

# ALMA Observations of Ethyl Formate toward Orion KL

YAPING PENG<sup>1,2</sup>, V. M. RIVILLA<sup>3</sup>, LI ZHANG<sup>1</sup>, J. X. GE<sup>4</sup>, BING ZHOU<sup>1,2</sup>

## ABSTRACT

Orion KL is one of the prime templates of astrochemical and prebiotic chemical studies. We wish to explore more organic molecules with increasing complexity in this region. In particular, we have searched for one of the most complex organic molecules detected in space so far, ethyl formate ( $\text{C}_2\text{H}_5\text{OCHO}$ ). This species is the next step in chemical complexity after the simplest member of esters (methyl formate,  $\text{CH}_3\text{OCHO}$ ). The mechanisms leading to its formation are still poorly known. We have used high angular resolution ( $\sim 1.''5$ ) ALMA observations covering a large bandwidth from 214 to 247 GHz. We have detected 82 unblended lines of  $\text{C}_2\text{H}_5\text{OCHO}$  (49 and 33 of the trans and gauche conformers, respectively). The line images showed that  $\text{C}_2\text{H}_5\text{OCHO}$  arises mainly from the compact ridge and the hot core-southwest regions. The derived rotational temperatures and column densities are  $122 \pm 34$  K,  $(0.9 \pm 0.3) \times 10^{16} \text{ cm}^{-2}$  for the hot core-SW, and  $103 \pm 13$  K,  $(0.6 \pm 0.3) \times 10^{16} \text{ cm}^{-2}$  for the compact ridge. The comparison of spatial distribution and abundance ratios with chemically related molecules (methyl formate, ethanol and formic acid) indicates that  $\text{C}_2\text{H}_5\text{OCHO}$  is likely formed on the surface of dust grains by addition of  $\text{CH}_3$  to functional-group radicals ( $\text{CH}_2\text{OCHO}$ ) derived from methyl formate ( $\text{CH}_3\text{OCHO}$ ).

*Subject headings:* ISM:abundances — ISM:individual (Orion KL) — ISM:molecules — radio lines: ISM — star:formation

---

<sup>1</sup>Department of Astronomy, Yunnan University, and Key Laboratory of Astroparticle Physics of Yunnan Province, Kunming, 650091, China; pyp893@163.com, lizhang@ynu.edu.cn, bingzhoukm@126.com

<sup>2</sup>College of Science, Yunnan Agricultural University, Kunming, 650201, China

<sup>3</sup>INAF-Osservatorio Astrofisico di Arcetri, Largo Enrico Fermi 5, I-50125, Firenze, Italia; rivilla@arcetri.astro.it

<sup>4</sup>Departamento de Astronomía, Universidad de Chile, Camino el Observatorio 1515, Las Condes, Santiago, Chile; gejixing666@gmail.com

## 1. INTRODUCTION

Almost 200 molecules have been detected in the interstellar medium (ISM) and circumstellar environments, of which more than 65 are considered complex organic molecules (COMs), molecules with  $\geq 6$  atoms containing carbon. The formation of these COMs in the ISM is still poorly understood, and is subject of intense debate. Two general theories have been proposed: gas-phase chemistry (e.g., Millar et al. 1991; Balucani et al. 2015; Taquet et al. 2016) and dust grain surface chemistry (e.g., Garrod & Herbst 2006; Fedoseev et al. 2015; Chuang et al. 2016).

Orion KL is a high mass star-forming region that provides a superb template for constraining the chemical models (e.g., Brouillet et al. 2013; Crockett et al. 2015; Feng et al. 2015; Favre et al. 2017; Carroll et al. 2017; Friedel & Looney 2017). Orion KL consists of different spatial and chemical components, namely: the hot core, the compact ridge, the extended ridge and the plateau (Blake et al. 1987). In particular two regions, the hot core and the compact ridge, have received special attention because they are very rich in organic species (e.g., Blake et al. 1987; Wang et al. 2011; Favre et al. 2011). While the hot core is rich in nitrogen-bearing molecules (Peng et al. 2013; Peng et al. 2017; Pagani et al. 2017), the compact ridge is richer in oxygen-bearing species (Blake et al. 1987; Beuther et al. 2005; Friedel & Snyder 2008; Gong et al. 2015). The hot core region may be heated by shocks from source I outflow (e.g., Goddi et al. 2011) or by explosive event occurred around 500 yr ago (e.g., Zapata et al. 2011; Rivilla et al. 2013; Bally et al. 2011, 2017; Wright & Plambeck 2017). Whether this explosive event impacted the release of complex molecules to the gas phase is under debate (e.g., Friedel & Looney 2017; Favre et al. 2017).

The ester family of molecules is essential for many prebiotic processes. The simplest representative is the 8 atom molecule methyl formate ( $\text{CH}_3\text{OCHO}$ , hereafter MF), which is relatively abundant in many high-mass (e.g., Favre et al. 2011; Rivilla et al. 2017b) and low-mass star-forming regions (e.g., Cazaux et al. 2003). Ethyl formate ( $\text{C}_2\text{H}_5\text{OCHO}$ , hereafter EF) is the next step in chemical complexity of esters, with eleven atoms. EF has two conformers: the *trans*-conformer (also called *anti*-conformer) where the heavy atoms C-C-O-C=O form a planar zigzag chain, and the *gauche*-conformer produced by an out-of-plane rotation of the ethyl group ( $\text{C}_2\text{H}_5$ ) around the O-C bond (Medvedev et al. 2009). The formation routes of EF are still poorly known. Several chemical pathways have been proposed, including reactions on the surface of dust grains and reactions in the gas-phase. On one hand, Charnley et al. (1995) used gas-phase reactions starting with the ethanol ( $\text{C}_2\text{H}_5\text{OH}$ , hereafter ET) to produce the EF. Recently, the formation of EF has been included in a new gas-phase chemical network (Taquet et al. 2016), in which formic acid ( $\text{HCOOH}$ ) and ammonia ( $\text{NH}_3$ ) favor the formation of EF. On the other hand, Garrod et al. (2008)

proposed an alternative scenario based on grain-surface chemistry, in which EF can be formed from ET and MF via cosmic ray-induced photodissociation.

The different chemical routes proposed should be checked with observations of EF and its chemically related species. However, since EF is a very complex and hence low abundant molecule, it has been detected so far only towards 4 sources: three massive star forming regions Sgr B2(N) (Belloche et al. 2009), W51 e2 (Rivilla et al. 2017b), Orion KL (Tercero et al. 2013, 2015), and one low-mass star forming region Barnard 1b (Marcelino et al. 2018). The works by Belloche et al. (2009), Rivilla et al. (2017b) and Tercero et al. (2013) all used single-dish IRAM 30m data. Single-dish observations give the line intensity integrated over a large beam area and do not provide the spatial distribution of EF nor an accurate value of the source-averaged column density. To better constrain the formation of this species, interferometric observations at high angular resolution and good sensitivity are needed. Tercero et al. (2015) provided an ALMA map of a single transition of EF (at 237.567 GHz, with  $E_u = 275.9$  K), which peaks mainly towards the compact ridge. However, a more complete multi-transition study involving many EF transitions at different energy levels is needed to: i) determine the excitation conditions of the molecule and thus the column density in the different components of Orion KL, and ii) compare the spatial distribution and abundances of EF with that of the molecules proposed to play a role in its formation.

With this purpose, we study in this paper multiple transitions of EF, covering the spectral range 214-247 GHz, and energy levels from 56 to 788 K, using interferometric ALMA observations with high angular resolution ( $\sim 1.''5$ ). We identified EF, and also the chemically related molecules ET, MF and HCOOH. We studied their relative abundances and relative spatial distributions, and we compared with the predictions of the theoretical gas-phase and grain-surface models, so that we can further understand the chemical routes of EF. This paper is organized as follows. In Section 2, we introduce the observations. The results and derivation of physical parameters are presented in Section 3 and Section 4, respectively. A general discussion is presented in Section 5. We summarize the results in Section 6.

## 2. OBSERVATIONS

We used data from the ALMA science verification (SV) program<sup>1</sup>. The observations were carried with 16 antennas of 12 m in January 2012. The phase center of the observations is R.A.(J2000)=05<sup>h</sup>35<sup>m</sup>14<sup>s</sup>.35 and Decl.(J2000)=−05°22′35″.00. The baseline lengths range

---

<sup>1</sup>The data are available to the public and can be accessed from the ALMA-SV website at <https://almascience.nrao.edu/alma-data/science-verification>.

from 17 to 265 m. A total of 20 spectral windows of 1.875 GHz completely cover a frequency range from 214 GHz to 247 GHz. Each spectral window consists of 3840 channels with a uniform spectral resolution of 0.448 MHz ( $\sim 0.7 \text{ km s}^{-1}$ ). Callisto and the quasar J0607-085 were used for the flux and phase calibration, respectively. The  $1 \text{ Jy beam}^{-1}$  correspond to a main beam brightness temperature of  $\sim 9 \text{ K}$ . The primary beam size of each 12 m antenna is about  $30''$ . The calibrated UV data were exported to Miriad format, and images were using the Miriad software package (Sault et al. 1995). The synthesized beam size with natural weighting for spectral images is approximately  $1.''8 \times 1.''3$  ( $\sim 745 \text{ AU} \times 538 \text{ AU}$ ) with a PA of  $-2.6^\circ$ .

### 3. RESULTS

#### 3.1. Line Identification

We identified spectral line transitions using the eXtended CASA Line Analysis Software Suite (XCLASS; Möller et al. 2017), which accesses the Cologne Database for Molecular Spectroscopy (CDMS<sup>2</sup>; Müller et al. 2001, 2005) and Jet Propulsory Laboratory (JPL<sup>3</sup>; Pickett et al. 1998) molecular databases. We used the CDMS entries for EF, ET and t-HCOOH. We used the JPL entry for MF. To identify lines, we set the following constraints (Snyder & Lovas. 2005; Brouillet et al. 2015): the rest frequency must be consistent with the value from laboratory measurement; all detected transitions for a given species must have similar Local standard of rest (LSR) velocity of the source; the transitions at different frequency have different beam dilution effect; for a specific species, transitions having similar excitations condition should have similar spatial distribution. Over the full spectral coverage, we identified 82 (above  $5\sigma$ ) unblended lines of EF (49 of the *trans* conformer and 33 of the *gauche* conformer) with upper level energies ( $E_u$ ) in the range 152–411 K, 469 lines of MF with  $E_u$  36–797 K, 204 lines of ET (67 *trans* and 137 *gauche*) with  $E_u$  ranging from 24 to 672 K, and 12 lines of *trans*-HCOOH with  $E_u$  of 59–262 K. In this work, all lines below the  $5\sigma$  detection level are ignored, where  $\sigma$  is the rms noise. In order to compute rms of a certain transition, we measured the rms value considering the line-free channels among the nearby 50 channels. We show in Figure 1 selected transitions of EF that appear unblended or only slightly blended towards the two selected positions (see below): the compact ridge and/or the hot core southwest region. We also present the full observed spectra (black curve) in Figure A.1, and overplot all the detectable transitions of EF (unblended and blended).

---

<sup>2</sup><http://cdms.de>

<sup>3</sup><http://spec.jpl.nasa.gov>

The observed spectra of MF and ET are showed in Figure 2 and t-HCOOH is showed in Figure 3. The spectra of EF, MF and ET are extracted from the positions of the intensity peaks of EF (see Figure 4a), which are R.A.=05<sup>h</sup>35<sup>m</sup>14<sup>s</sup>.430, Decl.=−05°22′34″.26 for the hot core-SW and R.A.=05<sup>h</sup>35<sup>m</sup>14<sup>s</sup>.107, Decl.=−05°22′36″.84 for the compact ridge. The spectra of t-HCOOH are extracted from the intensity peaks of t-HCOOH (see Figure 4d, R.A.=05<sup>h</sup>35<sup>m</sup>14<sup>s</sup>.485, Decl.=−05°22′32″.56 for the hot core-SW, and R.A.=05<sup>h</sup>35<sup>m</sup>14<sup>s</sup>.584, Decl.=−05°22′27″.46 for the hot core-N). The rest frequencies, quantum numbers, the line strength ( $S\mu^2$ ), and the upper level energies ( $E_u$ ) of selected lines of EF are listed in Table A.1. We performed Gaussian fits to every transition. The LSR velocity, full-width half maximum and peak intensities of each transitions are given in columns 5 to 7 (for the hot core-southwest) and 9 to 11 (for the compact ridge). The detection level of each transition is given in column 8 and 12 in Table A.1. The last column of Table A.1 lists the  $1\sigma$  channel rms noise level of each transition. Table A.2, A.3, A.4 list the unblended lines of MF, ET and formic acid, respectively. From the Figure 1 and A.1, one can see that EF lines are less blended toward the compact ridge than in the hot core-SW, and that the molecular lines have emission intensities slightly weaker toward the compact ridge than toward the hot core-SW.

### 3.2. Spatial Distributions

We show in Figure 4 the line integrated maps of EF, MF, ET and t-HCOOH at different (lower, intermediate and higher) upper level energies, with the aim of evaluating how the molecular emission varies with the energy of the transitions. It should be noted that it is difficult to present the EF integrated maps at low (e.g.,  $E_u = 222$  K) and high (e.g.,  $E_u = 596$  K) energies due to contamination from other species, especially toward the hot core-SW. We show three lines at intermediate energy levels (306–320 K) that are completely free from contamination in Figure 4a. In Figure 4, the peak positions of continuum hot core (R.A.=05<sup>h</sup>35<sup>m</sup>14<sup>s</sup>.543, Decl.=−05°22′31″.21) and compact ridge (R.A.=05<sup>h</sup>35<sup>m</sup>14<sup>s</sup>.064, Decl.=−05°22′36″.97) are marked as red crosses. The coordinates of two peak positions are from Peng et al. (2017) that used the same dataset.

The emission of EF distributes over the compact ridge and the hot core-SW. The gas map of MF with low-energy level ( $E_u = 236$  K) indicates widespread emission and has two main concentrations: the compact ridge and the hot core, in agreement with previous studies (e.g., Favre et al. 2011; Widicus Weaver & Friedel 2012; Favre et al. 2014; Sakai et al. 2015). However, at intermediate ( $E_u = 462$  K) and higher ( $E_u = 617$  K) energy levels, the emissions of MF becomes more compact and are mainly from the compact ridge and the hot core-SW.

We note that the emission of MF at the compact ridge is stronger than at the hot core for low energies, and emission at the hot core becomes stronger at higher upper level energies (e.g.,  $E_u = 617$  K; see Figure 2 and Figure 4(b)), consistent with the results presented by Favre et al. (2011). This indicates that lines having higher upper level energies are easily excited in hotter environment. A salient result is that the emission of EF and MF mainly come from the hot core-SW and compact ridge, and peak at the same position toward these two regions. Unlike EF and MF, ET has no strong emission in the compact ridge, and it mainly arises from the hot core-SW, which agrees with the previous works (e.g., Guélin et al. 2008; Feng et al. 2015).

The velocity integrated intensity maps of t-HCOOH with three different energies (70–215 K) are shown in Figure 4d. One emission peak of t-HCOOH is mainly at the hot core-SW, while another one is at the north of hot core (hereafter hot core-N). No compact emission of these relatively high energy transitions of HCOOH is detected towards the compact ridge molecular peak traced by EF and MF. We note that previous observations of lower excitation lines (14–70 K) of HCOOH (Liu et al. 2002; Widicus Weaver & Friedel 2012; Pagani et al. 2017) showed widespread distribution towards the S-SW of the compact ridge. However, this gas component, seen more clearly with poorer spatial resolution ( $3''$ - $6''$ ; Liu et al. 2002; Widicus Weaver & Friedel 2012), do not seem related with the compact gas traced by EF and MF.

## 4. DERIVATION OF PHYSICAL PARAMETERS

### 4.1. Rotational temperatures and column Densities

The combined usage of XCLASS and MAGIX (Modeling and Analysis Generic Interface for eXternal numerical codes; Möller et al. 2013, 2017) provides the best fit to the data. We have fitted the spectra extracted from the intensity peaks of EF in the hot core-SW and the compact ridge region, and spectra from the intensity peaks of HCOOH toward the hot core-SW and the hot core-N (see Section 3.1). Under the assumption of local thermodynamical equilibrium (LTE), XCLASS takes into account the beam dilution, the line opacity and line blending (Möller et al. 2017), and generates the synthetic spectrum of the different molecular species. The main modeling parameters of XCLASS for each molecule are the source size, the line full width at half maximum  $\Delta v$ , the velocity offset with respect to the systemic velocity of the object  $v_{\text{off}}$ , the rotational temperature  $T_{\text{rot}}$  and the column density  $N$ . We have derived the velocity offsets and line widths from Gaussian fits. We have derived the source size by performing two-dimension Gaussian fits to the line images, by using Miriad task IMFIT. We obtain the source sizes of  $1.6''$  for the hot core-SW and compact ridge based on the integrated

maps of EF. We have fixed the  $\Delta v$  and  $v_{\text{off}}$ . The rotational temperature and the column density are left as free parameters. These two parameters produced by XCLASS are used as initial guesses, and then MAGIX is used to optimize the fit and find the best solutions of  $T_{\text{rot}}$  and  $N$ , and provide corresponding error estimates. The algorithms we adopted are the Genetic, Levenberg-Marquardt and Error estimation using Interval-Nested-Sampling.

We stress that in the case of the conformers of EF and ET, we are able to fit both conformers using the same physical parameters. So both conformers of EF and ET are fitted together. We show the LTE model spectra overlaid on the observed spectra in Figure 1 (EF) and Figure 2 (MF and ET) toward the hot core-SW and the compact ridge. Figure 3 shows the LTE spectra of t-HCOOH toward the hot core-SW and the hot core-N. The derived parameters from two positions, including rotational temperature  $T_{\text{rot}}$ , total column density  $N$  and abundance  $\chi$  are listed in Table 1. See more details about abundances in section 4.2. In the following we comment individually the rotational temperature and column density obtained from each species:

**EF (C<sub>2</sub>H<sub>5</sub>OCHO):** The detected unblended transitions cover a large  $E_u$  range (152–411 K), which allow to constrain well the rotational temperature, and then the column density. We have obtained  $T_{\text{rot}} = 122 \pm 34$  K, and a column density of  $N = (9.0 \pm 3.0) \times 10^{15} \text{ cm}^{-2}$  for the hot core-SW, and  $T_{\text{rot}} = 103 \pm 13$  K,  $N = (6.0 \pm 3.0) \times 10^{15} \text{ cm}^{-2}$  for the compact ridge. Meanwhile, for the purpose of comparison with other works, we list the number of detected lines, corresponding  $E_u$  range, observations information and source size they used in Table 2. The temperature  $T_{\text{rot}}$  we obtained is similar to that derived in W51 ( $78 \pm 10$  K) by Rivilla et al. (2017b), and to that assumed in Orion KL compact ridge ( $100 \pm 20$  K) by Tercero et al. (2015) and Sgr B2(N) (100 K) by Belloche et al. (2009). The column density we obtained in the compact ridge is higher to that of Tercero et al. (2015). They assumed  $T_{\text{rot}}$  of 100 K and  $\theta_s$  of  $3''$  for one single transition to obtain column density  $N$  of  $(0.2 \pm 0.04) \times 10^{16} \text{ cm}^{-2}$ . This value would be  $0.7 \times 10^{16} \text{ cm}^{-2}$ , similar to our value, if we consider the same source size of  $1.6''$ .

As mentioned before, multiple unblended or slightly blended lines of the both conformers of EF are clearly identified, as shown in Figure 1. We note that a few transitions (e.g., 218.74259 GHz, 218.74470 GHz, 220.00368 GHz, 223.89863 GHz, 224.28239 GHz) are weaker than the LTE fit. A possible explanation is a poor baseline subtraction at these spectral ranges, since Orion is a line-rich source, and it is difficult to find free-line channels, and then the continuum is not perfectly subtracted. On the other hand, some of the observed lines might be weaker than the LTE fit due to the presence of nearby absorption lines from other species (e.g. 218.752 GHz, 219.658 GHz and 225.240 GHz). There are some lines, at 219.40243 GHz, 219.65815 GHz, 219.78133 GHz, 219.78771 GHz and 220.17206 GHz, for

which the LTE fit predicts higher line intensities than observed. We found that the spectroscopic parameters (in particular  $S\mu^2$ ) of these five transitions show discrepancies between the CDMS and the JPL entries. Other lines that have similar spectroscopic parameters in two database have good fitting results. We suspect that there are some issues affecting the spectroscopic information of some of the transitions with discrepancies.

**MF (CH<sub>3</sub>OCHO):** We note that the stronger lines are overestimated toward the hot core-SW, this could be due to line opacity effects. These stronger lines have high  $S\mu^2$ . If we leave the source size as a free parameter, all lines of MF can be fitted better, including high  $S\mu^2$  lines, which appears saturated with optical depth of  $\sim 4$ . The strong lines are expected to have more extended gas distribution, and interferometric observations of ALMA will partially filter out diffuse gas component. This is likely to cause decreasing intensities of strong lines. The best fit parameters of MF are  $T_{\text{rot}} = 135 \pm 5$  K and  $N = (7 \pm 3) \times 10^{17}$  cm<sup>-2</sup> toward the hot core-SW, and  $93 \pm 5$  K and  $(9 \pm 4) \times 10^{17}$  cm<sup>-2</sup> for the compact ridge. Our derived rotational temperatures in the hot core-SW and compact ridge are mostly consistent with the other works, but column densities in the two regions are larger than the values provided by others (see Table 2, e.g., Favre et al. 2011; Feng et al. 2015; Tercero et al. 2015). Our column density is higher than results from Favre et al. (2011) by a factor of  $\sim 4$ – $5$  probably because they cover lower  $E_u$  transitions, especially in the compact ridge. The lower column densities found by Feng et al. (2015) is easily explained because of their large beam ( $5.''0 \times 4.''0$ ), which also includes less dense gas. The difference of column density between our work and Tercero et al. (2015) can be easily explained due to the different source size used. If one consider  $\theta_s$  of  $1.6''$  instead of  $3''$ , the Tercero et al. (2015) estimate would be  $84 \times 10^{16}$  cm<sup>-2</sup>, in remarkably agreement with our results.

**ET (C<sub>2</sub>H<sub>5</sub>OH):** Regarding ET, we have found significant discrepancies in the spectroscopic parameters between the CDMS and JPL entries affecting some transitions, e.g., those at 213.760 and 213.856 GHz. Comparing the LTE spectra of both databases, we have seen that the CDMS entry is more consistent with the observed spectrum, so that we have used it to derive the physical properties. The LTE fitting gives  $T_{\text{rot}} = 144 \pm 13$  K and  $N = (1.3 \pm 0.5) \times 10^{17}$  cm<sup>-2</sup> toward the hot core-SW, and  $111 \pm 15$  K and  $(2.0 \pm 0.5) \times 10^{16}$  cm<sup>-2</sup> for the compact ridge. The column densities derived from our work are higher than those reported in Feng et al. (2015) (see Table 2), owing to our higher angular resolution. Again for result from Tercero et al. (2015), if one consider  $\theta_s = 1.6''$ , the column density would be  $21 \times 10^{16}$  cm<sup>-2</sup>, which is of the same order than our value (less than a factor of 2).

**Formic acid (t-HCOOH):** We derive  $T_{\text{rot}} = 120 \pm 16$  K and  $N = (6.2 \pm 1.8) \times 10^{15}$  cm<sup>-2</sup> toward the hot core-SW peak, and  $106 \pm 27$  K and  $(2.8 \pm 0.8) \times 10^{15}$  cm<sup>-2</sup> toward the hot core-N.



We give in Table 3 the ratios of [MF/EF] and [MF/ET] from our work and a few other works toward the hot core-SW and the compact ridge. The [MF/EF] of  $140 \pm 81$  toward the compact ridge in our work is reasonable agreement with the ratio of 120 in Tercero et al. (2015). Toward the hot core-SW, the [MF/ET] of  $6 \pm 3$  is in agreement with that of  $4 \pm 3$  in Feng et al. (2015), and toward the compact ridge our result of  $42 \pm 24$  is similar to those from Feng et al. (2015) ( $17 \pm 12$ ) and Crockett et al. (2014) (20) if considering the uncertainties.

## 4.2. Molecular abundances

The fractional abundance of a certain molecule relative to  $H_2$  depends on the column density of the certain molecule,  $N$ , and that of the  $H_2$  molecule ( $\chi = N/N_{H_2}$ ). The estimations of  $N_{H_2}$  for each Orion KL component are presented in many works (e.g., Tercero et al. 2010; Crockett et al. 2014; Favre et al. 2011; Feng et al. 2015), and  $N_{H_2}$  varies in every work because of different spatial resolutions. We used the dust continuum emission of the ALMA observations to estimate the column density of  $H_2$ . In the assumption of optically thin emission from dust, and taking a grain radius of  $0.1 \mu\text{m}$ , a grain density of  $3 \text{ g cm}^{-3}$ , and a gas-to-dust ratio of 100, the column density of  $H_2$  can be derived by the formula (e.g., Lis et al. 1991; Qin et al. 2010):

$$N_{H_2} = 8.1 \times 10^{17} \frac{e^{h\nu/\kappa T_d} - 1}{Q_\nu \Omega} \left( \frac{S_\nu}{\text{Jy}} \right) \left( \frac{\nu}{\text{GHz}} \right)^{-3} (\text{cm}^{-2}), \quad (1)$$

where  $T_d$  is the dust temperature,  $Q_\nu$  is the grain emissivity at frequency  $\nu$ ,  $S_\nu$  is the peak intensity of the continuum and  $\Omega$  is the beam solid angle. We assumed that the dust temperature equals to the rotation temperature of the core. We used dust temperature of 200 K for the hot core and 100 K for the compact ridge (e.g., Wu et al. 2014; Favre et al. 2011), and grain emissivity of  $2 \times 10^{-5}$  at 230 GHz (Lis et al. 1991). We adopt  $S_\nu$  of  $1.34 \pm 0.06 \text{ Jy beam}^{-1}$  for the hot core and  $0.28 \pm 0.03 \text{ Jy beam}^{-1}$  for the compact ridge from Wu et al. (2014) that used same ALMA data. Therefore we obtain  $H_2$  column densities of  $(4.7 \pm 0.2) \times 10^{24} \text{ cm}^{-2}$  and  $(2.0 \pm 0.2) \times 10^{24} \text{ cm}^{-2}$  for the hot core and the compact ridge, respectively. We list the abundances relative to  $H_2$  of EF, MF, ET and t-HCOOH toward the two positions in Table 1. In comparison with abundances for each species from other works (see Table 2), one can see that:

1) The abundance of EF towards the hot core and the compact ridge are very similar,  $0.19 \times 10^{-8}$  and  $0.3 \times 10^{-8}$  respectively. This value is in good agreement with the ones derived in the other two massive star forming regions where EF has been detected:  $1 \times 10^{-8}$  in W51 (Rivilla et al. 2017b) and  $0.36 \times 10^{-8}$  on Sgr B2(N) (Belloche et al. 2009).

2) The abundances of ET and MF we have derived are in better agreement with those from Feng et al. (2015), compared with the column densities. This is because the effect of the different beams are compensated by dividing by  $N_{\text{H}_2}$  (namely, their  $N$  is lower but also their  $N_{\text{H}_2}$ ).

3) The abundances of MF from Favre et al. (2011) are lower, especially in the compact ridge ( $3.1 \times 10^{-8}$ ). This could be because the range of energies of the lines used in the compact ridge by Favre et al. (2011) is much lower than the one we have used (see Table 2), and thus they are tracing less dense gas.

4) Our derived abundance of MF ( $(42 \pm 20) \times 10^{-8}$ ) in the compact ridge agrees very well with those derived by Gong et al. (2015) ( $(47 \pm 6) \times 10^{-8}$ ) and Crockett et al. (2014) ( $33 \times 10^{-8}$ ).

We compare graphically the abundances (Figure 5a) and rotational temperatures (Figure 5b) of each molecule derived in different regions (Orion KL, W51 and Sgr B2(N)) with the theoretical values from the grain-surface model by Garrod et al. (2008) and gas-phase model by Taquet et al. (2016). In the next section we will discuss which of the two proposed chemistries is in better agreement with the observations in star-forming regions.

## 5. Discussion

We have shown that both conformers of EF can be well fitted simultaneously, and hence that they share the same abundance. The relative abundance of the two conformers is  $N_g/N_t = 2e^{-\Delta E/T_{\text{kin}}}$  (Rivilla et al. 2017b), where  $T_{\text{kin}}$  is kinetic temperature of the gas and  $\Delta E$  is energy difference between the two ground states of two conformers.  $\Delta E$  is in the range of 64–124 K (Riveros & Wilson. 1967), which implies a  $T_{\text{kin}}$  in the range 93–178 K when considering  $N_g/N_t = 1$ . The  $T_{\text{kin}}$  would be equal to the rotational temperature  $T_{\text{rot}}$ , if we assume that EF is thermalized. The  $T_{\text{rot}}$  derived in our work ( $122 \pm 34$  K for hot core-SW and  $103 \pm 13$  K for compact ridge, see Table 1) are compatible to the range of 93–178 K, which suggests that EF is indeed thermalized.

As we stated above, three molecules (MF, ET and HCOOH) may play a important role in forming EF, so it is necessary to take these related species into account to study the proposed chemical routes to EF. Table 1 and Figure 5b showed that  $T_{\text{rot}}$  in the hot core are in the range of 120–144 K, and 93–111 K in the compact ridge, indicating that these four molecules share similar excitation conditions, and hence they are expected to trace similar gas components. This means that if there is no emission in some region (for instance ET in the compact ridge), this is due to a chemical effect.

Two main pathways have been proposed to form EF, one based on gas-phase chemistry and other based on chemistry on the surface of dust grains. We compare in the following the result found in star-forming regions (Orion KL, W51 and Sgr B2(N)) with the predictions of the proposed models.

1) Gas-phase formation. Based on the model from Charnley et al. (1995), their gas-phase route is able to produce EF abundance of  $\sim 10^{-10}$  in  $10^4$ - $10^5$  yr ( $C_2H_5OH + H^+ \rightarrow C_2H_5OH_2^+$ ,  $C_2H_5OH_2^+ + H_2CO \rightarrow HC(OH)OC_2H_5^+ + H_2$ ,  $HC(OH)OC_2H_5^+ + e^- \rightarrow C_2H_5OCHO + H$ ). The observed EF abundances of  $0.2 \times 10^{-8}$  (hot core) and  $0.3 \times 10^{-8}$  (compact ridge) (see Table 1) are much larger than that predicted by gas-phase route. The estimated abundances in W51 ( $1.0 \times 10^{-8}$ ) and Sgr B2(N) ( $3.6 \times 10^{-9}$ ) are also larger than that predicted ones. So this gas-phase reaction can not produce enough abundance of EF. A new gas-phase network for the formation of COMs have been proposed by Taquet et al. (2016). Considering proton transfer (PT) reaction with HCOOH and  $NH_3$  ( $C_2H_5OH_2^+ + HCOOH \rightarrow HC(OH)OC_2H_5^+ + H_2O$ ,  $HC(OH)OC_2H_5^+ + NH_3 \rightarrow C_2H_5OCHO + NH_4^+$ ), their model is able to produce the observed EF abundances of  $10^{-8}$ - $10^{-7}$  in a reasonable timescale for hot molecular cores of  $10^4 - 10^5$  yr. In the hot core-SW, our derived HCOOH abundance of  $(1.3 \pm 0.4) \times 10^{-9}$  is much lower than those required for gas-phase model (see panel a(4) of Figure 5). Moreover, the ALMA maps show that there is no similarity in spatial distributions and emission peaks between HCOOH and EF (see Figure 4).

Regarding the distribution of  $NH_3$  (transitions with  $E_u > 408$  K) detected by Goddi et al. (2011), it peaks towards the hot core and IRC7 regions, while no emission is detected towards the compact ridge peak traced by EF and MF (see their Fig. 2). Since both the hydrogen column densities and rotational temperatures found towards the two positions studied in our work, hot core-SW ( $N_{H_2} = (4.7 \pm 0.2) \times 10^{24} \text{ cm}^{-2}$ ,  $T_{rot} = 120$ - $144$  K) and compact ridge ( $N_{H_2} = (2.0 \pm 0.2) \times 10^{24} \text{ cm}^{-2}$ ,  $T_{rot} = 93$ - $111$  K), are relatively similar, the clear presence of  $NH_3$  in the hot core region and the lack in the compact ridge peak, point to a chemical differentiation and not to excitation effects. Therefore, similarly to HCOOH, there is no spatial coincidence between  $NH_3$  and EF. In the hot core region, Goddi et al. (2011) derived a column density of  $NH_3$  of  $(1-4) \times 10^{17} \text{ cm}^{-2}$ , which implies an abundance of  $(2-9) \times 10^{-8}$ . This value is lower than the gas model value by more than an order of magnitude. In summary, the molecular abundances and spatial distributions of HCOOH and  $NH_3$  indicate that the proposed gas-phase routes are not able to produce the observed EF abundance in Orion KL, as also noted by Rivilla et al. (2017b) in W51.

2) Grain-surface formation. According to the coupled gas-phase and grain-surface chemical network by Garrod et al. (2008), EF can be formed on grain surfaces by the reactions between radicals  $CH_3$  and  $CH_2OCHO$  or between HCO and  $C_2H_5O$ . MF is the primary

source of precursor radical of EF ( $\text{CH}_3\text{OCHO} + h\nu \rightarrow \text{CH}_2\text{OCHO}$ ,  $\text{CH}_2\text{OCHO} + \text{CH}_3 \rightarrow \text{C}_2\text{H}_5\text{OCHO}$ ). When MF evaporates, ET ( $\text{C}_2\text{H}_5\text{OH}$ ) becomes dominant in forming EF ( $\text{C}_2\text{H}_5\text{OH} + h\nu \rightarrow \text{C}_2\text{H}_5\text{O}$ ;  $\text{C}_2\text{H}_5\text{O} + \text{HCO} \rightarrow \text{C}_2\text{H}_5\text{OCHO}$ ). The predicted abundance of EF is  $2.3 \times 10^{-9}$  in this model (see Belloche et al. 2009), which is in reasonably agreement with the range of observed values in our work ( $(2-3) \times 10^{-9}$ ) and in W51 e2 and Sgr B2(N) ( $(3.6-10) \times 10^{-9}$ ). In addition, the predicted molecular ratio MF/EF is 72/1 (in Basic model, see Table 15 of Belloche et al. 2009), which is close to our observed ratio values of  $(79 \pm 36)/1$  for the hot core and  $(140 \pm 81)/1$  for the compact ridge. The excitation temperature of EF ( $122 \pm 34$  K for the hot core and  $103 \pm 13$  K for the compact ridge) and MF ( $135 \pm 5$  K for the hot core and  $93 \pm 5$  K for the compact ridge) derived in Orion KL are also close to the temperature associated with the peak gas-phase temperatures of Garrod et al. (2008) model (110 K for EF and 81 K for MF) (see Figure 5b). The abundances of ET derived from our fitting ( $(2.7 \pm 1.0) \times 10^{-8}$  for the hot core and  $(1.0 \pm 0.3) \times 10^{-8}$  for the compact ridge),  $7.9 \times 10^{-8}$  in W51 and  $5.7 \times 10^{-8}$  in Sgr B2(N) (see Table 2 and Figure 5a) are lower than abundance from Garrod et al. (2008) model ( $1.0 \times 10^{-7}$ ). This may indicate that the dominant route to the formation of EF is grain surface chemistry from MF and not from ET. This is also supported by the spatial distribution of the different molecules revealed by the ALMA observations (see Figure 4): EF and MF share the same intensity peaks toward the hot core-SW and the compact ridge, while there is no strong ET emission towards the compact ridge. Considering all this together, EF is likely formed on grains by addition of  $\text{CH}_3$  to functional-group radicals ( $\text{CH}_2\text{OCHO}$ ) derived from  $\text{CH}_3\text{OCHO}$  and then evaporated to the gas phase.

## 6. Summary

As the the next step in chemical complexity of esters, ethyl formate ( $\text{C}_2\text{H}_5\text{OCHO}$ ) is a low abundant molecule and it is detected so far only toward three sources. The formation routes of EF are still poorly known. Multiple transitions of EF covering a wide range of energy levels are needed to explore it's excitation conditions and formation routes. The different chemical routes proposed should be checked with observations of EF and its chemically related species (methyl formate ( $\text{CH}_3\text{OCHO}$ ), ethanol ( $\text{C}_2\text{H}_5\text{OH}$ ) and trans-HCOOH). We have identified and imaged multiple lines of EF, MF, ET and t-HCOOH observed with ALMA at band 6 (214–247 GHz). The identified transitions of three molecules span a wide range of upper-level energy so that we can perform a detailed LTE analysis to derive accurate physical parameters. We have compared our results with the two main chemical routes proposed to the formation of EF (gas-phase chemistry and grain surface chemistry). The main findings are as follows:

1. We have identified 82 unblended lines of EF (49 of the trans conformer and 33 of the gauche conformer), 469 lines of MF, 204 lines of ET (67 of the trans conformer and 137 of the gauche conformer) and 12 lines of t-HCOOH over the full ALMA band 6.

2. The spatial distribution of EF exhibits two main emission regions (compact ridge and hot core-SW). The gas emission of MF is very similar to that of EF, while ET mainly originates from the hot core-SW but not from the compact ridge. t-HCOOH mainly originate from the south-west of hot core and hot core-N.

3. The derived rotational temperatures and column densities of EF are  $122 \pm 34$  K,  $(9.0 \pm 3.0) \times 10^{15} \text{ cm}^{-2}$  for the hot core-SW, and  $103 \pm 13$  K,  $(6.0 \pm 3.0) \times 10^{15} \text{ cm}^{-2}$  for the compact ridge. We also derived the best fit parameters of chemically related molecules MF, ET and t-HCOOH.

4. We have compared our results with the two proposed routes to form EF, based on gas-phase chemistry (Taquet et al. 2016) and grain surface chemistry (Garrod et al. 2008; Belloche et al. 2009). The observed abundances of  $\text{NH}_3$  and HCOOH are much lower than those required for gas-phase model to produce the observed abundances of EF. Moreover, there is no similarity in spatial distributions and emission peaks among HCOOH,  $\text{NH}_3$  and EF. So these gas-phase routes may not produce the observed EF abundance in Orion KL and other star-forming regions. The derived EF abundance of  $(2-3) \times 10^{-9}$  is in good agreement with the one predicted by the grain surface model. The observed ratios of MF/EF ( $(79 \pm 36)/1$  for the hot core and  $(140 \pm 81)/1$  for the compact ridge) are also in good agreement with the grain-surface model. In addition, the gas emissions of EF and MF peak at same position in the hot core and compact ridge, while ET spatial distribution is different, lacking in the compact ridge. Altogether, these results suggest that EF is likely formed on grains by addition of  $\text{CH}_3$  to functional-group radicals ( $\text{CH}_2\text{OCHO}$ ) derived from  $\text{CH}_3\text{OCHO}$  and then evaporated to the gas phase.

This paper makes use of the following ALMA data: ADS/JAO.ALMA# 2011.0.00009.SV. ALMA is a partnership of ESO (representing its member states), NSF (USA), and NINS (Japan), together with NRC (Canada) and NSC and ASIAA (Taiwan), in cooperation with the Republic of Chile. The Joint ALMA Observatory is operated by ESO, AUI/NRAO, and NAOJ. We thank Sheng-Li Qin for carefully reading the paper and providing useful comments and suggestions. This work has been supported by the National Natural Science Foundation of China under grant No. 11433004. V.M. R. has received funding from the European Union's Horizon 2020 research and innovation programme under the Marie Skłodowska-Curie grant agreement No 664931, and from the Italian Ministero dell'Istruzione, Università e Ricerca through the grant Progetti Premiali 2012 - iALMA (CUP C52I13000140001). JX acknowl-

edges support from FONDECYT grant 3170768 and the "Light of West China" program of Chinese Academy of Sciences (CAS).

## REFERENCES

- Bally, J., Cunningham, N. J., Moeckel, N., et al. 2011, *ApJ*, 727, 113
- Bally, J., Ginsburg, A., Arce, H., et al. 2017, *ApJ*, 837, 60
- Balucani, N., Ceccarelli, C., & Taquet, V. 2015, *MNRAS*, 449, 16
- Belloche, A., Garrod, R. T., Müller, H. S. P., et al., 2009, *A&A*, 499, 215
- Beuther, H., Zhang, Q., Greenhill, L. J., et al. 2005, *ApJ*, 632, 355
- Beuther, H., Zhang, Q., Reid, M. J., et al. 2006, *ApJ*, 636, 323
- Blake, G. A., Sutton, E. C., Masson, C. R., & Phillips, T. G. 1987, *ApJ*, 315, 621
- Brouillet, N., Despois, D., Baudry, A., et al., 2013, *A&A*, 550, A46
- Brouillet, N., Despois, D., Lu, X. H., Baudry, A., et al. 2015, *A&A*, 576, A129
- Carroll, B., Crockett, N. R., Wilkins, O. H., Bergin, E. A., et al. 2017, in 72nd International Symposium on Molecular Spectroscopy
- Cazaux, S., Tielens, A. G. G. M., Ceccarelli, C., et al., 2003, *ApJL*, 593, L51
- Chuang, K. -J., Fedoseev, G., Ioppolo, S., van Dishoeck, E. F., & Linnartz, H. 2016, *MNRAS*, 455, 1702
- Crockett, N. R., Bergin, E. A., Neill, J. L., et al. 2014, *ApJ*, 787, 112
- Crockett, N. R., Bergin, E. A., Neill, J. L., et al. 2015, *ApJ*, 806, 239
- Charnley, S. B., Kress, M. E., Tielens, A. G. G. M., & Millar, T. J. 1995, *ApJ*, 448,232
- Curl, R. F. 1959, *J. Chem. Phys.*, 30, 1529
- Favre, C., Despois, D., Brouillet, N., et al., 2011, *A&A*, 532, A32
- Favre, C., Carvajal, M., Field, D., et al., 2014, *ApJS*, 215, 25
- Favre, C., Pagani, L., Goldsmith, P., et al., 2017, *A&A*, 604, 2

- Fedoseev, G., Ioppolo, S., Zhao, D., Lamberts, T., & Linnartz, H. 2015, *MNRAS*, 446, 439
- Feng, S., Beuther, H., Henning, Th., et al. 2015, *A&A*, 581, 71
- Friedel, D. N., & Snyder, L. E. 2008, *ApJ*, 672, 962
- Friedel, D. N., & Looney, L. W. 2017, *AJ*, 154, 152
- Fontani, F., Pascucci, I., Caselli, P., Wyrowski, F., Cesaroni, R., Walmsley, C. M., 2007, *A&A*, 470, 639
- Garrod, R. T., & Herbst, E. 2006, *A&A*, 457, 927
- Garrod, R. T., Weaver, S. L. W., Herbst, E., 2008, *ApJ*, 682, 283
- Greenhill, L. J., Gezari, D. Y., Danchi, W. C., et al. 2004, *ApJ*, 605, L57
- Goddi, C., Greenhill, L. J., Humphreys, E. M. L., Chandler, C. J., & Matthews, L. D. 2011, *ApJL*, 739, L13
- Gong, Y., Henkel, C., Thorwirth, S., et al., 2015, *A&A*, 581, 48
- Gómez, L., Godríguez, L. F., Loinard, L., et al. 2008, *ApJ*, 685, 333
- Guélin, M., Brouillet, N., Cernicharo, J., Combes, F., & Wootten, A. 2008, *Ap&SS*, 313, 45
- Hirota, T., Machida, M. N., Matsushita, Y., et al. 2017, *Nature Astronomy*, 1, 0146
- Lis, D. C., Carlstrom, J. E., & Keene, J. 1991, *ApJ*, 380, 429
- Liu, S.-Y., Girart, J. M., Remijan, A., Snyder, L. E. 2002, *ApJ*, 576, 255
- Marcelino, N., Gerin, M., Cernicharo, J., Fuente, A., et al. 2018, *A&A*, 2018arXiv180908014M
- Medvedev, I. R., De Lucia, F. C., Herbst, E. 2009, *ApJS*, 181, 433
- Menten K. M., & Reid, M. J. 1995, *ApJ*, 445, 157
- Millar, T. J., Bennett, A., Rawlings, J. M. C., et al., 1991, *A&AS*, 87, 585
- Möller, T., Bernst, I., Panoglou, D., et al. 2013, *A&A*, 549, 21
- Möller, T., Endres, C., Schilke, P. 2017, *A&A*, 598, 7
- Müller, H. S. P., Thorwirth, S., Roth, D. A., & Winnewisser, G. 2001, *A&A*, 370, 49

- Müller, H. S. P., Schlöder, F., Stutzki, J., & Winnewisser, G. 2005, *Journal of Molecular Structure*, 742, 215
- Pagani, L., Favre, C., Goldsmith, P. F., et al., 2017, *A&A*, 604, 32
- Peng, Y. P., Qin, S. L., Schilke, P., et al., 2017, *ApJ*, 837, 49
- Peng, T.-C., Despois, D., Brouillet, N., et al. 2013, *A&A*, 554, A78
- Pickett, H. M., Poynter, R. L., Cohen, E. A., et al. 1998, *Quant. Spectrosc. & Rad. Transfer*, 60, 883
- Qin, S.-L., Wu, Y., Huang, M., et al. 2010, *ApJ*, 711, 399
- Riveros, J. M., & Wilson, E. B. 1967, *JChPh*, 46, 4605
- Rivilla, V. M., Martín-Pintado, J., Jiménez-Serra, I., Rodríguez-Franco, A. 2013, *A&A*, 554, A48
- Rivilla, V. M., Beltrán, M. T., Cesaroni, R., et al., 2017a, *A&A*, 598, 59
- Rivilla, V. M., Beltrán, M. T., Martín-Pintado, J., et al., 2017b, *A&A*, 599, 26
- Rizzo, J. R., Tercero, B., & Cernicharo, J. 2017, *A&A*, 605, A76
- Sakai, Y., Kobayashi, K., & Hirota, T. 2015, *ApJ*, 803, 97
- Sault, R. J., Teuben, P. J., & Wright, M. C. H. 1995, in *ASP Conf. Ser. 77, Astronomical Data Analysis Software and Systems IV* (San Francisco: ASP), 433
- Shuping, R., Morris, M., & Bally, J. 2004, *AJ*, 128, 363
- Simpson, J. P., Colgan, S. W. J., Erickson, E. F., et al. 2006, *ApJ*, 642, 339
- Snyder, L. E., Lovas, F. J., Hollis, J. M., et al. 2005, *ApJ*, 619, 914
- Taquet, V., Wirström, E. S., Charnley, S. B. 2016, *ApJ*, 821, 46
- Tercero, B., et al., 2015, *A&A*, 582, L1
- Tercero, B., Kleiner, I., Cernicharo, J., et al., 2013, *ApJL*, 770, L13
- Tercero, B., Cernicharo, J., Pardo, J. R., & Goicoechea, J. R. 2010, *A&A*, 517, A96
- Wang, S., Bergin, E. A., Crockett, N. R., et al. 2011, *A&A*, 527, A95



Widicus Weaver, S. L., & Friedel, D. N. 2012, *ApJS*, 201, 16

Wright, M. C. H., & Plambeck, R. L. 2017, *ApJ*, 843, 83

Wu, Y.F., Liu, T., & Qin, S. L. 2014, *ApJ*, 791, 123

Zapata, L. A., Schmid-Burgk, J., & Menten, K. M. 2011, *A&A*, 529, A24

Zapata, L. A., Rodríguez, L. S., Schmid-Burgk, J., et al. 2012, *ApJL*, 754, 17

Zhang, C.-P., Wang, J.-J., Xu, J.-L., et al., 2014, *ApJ*, 784, 107

Table 1. Model fitting results of EF, MF, ET and t-HCOOH.

Molecular name	hot core-SW					compact ridge				
	$v_{\text{LSR}}^{\text{a}}$ ( $\text{km s}^{-1}$ )	$\Delta v^{\text{a}}$ ( $\text{km s}^{-1}$ )	$T_{\text{rot}}$ (K)	$N$ ( $10^{16} \text{cm}^{-2}$ )	$\chi$ ( $10^{-8}$ )	$v_{\text{LSR}}^{\text{a}}$ ( $\text{km s}^{-1}$ )	$\Delta v^{\text{a}}$ ( $\text{km s}^{-1}$ )	$T_{\text{rot}}$ (K)	$N$ ( $10^{16} \text{cm}^{-2}$ )	$\chi$ ( $10^{-8}$ )
C <sub>2</sub> H <sub>5</sub> OCHO	6.8±0.1	3.0±0.1	122±34	0.9±0.3	0.19±0.06	7.2±0.2	2.2±0.1	103±13	0.6±0.3	0.3±0.1
CH <sub>3</sub> OCHO	7.3±0.1	3.2±0.1	135±5	70.0±26.0	15±5	7.1±0.1	2.5±0.2	93±5	85.0±40.0	42±20
C <sub>2</sub> H <sub>5</sub> OH	7.1±0.1	3.5±0.1	144±13	12.9±4.8	2.7±1.0	7.7±0.1	2.5±0.1	111±15	2.0±0.5	1.0±0.3
t-HCOOH	6.7±0.1	4.0±0.2	120±16	0.6±0.2	0.13±0.04	...	...	...	...	...

<sup>a</sup>The  $v_{\text{LSR}}$  and  $\Delta v$  toward two positions are the average values from the Gaussian fitting of several completely unblended lines.

Table 2. Parameters of EF, MF and ET from best-fit LTE analysis in three sources (Orion KL, W51 and Sgr B2(N)).

Species	Source	Num. <sup>1</sup>	$E_{\text{u}}$ range (K)	Obs. <sup>2</sup>	$\theta_{\text{s}}^{\text{3}}$ ( $''$ )	$T_{\text{rot}}$ (K)	$N$ ( $10^{16} \text{cm}^{-2}$ )	$\chi$ ( $10^{-8}$ )	reference
EF	Orion KL (hc)	34	152–387	(ALMA)1.''8×1.''3	1.6	122±34	0.9±0.3	0.19±0.06	this work
	Orion KL (cr)	51	170–411	(ALMA)1.''8×1.''3	1.6	103±13	0.6±0.3	0.3±0.1	this work
	Orion KL (cr)	1	276–276	(ALMA)2.''0×1.''5	3.0	100±20	0.2±0.04	...	Tercero et al. (2015)
	Orion KL (cr)	90	...	(IRAM 30m)11''–29''	15.0	150±20	0.045±0.01	...	Tercero et al. (2013)
	W51	46	42–213	(IRAM 30m)10''–27''	2.4	78±10	2.0±0.3	1.0	Rivilla et al. (2017b)
Sgr B2(N)	46	34–253	(IRAM 30m)22''–29''	3.0	100	5.4	0.36	Belloche et al. (2009)	
MF	Orion KL (hc)	350	36–797	(ALMA)1.''8×1.''3	1.6	135±5	70.0±26.0	15±5	this work
	Orion KL (hc)	20	57–312	(SMA+IRAM 30m)5.''0×4.''0	...	126±13	2.7±1.1	2±1	Feng et al. (2015)
	Orion KL (hc)	14	36–618	(PdBI)1.''79×0.''79	...	128±9	16.0±2.0	5.2	Favre et al. (2011)
	Orion KL (cr)	458	23–797	(ALMA)1.''8×1.''3	1.6	93±5	85.1±40.0	42±20	this work
	Orion KL (cr)	1	122–122	(ALMA)2.''0×1.''5	3.0	100±20	24.0±5.0	...	Tercero et al. (2015)
	Orion KL (cr)	27	57–312	(SMA+IRAM 30m)5.''0×4.''0	...	102±5	9.7±2.1	15±3	Feng et al. (2015)
	Orion KL (cr)	12	2–143	(Effelsberg-100m)35''–50''	10	92±14	18±2	47±6	Gong et al. (2015)
	Orion KL (cr)	...	...	(HIFI, IRAM 30m)	10	110	13	33	Crockett et al. (2014)
	Orion KL (cr) <sup>a</sup>	20	36–366	(PdBI)1.''79×0.''79	...	79±2	16.0±1.0	3.1	Favre et al. (2011)
	W51	38	28–365	(IRAM 30m)10''–27''	2.4	112±3	50.1±0.6	25	Rivilla et al. (2017b)
Sgr B2(N)	...	...	(IRAM 30m)22''–29''	4.0	80	45	3.5	Belloche et al. (2009)	
ET	Orion KL (hc)	186	24–672	(ALMA)1.''8×1.''3	1.6	144±13	12.9±4.8	2.7±1.0	this work
	Orion KL (hc)	5	86–263	(SMA+IRAM 30m)5.''0×4.''0	...	137±33	0.8±0.5	0.6±0.5	Feng et al. (2015)
	Orion KL (hc)	1	316–316	(ALMA)2.''0×1.''5	3.0	100±20	6.0	...	Tercero et al. (2015)
	Orion KL (cr)	162	24–548	(ALMA)1.''8×1.''3	1.6	127±17	2.0±0.5	1.0±0.3	this work
	Orion KL (cr)	5	86–263	(SMA+IRAM 30m)5.''0×4.''0	...	68±11	0.6	0.9±0.5	Feng et al. (2015)
	Orion KL (cr)	...	...	(HIFI, IRAM 30m)	10	110	0.7	1.7	Crockett et al. (2014)
	W51	14	35–327	(IRAM 30m)10''–27''	2.4	95±3	15.8±0.4	7.9	Rivilla et al. (2017b)
Sgr B2(N)	...	...	(IRAM 30m)22''–29''	3.0	100	84	5.7	Belloche et al. (2009)	

<sup>a</sup>toward the 7.6 km s<sup>−1</sup> component for the compact ridge

Note. — "hc" and "cr" indicate hot core and compact ridge, respectively. <sup>1</sup> Number of identified lines. <sup>2</sup> information of observations, including telescope name, synthesized beam size for interferometric observations and HPBW beam size for single-dish observations. <sup>3</sup> source size for modeling. The "..." in  $\theta_{\text{s}}$  means that they derived column density and rotational temperature by rotation temperature diagram (RTD) method.

Table 3. Molecular column density ratios toward Orion KL in different works.

	[MF/EF]		[MF/ET]		
	this work	Tercero et al. (2015)	this work	Feng et al. (2015)	Crockett et al. (2014)
hot core-SW	$79 \pm 36$	–	$6 \pm 3$	$4 \pm 3$	–
compact ridge	$140 \pm 81$	$\simeq 120$	$42 \pm 24$	$17 \pm 12$	20

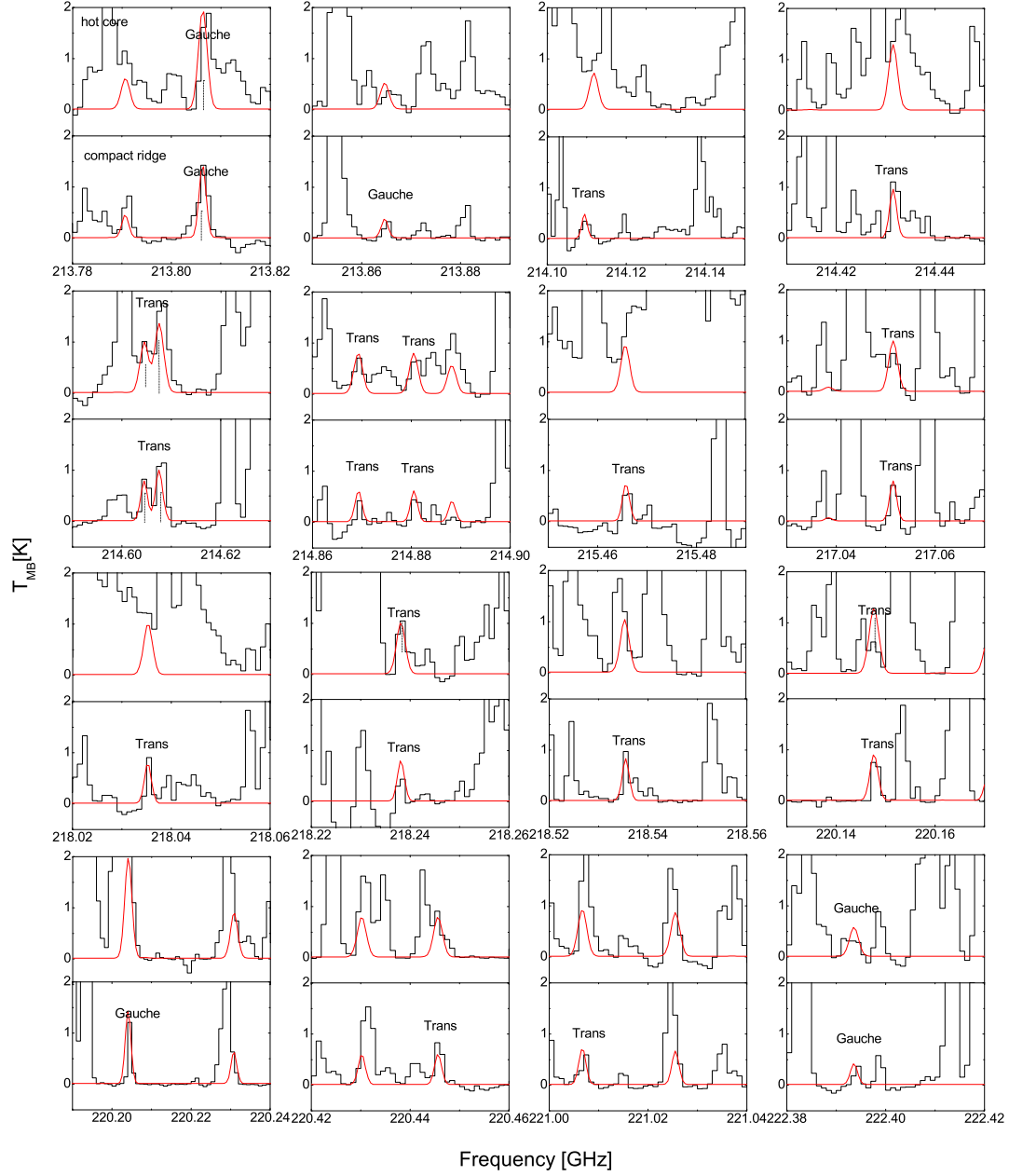


Fig. 1.— Unblended or slightly blended transitions of the *trans* and *gauche* conformers of FF ( $\text{C}_2\text{H}_2\text{OCHO}$ ) from transitions 213 807 GHz to 246 129 GHz toward the hot core-SW

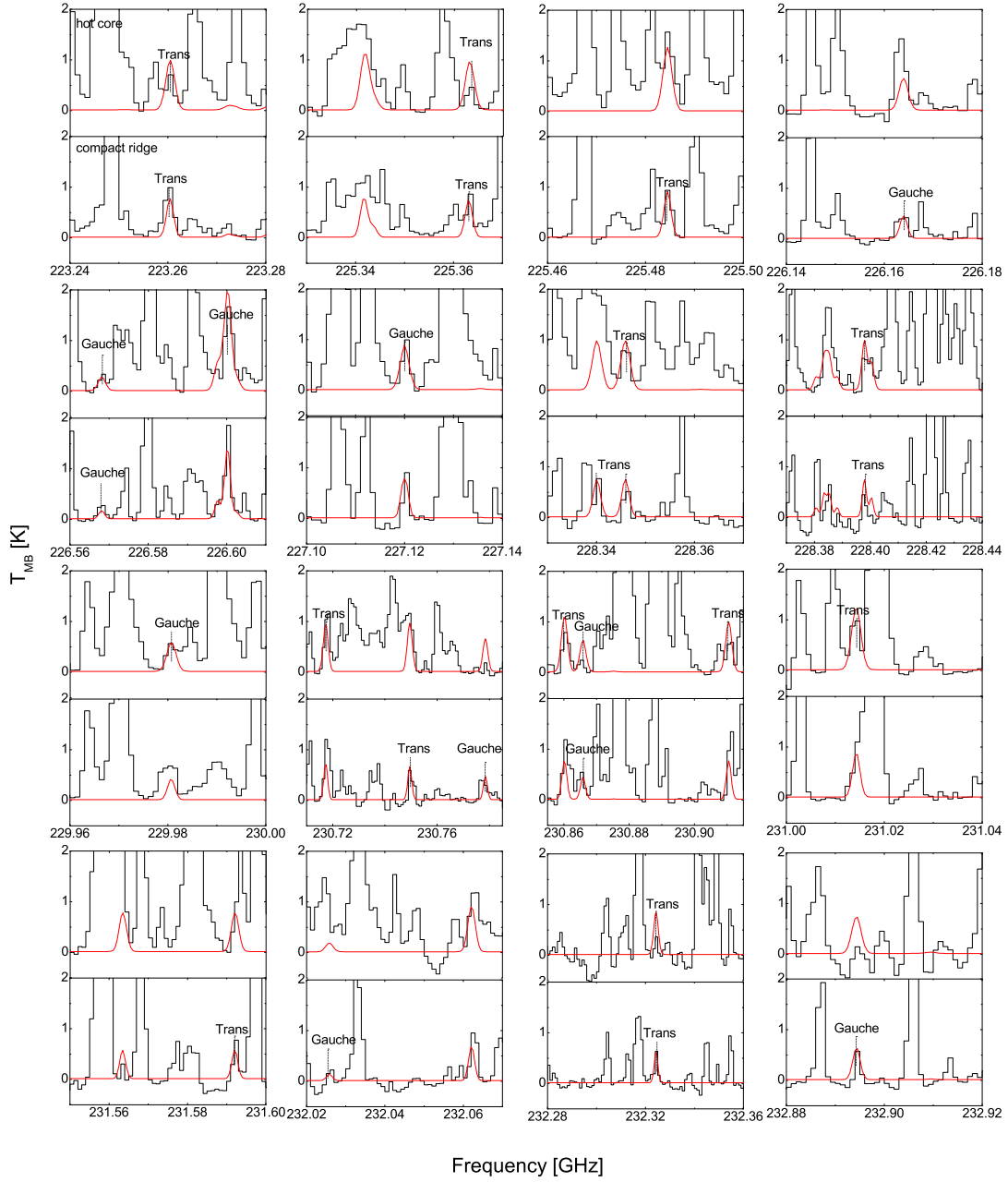


Fig. 1.— Continued.

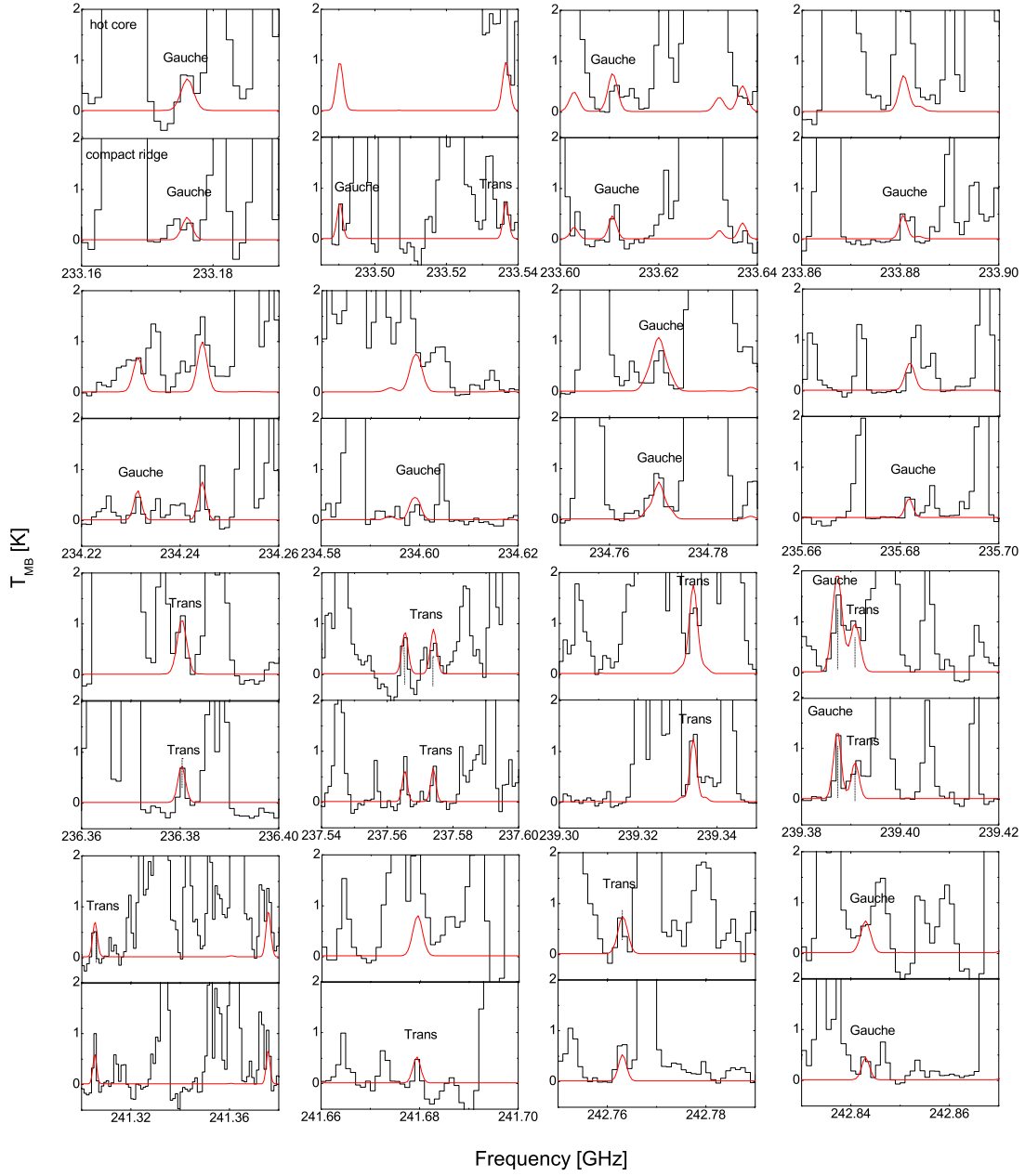


Fig. 1.— Continued.

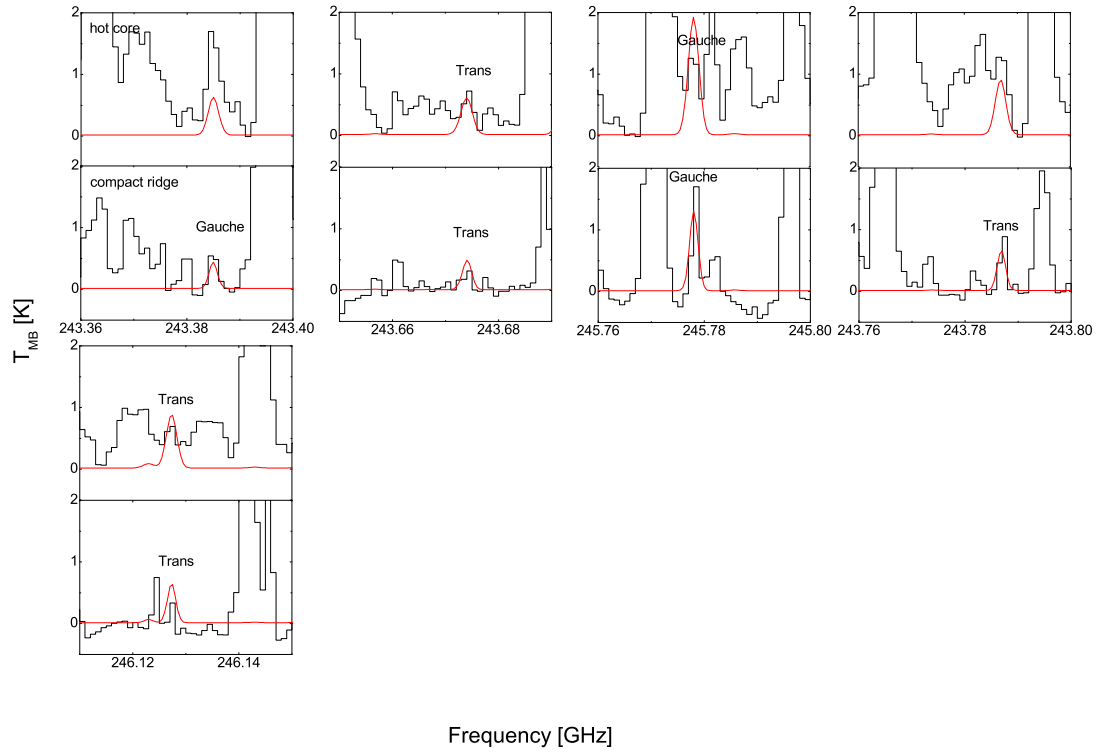


Fig. 1.— Continued.

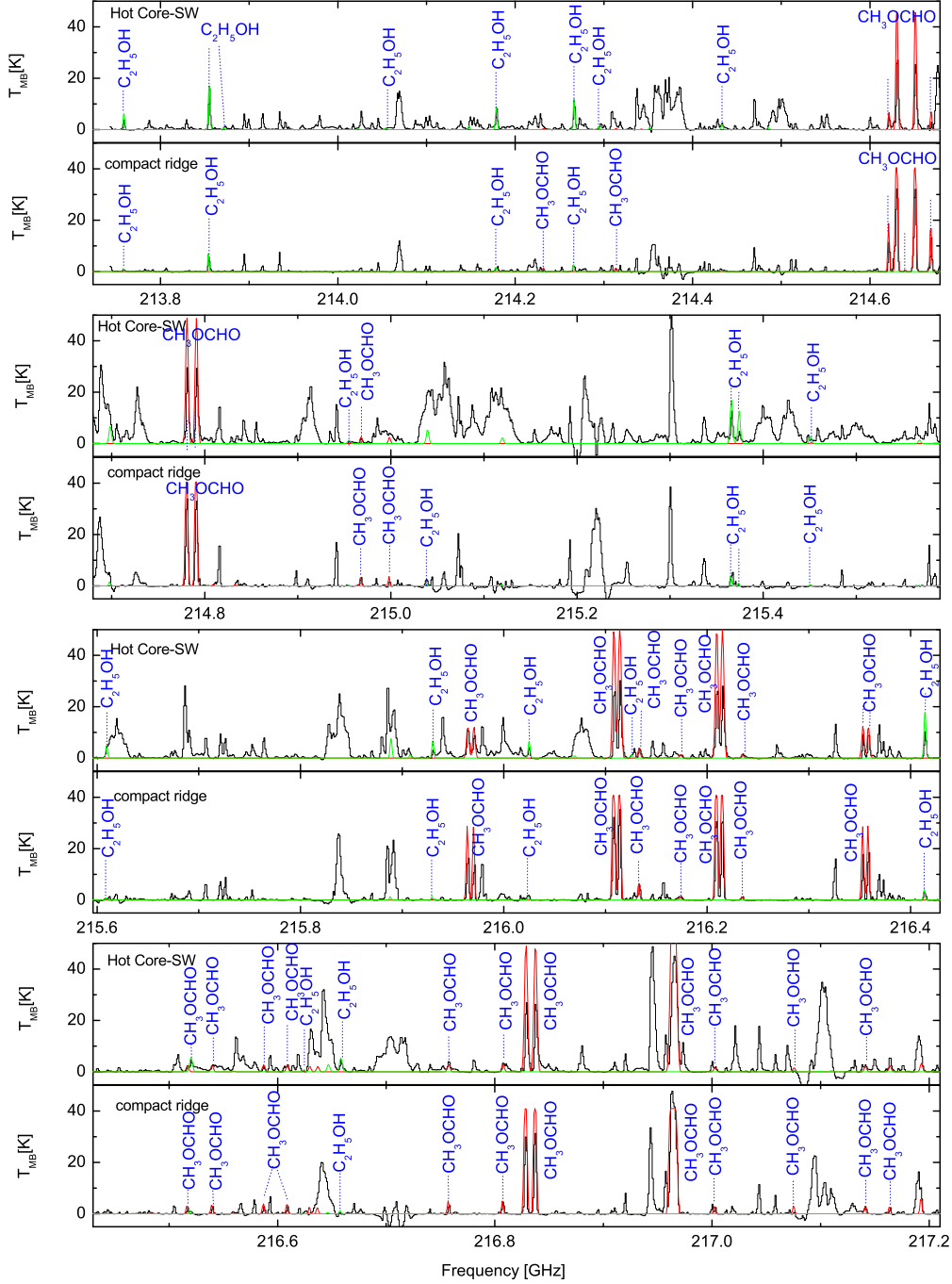


Fig. 2.— Spectra of ET and MF detected in the Orion KL from 213 GHz to 217 GHz. Each panel consists of two plots: the top and bottom plots show the spectrum from the hot core and the compact ridge, respectively. The black curve is the observed spectra, and red curve (MF) and green curve (ET) indicate the simulated LTE spectra.



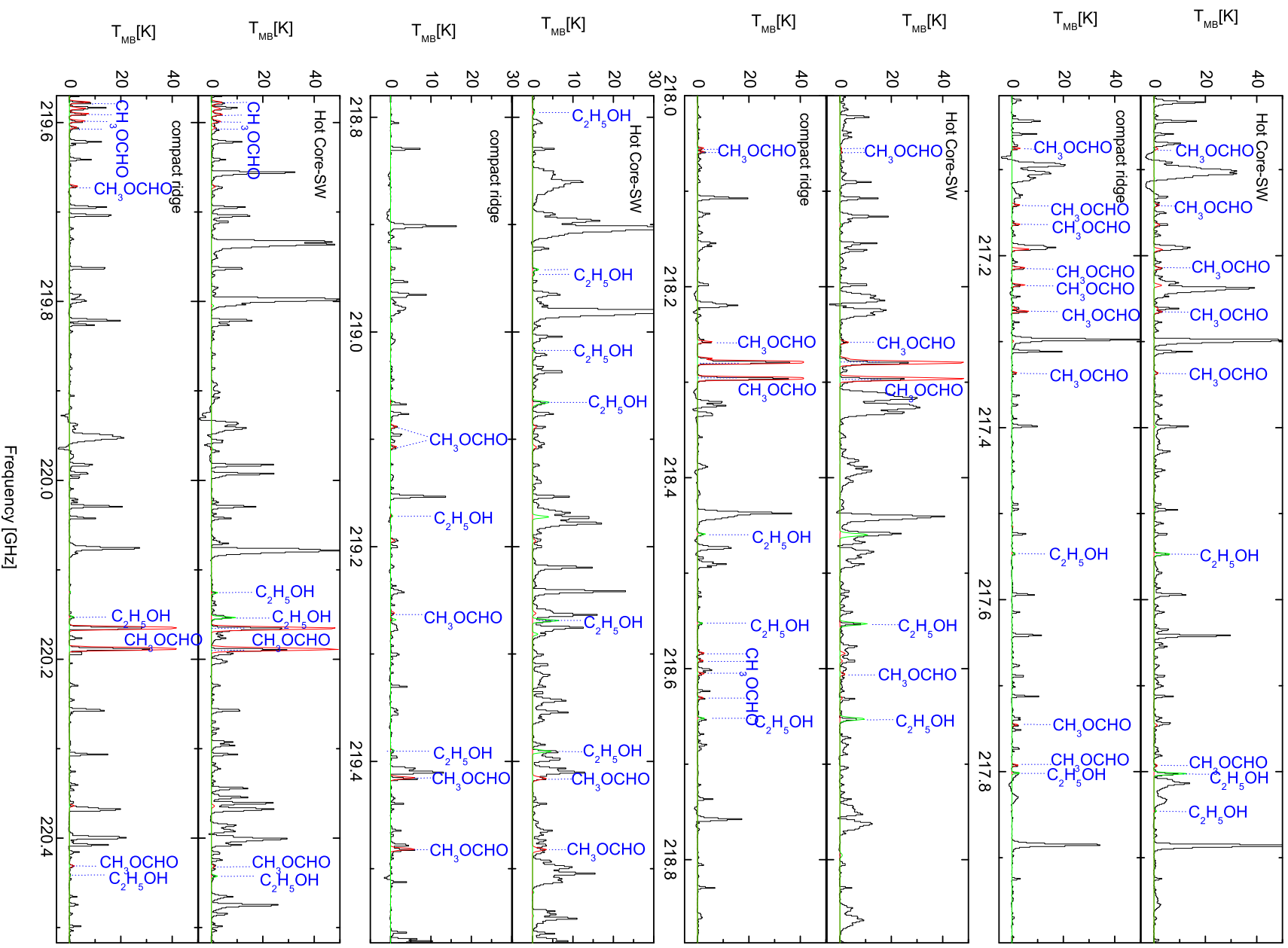


Fig. 2. — continued.

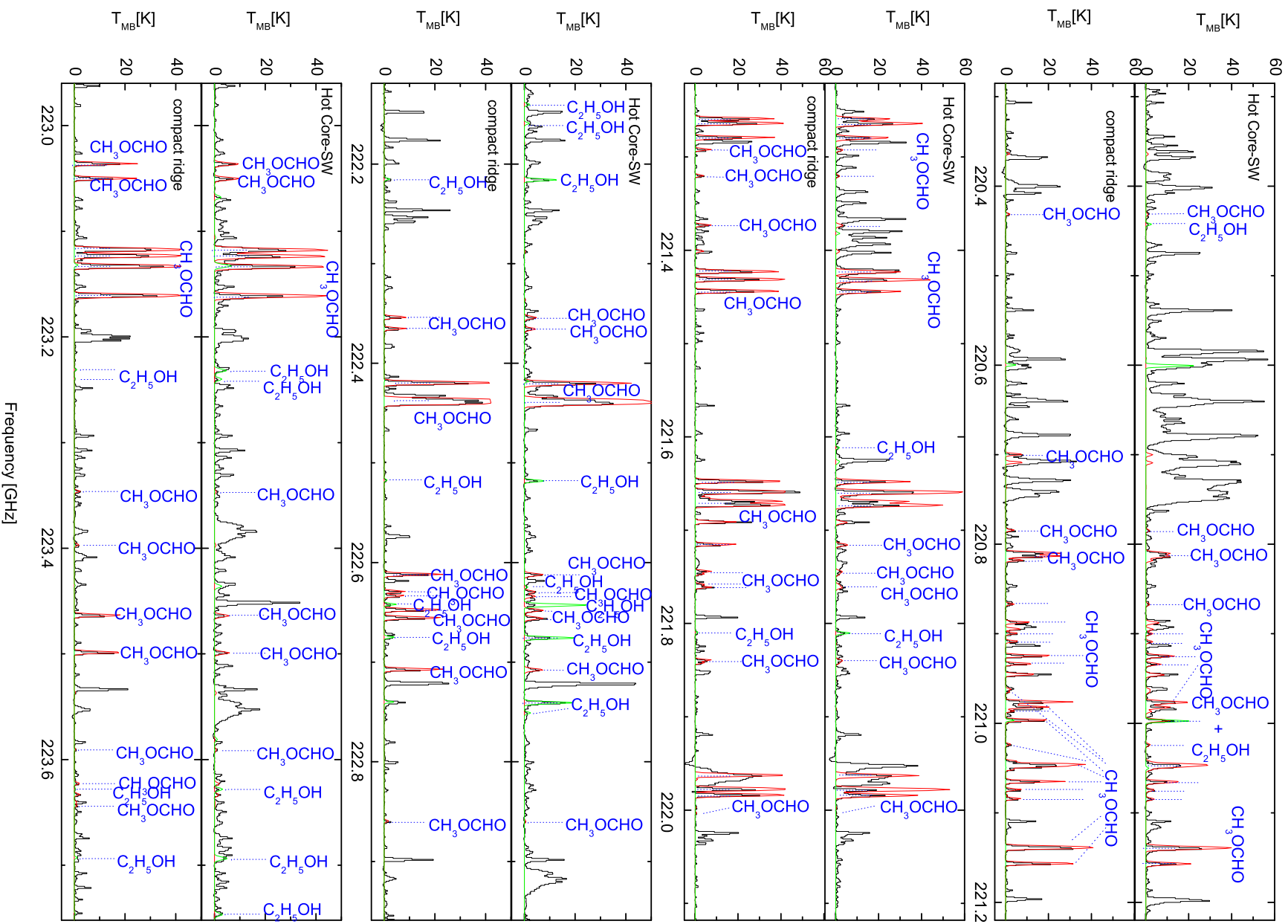


Fig. 2. — continued.

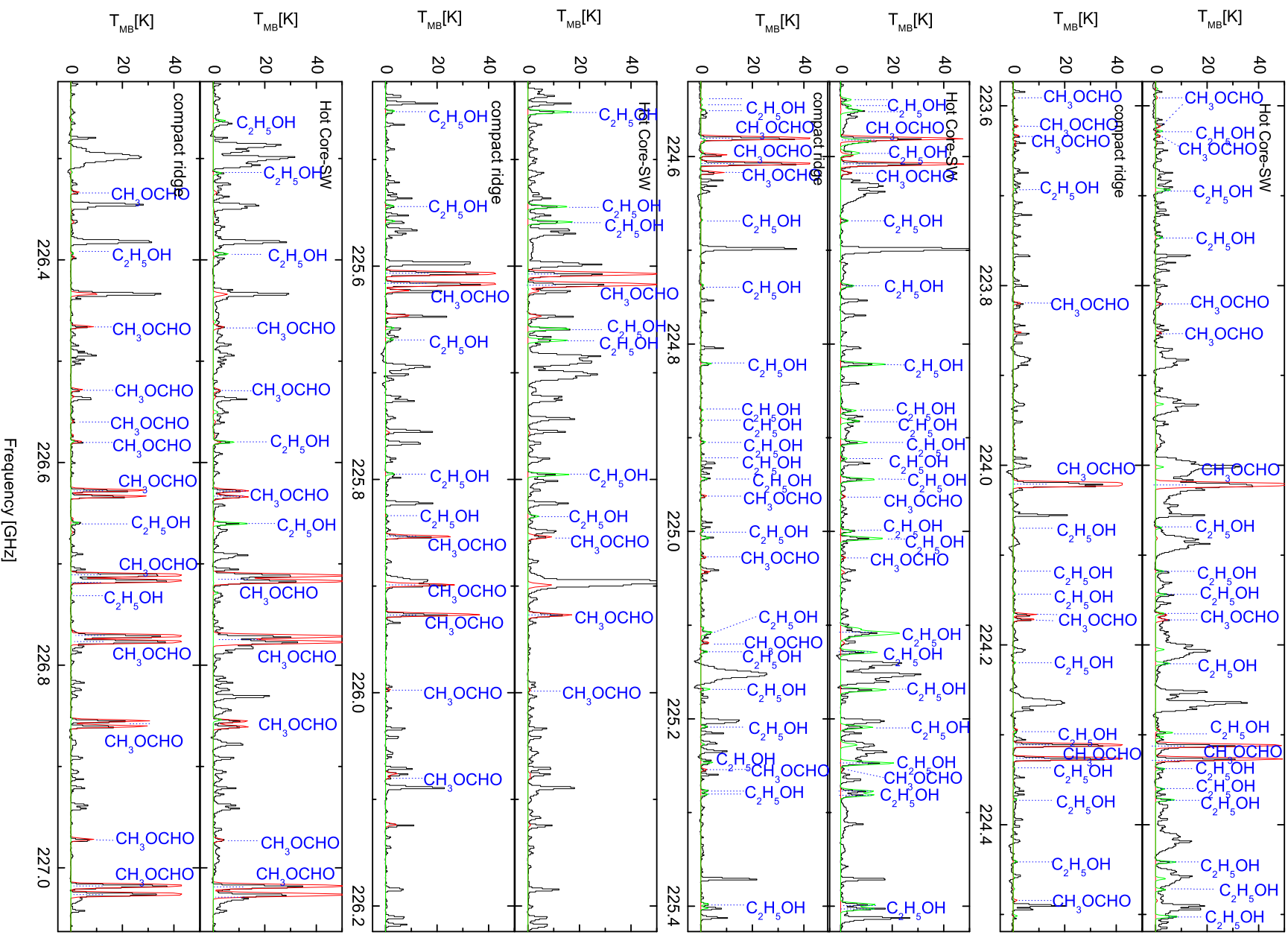


Fig. 2. — continued.



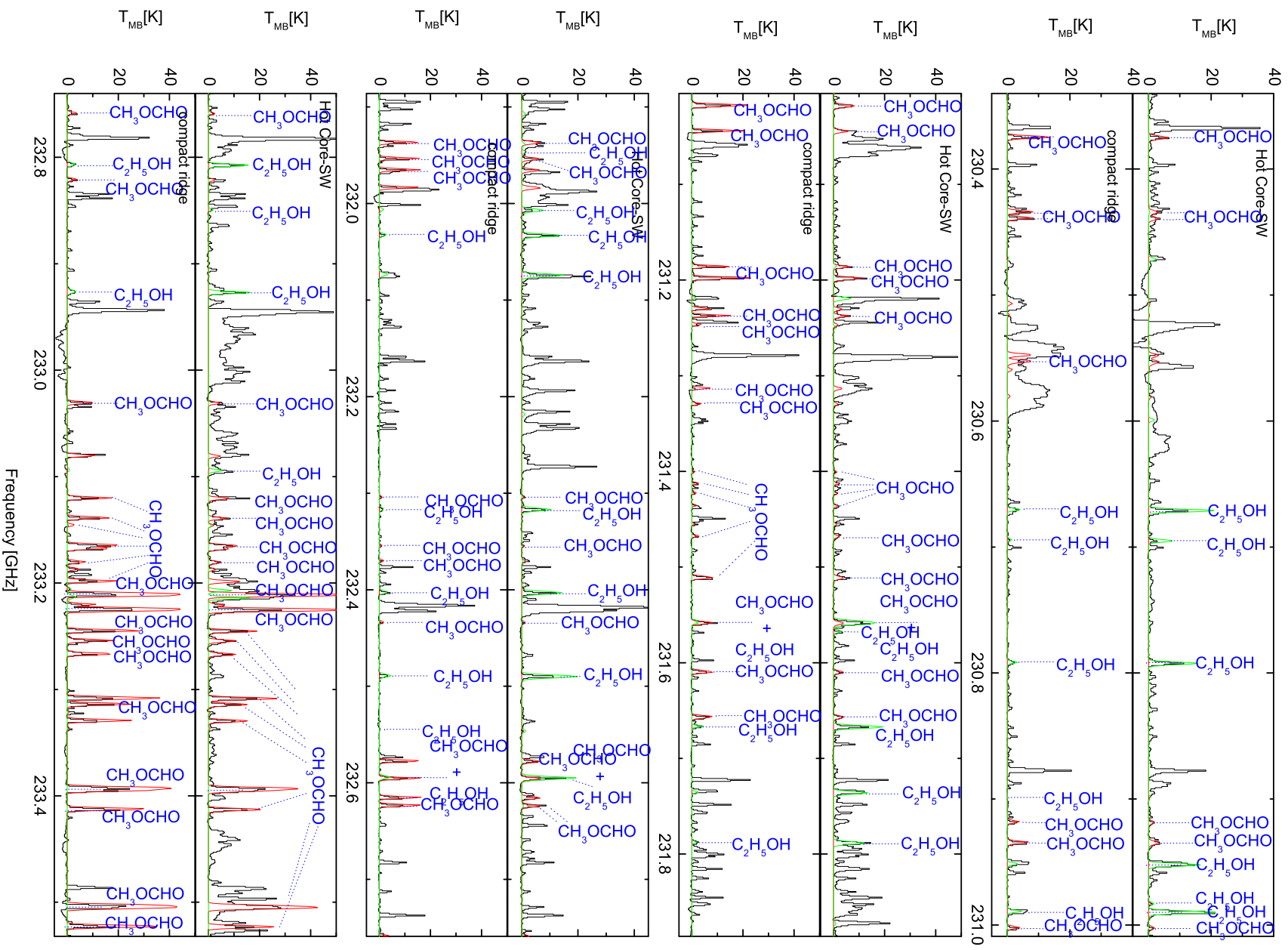


Fig. 2. — continued.



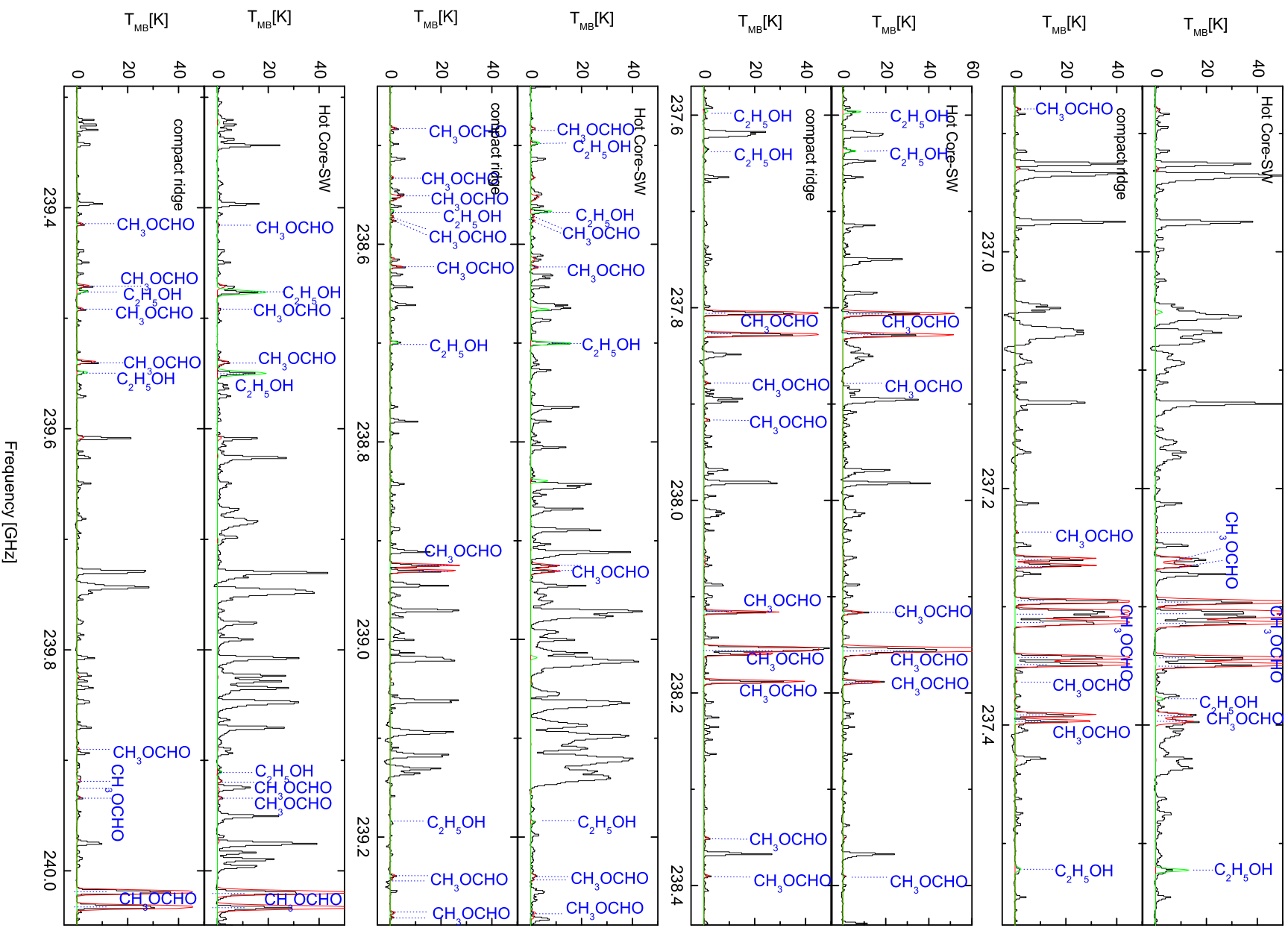


Fig. 2. — continued.





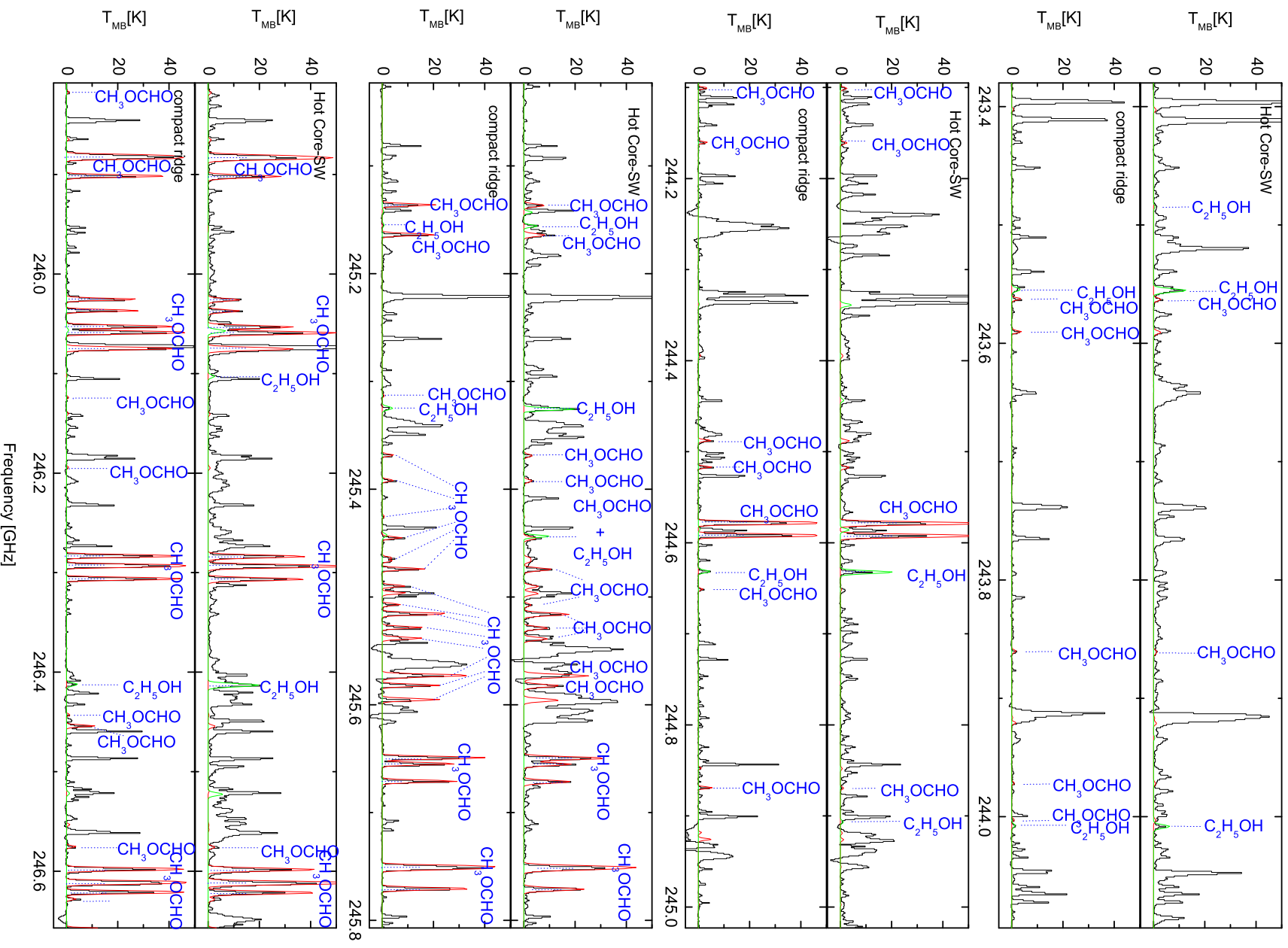


Fig. 2. — continued.

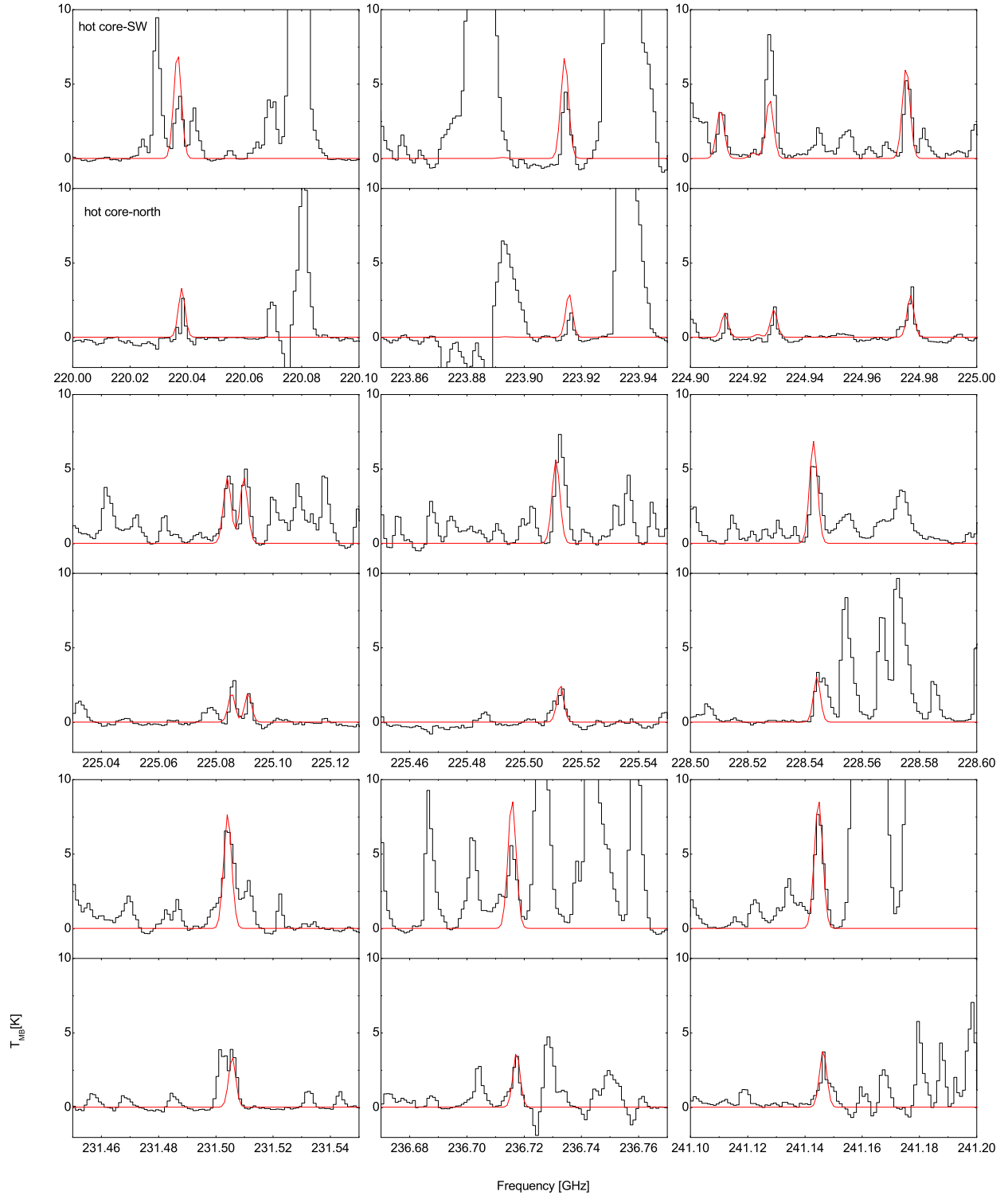


Fig. 3.— Spectra of twelve transitions of t-HCOOH toward the hot core-SW and hot core-N. The black curve is the observed spectra, and red curve indicates the simulated LTE spectra.

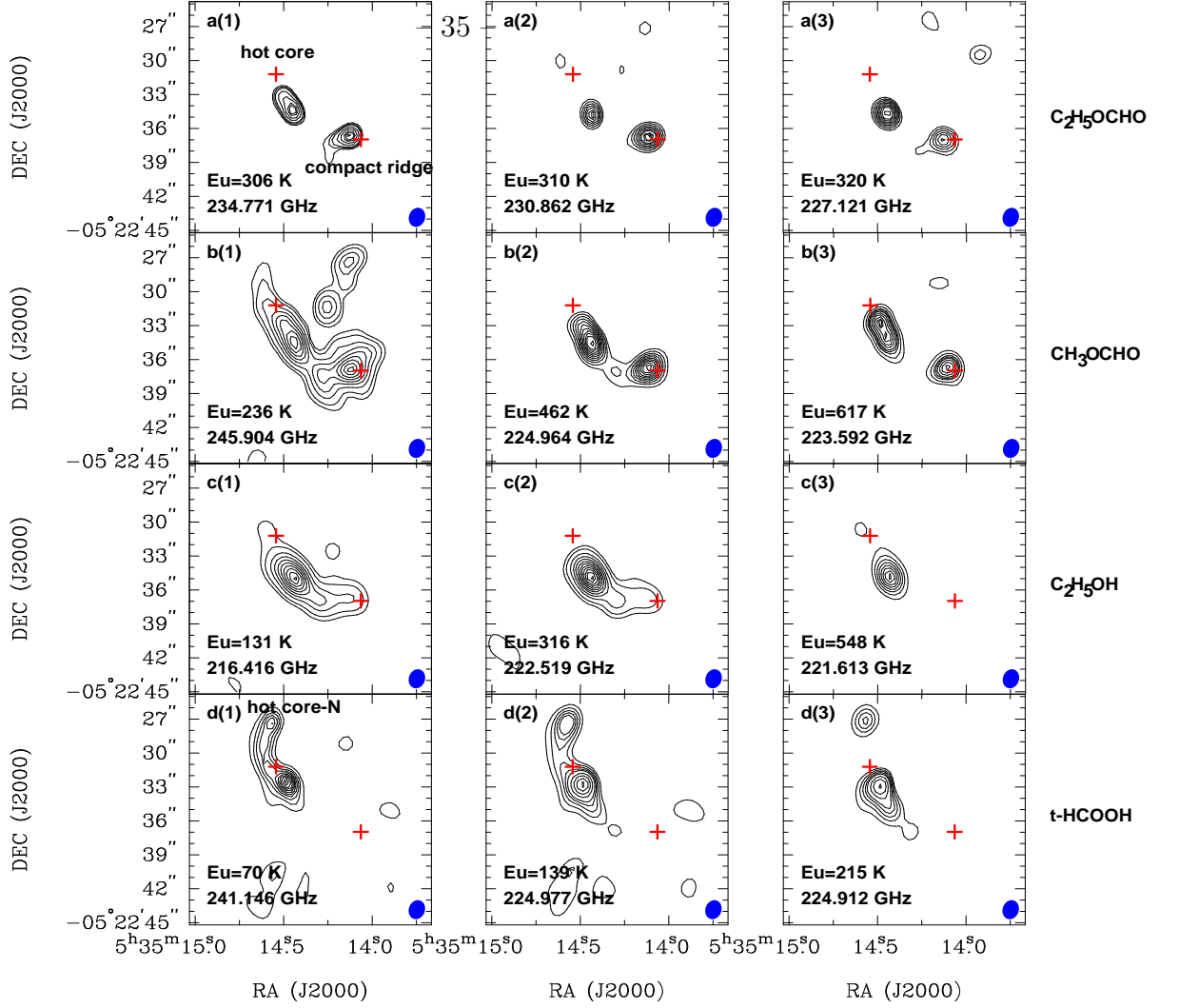


Fig. 4.— The velocity integrated intensity maps of EF (panel a), MF (panel b), ET (panel c) and  $t-HCOOH$  (panel d) at different upper level energies. The upper state energy and frequency are indicated on each plot. The synthesized beam is shown in the bottom right corner. The contour levels are: a(1) (5, 6, 7, 9, 10, 11, 12, 12.8)  $\times 0.02$  Jy beam $^{-1}$  km s $^{-1}$ , a(2) (5, 7, 9, 11, 13, 15, 16.5, 19, 20, 21)  $\times 0.007$  Jy beam $^{-1}$  km s $^{-1}$ , a(3) (5, 7, 9, 11, 13, 15, 17, 19, 22)  $\times 0.008$  Jy beam $^{-1}$  km s $^{-1}$ , b(1) (5, 10, 20, 30, 40, 50, 60, 70, 78)  $\times 0.095$  Jy beam $^{-1}$  km s $^{-1}$ , b(2) (5, 8, 11, 14, 17, 20, 23, 26, 29, 32, 36)  $\times 0.014$  Jy beam $^{-1}$  km s $^{-1}$ , b(3) (5, 8, 11, 13, 15, 18, 21, 24, 27)  $\times 0.01$  Jy beam $^{-1}$  km s $^{-1}$ , c(1) (5, 10, 20, 30, 40, 50, 60, 70, 80, 87)  $\times 0.05$  Jy beam $^{-1}$  km s $^{-1}$ , c(2) (5, 10, 20, 30, 40, 50, 60, 70, 80, 90, 100, 108)  $\times 0.018$  Jy beam $^{-1}$  km s $^{-1}$ , c(3) (5, 9, 13, 17, 21, 25, 29, 32.5)  $\times 0.018$  Jy beam $^{-1}$  km s $^{-1}$ , d(1) (5, 10, 15, 20, 25, 30, 35, 40, 45, 50)  $\times 0.045$  Jy beam $^{-1}$  km s $^{-1}$ , d(2) (5, 10, 15, 20, 25, 35, 45, 55, 65)  $\times 0.028$  Jy beam $^{-1}$  km s $^{-1}$ , and d(3) (5, 10, 15, 20, 25, 35, 45, 57)  $\times 0.02$  Jy beam $^{-1}$  km s $^{-1}$ . The cross symbols mark the continuum peak positions of hot core and compact ridge. The coordinates of two continuum peaks are presented in Section 3.2.

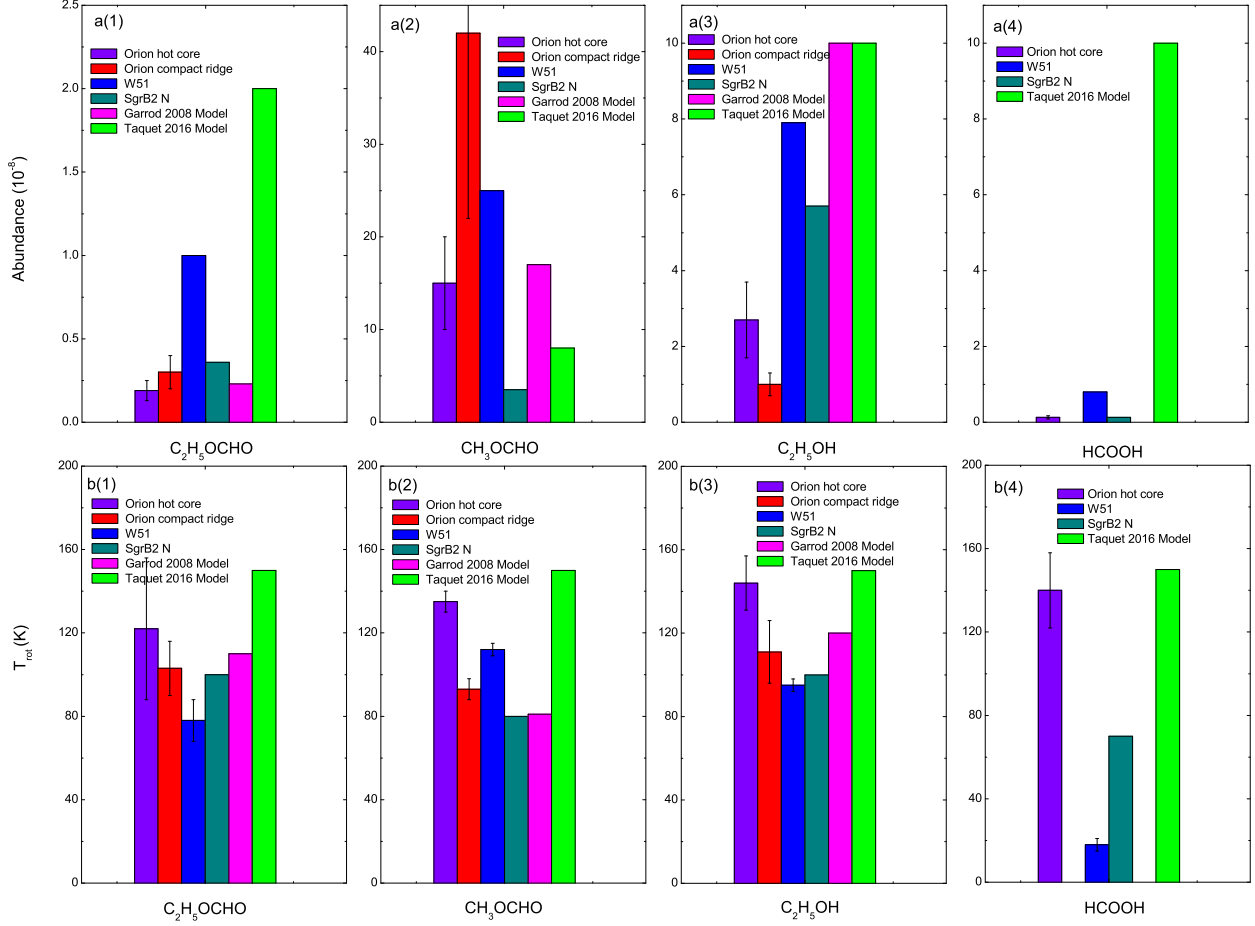


Fig. 5.— The abundances (top panels) and rotational temperatures (bottom panels) of each molecule (EF, MF, ET and HCOOH) derived in different regions (Orion KL, W51 and Sgr B2(N)), and the theoretical values from the grain-surface model by Garrod et al. (2008) and gas-phase model by Taquet et al. (2016). The theoretical abundances of around  $2 \times 10^{-8}$  for EF,  $8 \times 10^{-8}$  for MF,  $1 \times 10^{-7}$  for ET and a few  $10^{-7}$  for HCOOH, in a reasonable timescale for hot core sources of  $5 \times 10^4$  yr, from Taquet et al. (2016) are the values obtained by considering PT reactions. For the estimated abundances and temperatures of EF, MF and ET in grain-surface model, the values are from Belloche et al. (2009) (in Basic model, see their Table 15), which uses Garrod et al. (2008) chemical network.

Table A.1. Selected unblended transitions of the *Trans* and *Gauche* conformers of EF observed with the ALMA.

Rest Frequency (GHz)	Transition	$S_{ij}\mu^2$ (Debye <sup>2</sup> )	E <sub>u</sub> (K)	hot core-SW				compact ridge				$\sigma$ (K)
				$v_{\text{LSR}}$ (km s <sup>-1</sup> )	$\Delta V$ (km s <sup>-1</sup> )	$I_{\text{p}}$ (K)	Detection Level	$v_{\text{LSR}}$ (km s <sup>-1</sup> )	$\Delta V$ (km s <sup>-1</sup> )	$I_{\text{p}}$ (K)	Detection Level	
<i>Trans</i> conformer												
214.11074	39(13, 26) – 38(13, 25)	118.64	327			B		7.2±0.1	1.7±0.3	0.42±0.07	7σ	0.06
214.43282	39(9, 31) – 38(9, 30)	126.36	264			B		7.0±0.1	2.0±0.1	1.09±0.05	23σ	0.05
214.43284	39(9, 30) – 38(9, 29)	126.36	264									
214.60560	39(4, 36) – 38(4, 35)	131.98	218			B		7.0±0.1	2.0±0.1	0.65±0.05	11σ	0.06
214.60858	39(8, 32) – 38(8, 31)	127.85	251	6.5±0.1	4.2±0.1	1.40±0.04	25σ	6.9±0.1	2.5±0.1	1.15±0.05	20σ	0.06
214.60911	39(8, 31) – 38(8, 30)	127.85	251									
214.87062	39(7, 33) – 38(7, 32)	129.18	241	7.3±0.2	4.0±0.4	0.78±0.05	14σ	7.4±0.1	1.7±0.3	0.59±0.06	10σ	0.06
214.88185	39(7, 32) – 38(7, 31)	129.17	241	6.8±0.1	3.7±0.3	0.80±0.04	14σ	7.2±0.1	2.1±0.2	0.61±0.06	11σ	0.06
215.46693	39(5, 35) – 38(5, 34)	131.27	224			B		7.1±0.1	1.7±0.1	0.84±0.06	15σ	0.06
217.05267	40(3, 38) – 39(3, 37)	135.84	222	7.1±0.1	2.5±0.3	0.86±0.6	13σ	7.0±0.1	1.8±0.2	0.78±0.07	12σ	0.07
218.03650	41(2, 40) – 40(2, 39)	139.64	225			B		7.2±0.1	1.7±0.2	0.81±0.09	11σ	0.08
218.23915	40(2, 38) – 39(2, 37)	135.92	222	6.9±0.1	3.0±0.2	1.18±0.07	14σ	7.1±0.1	1.8±0.3	0.66±0.09	8σ	0.09
218.53650	39(3, 36) – 38(3, 35)	132.54	216			PB		6.9±0.1	1.7±0.1	1.13±0.07	17σ	0.07
220.14861	40(8, 33) – 39(8, 32)	131.42	262			B		7.0±0.1	2.0±0.1	0.86±0.05	18σ	0.05
220.14940	40(8, 32) – 39(8, 31)	131.42	262									
220.44705	40(7, 33) – 39(7, 32)	132.70	252			PB		7.1±0.1	2.3±0.2	0.84±0.06	15σ	0.06
221.00793	40(5, 36) – 39(5, 35)	134.73	235			B		7.0±0.1	1.8±0.2	0.82±0.07	12σ	0.07
223.26160	42(1, 41) – 41(1, 40)	143.07	236	7.3±0.1	2.7±0.3	0.72±0.04	15σ			PB		0.05
225.36427	41(4, 38) – 40(4, 37)	138.86	239	7.0±0.2	2.1±0.5	0.40±0.06	6σ	7.0±0.1	1.7±0.2	0.87±0.07	13σ	0.07
225.48591	41(9, 33) – 40(9, 32)	133.57	285			B		7.1±0.1	2.0±0.1	1.13±0.05	24σ	0.05
225.48595	41(9, 32) – 40(9, 31)	133.57	285									
228.34140	43(2, 42) – 42(2, 41)	146.49	247			B		7.2±0.1	1.9±0.1	0.78±0.05	17σ	0.05
228.34705	42(2, 40) – 41(2, 39)	142.72	243	7.2±0.1	2.7±0.2	0.67±0.04	14σ	7.0±0.1	1.5±0.1	0.66±0.05	14σ	0.05
228.39919	43(1, 42) – 42(1, 41)	146.48	247	6.0±0.1	4.2±0.3	0.56±0.09	12σ	7.2±0.1	1.4±0.1	0.47±0.05	10σ	0.05
230.71849	42(4, 39) – 41(4, 38)	142.31	250	6.3±0.1	3.3±0.1	1.06±0.04	22σ			PB		0.05
230.75105	42(11, 32) – 41(11, 31)	133.90	325			B		7.2±0.2	2.8±0.6	0.59±0.05	10σ	0.06
230.861687	42(10, 33) – 41(10, 32)	135.61	310									
230.861689	42(10, 32) – 41(10, 31)	135.61	310	6.4±0.1	3.8±0.3	0.79±0.03	21σ			B		0.04
230.91185	41(4, 37) – 40(4, 36)	139.12	241	7.1±0.1	2.3±0.2	0.60±0.05	13σ			B		0.05
231.01571	42(9, 24)–41(9, 33)	137.16	296	7.9±0.1	2.3±0.1	1.01±0.05	21σ			B		0.05
231.59355	42(7, 35) – 41(7, 34)	139.74	274			B		7.5±0.1	1.9±0.3	0.58±0.06	10σ	0.06
232.32584	42(6, 36) – 41(6, 35)	140.82	265	7.9±0.2	1.8±0.3	0.28±0.05	6σ	7.7±0.1	1.9±0.2	0.63±0.05	13σ	0.05
233.53793	44(1, 43) – 43(1, 42)	149.90	258			B		7.1±0.1	1.8±0.2	0.70±0.08	9σ	0.08
236.381882	43(10, 34) – 42(10, 33)	139.22	321	8.0±0.1	2.7±0.2	1.19±0.07	16σ	7.6±0.1	1.6±0.3	0.68±0.11	9σ	0.08
236.381885	43(10, 33) – 42(10, 32)	139.22	321									
237.56673	43(6, 38) – 42(6, 37)	144.31	276	7.8±0.1	1.5±0.2	0.70±0.07	12σ			PB		0.06
237.57528	43(5, 39) – 42(5, 38)	145.14	268	7.0±0.1	2.9±0.3	0.53±0.04	11σ	7.3±0.1	1.9±0.1	0.80±0.05	17σ	0.05
239.33504	46(1, 46) – 45(1, 45)	157.20	272									
239.33580	46(0, 46) – 45(0, 45)	157.20	272			PB		7.1±0.1	2.3±0.1	1.32±0.06	20σ	0.07
239.39187	43(3, 40) – 42(3, 39)	146.09	260	7.2±0.1	3.0±0.2	0.99±0.05	15σ	6.9±0.1	1.8±0.1	0.81±0.07	12σ	0.07
241.30348	32(4, 28) – 32(1, 31)	0.30	152	3.8±0.1	1.7±0.2	0.42±0.05	9σ			PB		0.05
241.68105	44(12, 32) – 43(12, 31)	139.38	364			B		7.8±0.2	1.5±0.3	0.35±0.06	6σ	0.06
242.76463	44(7, 37) – 43(7, 36)	146.78	297	7.8±0.1	2.2±0.1	0.82±0.07	14σ			PB		0.06
243.56050	45(2, 43) – 44(2, 42)	152.99	278			B		7.0±0.1	2.2±0.1	0.128±0.006	19σ	0.007
243.67449	46(1, 45) – 45(2, 44)	16.76	281	6.1±0.1	2.9±0.3	0.70±0.04	15σ	6.4±0.1	2.1±0.3	0.32±0.05	7σ	0.05
243.78836	46(2, 45) – 45(2, 44)	156.77	281			B		7.3±0.1	1.6±0.2	0.72±0.05	15σ	0.05

Table A.1—Continued

Rest Frequency (GHz)	Transition	$S_{ij}\mu^2$ (Debye <sup>2</sup> )	Eu (K)	hot core-SW				compact ridge				$\sigma$ (K)
				$v_{\text{LSR}}$ (km s <sup>-1</sup> )	$\Delta V$ (km s <sup>-1</sup> )	$I_{\text{p}}$ (K)	Detection Level	$v_{\text{LSR}}$ (km s <sup>-1</sup> )	$\Delta V$ (km s <sup>-1</sup> )	$I_{\text{p}}$ (K)	Detection Level	
246.12899	44(5, 39) – 43(5, 38)	148.70	281	7.5±0.1	3.5±0.2	0.70±0.05	15 $\sigma$	7.7±1.3	1.3±0.9	0.35±0.09	7 $\sigma$	0.05
<i>Gauche</i> conformer												
213.807356	33(1, 33) – 32(1, 32)	68.12	272	6.0±0.1	3.7±0.1	1.76±0.05	31 $\sigma$	6.9±0.1	2.4±0.1	1.32±0.04	23 $\sigma$	0.06
213.807357	33(0, 33) – 32(0, 32)	68.12	272									
213.86579	30(9, 22) – 29(9, 21)	56.64	279	5.8±0.3	3.4±0.8	0.28±0.06	5 $\sigma$	7.0±0.2	1.6±0.4	0.30±0.05	6 $\sigma$	0.06
220.2051952	34(1, 34) – 33(1, 33)	70.19	283									
220.2051959	34(0, 34) – 33(0, 33)	70.19	283					7.0±0.1	1.9±0.1	1.21±0.05	21 $\sigma$	0.06
222.39509	31(8, 23) – 30(8, 22)	60.04	285	7.2±0.2	3.0±0.5	0.29±0.04	6 $\sigma$	7.1±0.1	1.7±0.2	0.46±0.05	10 $\sigma$	0.05
226.16523	33(4, 30) – 32(4, 29)	66.58	289					7.2±0.1	2.1±0.2	0.41±0.04	11 $\sigma$	0.04
226.56953	32(21, 11) – 31(21, 10)	37.80	411	7.0±0.3	2.1±0.6	0.21±0.04	5 $\sigma$	7.1±0.2	2.1±0.5	0.21±0.04	5 $\sigma$	0.04
226.6013827	35(1, 35) – 34(1, 34)	72.27	294									
226.6013832	35(0, 35) – 34(0, 34)	72.27	294	6.5±0.1	3.4±0.1	1.75±0.04	37 $\sigma$					0.05
227.12119	32(12, 21) – 31(12, 20)	57.07	320	6.7±0.1	2.5±0.2	1.10±0.04	23 $\sigma$					0.05
227.12122	32(12, 20) – 31(12, 19)	57.07	320									
229.98245	32(8, 24) – 31(8, 23)	62.25	296	7.9±0.1	2.6±0.3	0.51±0.05	11 $\sigma$					0.05
230.77940	32(5, 27) – 31(5, 26)	64.13	287		...		≤3 $\sigma$	7.1±0.2	2.6±0.4	0.30±0.04	8 $\sigma$	0.04
230.86702	33(4, 29) – 32(4, 28)	66.21	294	8.0±0.4	2.1±0.8	0.16±0.05	3 $\sigma$	8.1±0.1	2.5±0.3	0.45±0.05	10 $\sigma$	0.05
232.02663	33(5, 29) – 32(4, 28)	18.18	294					6.8±0.4	1.8±0.7	0.20±0.07	4 $\sigma$	0.06
232.89572	12(11, 2) – 11(11, 1)	25.44	170		...		<3 $\sigma$	7.4±0.1	1.7±0.2	0.57±0.04	15 $\sigma$	0.04
233.17815	32(7, 25) – 31(7, 24)	63.36	292	8.1±0.3	3.6±0.3	0.60±0.05	11 $\sigma$	8.2±0.2	2.0±0.4	0.33±0.06	6 $\sigma$	0.06
233.61188	33(18, 15) – 32(18, 14)	48.10	387	6.5±0.2	2.2±0.4	0.42±0.06	6 $\sigma$	6.9±0.1	1.8±0.2	0.57±0.07	9 $\sigma$	0.07
233.61188	33(18, 16) – 32(18, 15)	48.10	387									
233.88192	33(14, 19) – 32(14, 18)	56.15	347					6.7±0.2	2.7±0.4	0.37±0.04	8 $\sigma$	0.05
234.23279	14(10, 5) – 13(10, 4)	23.33	171					7.3±0.1	2.0±0.3	0.31±0.03	8 $\sigma$	0.04
234.59985	33(11, 23) – 32(11, 22)	60.86	324									
234.60109	33(11, 22) – 32(11, 21)	60.86	324					6.2±0.2	2.0±0.5	0.18±0.04	5 $\sigma$	0.04
234.77083	35(3, 33) – 34(3, 32)	71.17	306	6.2±0.1	2.8±0.3	0.85±0.06	13 $\sigma$					0.07
234.77186	35(2, 33) – 34(2, 32)	71.17	306									
235.68320	33(9, 25) – 32(9, 24)	63.38	312					7.2±0.2	2.1±0.4	0.36±0.06	13 $\sigma$	0.06
239.38860	37(1, 37) – 36(1, 36)	76.43	316	7.0±0.1	3.5±0.1	1.57±0.04	28 $\sigma$	7.3±0.1	2.1±0.1	1.27±0.06	22 $\sigma$	0.06
239.38861	37(0, 37) – 36(0, 36)	76.43	316									
242.84401	34(5, 29) – 33(5, 28)	68.08	310					7.0±0.2	1.7±0.4	0.38±0.07	6 $\sigma$	0.07
243.38631	35(4, 31) – 34(4, 30)	70.32	317					7.3±0.1	1.6±0.3	0.44±0.06	9 $\sigma$	0.05
245.7795365	38(1, 38) – 37(1, 37)	78.49	328									
245.7795366	38(0, 38) – 37(0, 37)	78.49	328	8.0±0.1	2.8±0.2	1.29±0.09	17 $\sigma$	7.5±0.1	1.6±0.3	1.73±0.08	23 $\sigma$	0.08

Note. — Abbreviations in the "Detection" column are B: blended; PB: partial blend.

Table A.2. Selected unblended transitions of MF observed with the ALMA.

Rest Frequency	Transition	$S_{ij}\mu^2$	$E_u$	Detection	
				hot core-SW	compact ridge
(GHz)		(Debye <sup>2</sup> )	(K)		
214.23362	13(4, 9) – 13(1, 12) <i>E</i>	0.13	65	B	✓
214.31522	13(4, 9) – 13(1, 12) <i>A</i>	0.13	65	B	✓
214.62285	10(4, 7) – 9(3, 6) <i>E</i>	1.71	43	✓	✓
214.63169	17(5, 12) – 16(5, 11) <i>E</i>	41.28	108	✓	✓
214.65259	17(5, 12) – 16(5, 11) <i>A</i>	41.28	108	✓	✓
214.67036	10(4, 7) – 9(3, 6) <i>A</i>	1.75	43	✓	✓
214.78236	18(3, 16) – 17(3, 15) <i>E</i>	46.05	106	✓	✓
214.79249	18(3, 16) – 17(3, 15) <i>A</i>	45.98	106	✓	✓
214.96936	34(7, 28) – 34(6, 29) <i>E</i>	8.23	388	✓	✓
214.99967	34(7, 28) – 34(6, 29) <i>A</i>	8.34	388	B	✓
215.96593	19(3, 17) – 18(2, 17) <i>E</i>	6.59	109	✓	✓
215.97199	19(1, 18) – 18(2, 17) <i>A</i>	6.59	109	✓	✓
216.10973	19(2, 18) – 18(2, 17) <i>E</i>	49.29	109	✓	✓
216.11549	19(2, 18) – 18(2, 17) <i>A</i>	49.28	109	✓	✓
216.13438	29(9, 20) – 29(6, 23) <i>E</i>	7.68	312	✓	✓
216.17531	39(7, 32) – 39(6, 33) <i>E</i>	9.84	507	✓	✓
216.21086	19(3, 17) – 18(3, 16) <i>E</i>	49.29	109	✓	✓
216.21646	19(1, 18) – 18(1, 17) <i>A</i>	49.29	109	✓	✓
216.23612	39(7, 32) – 39(6, 33) <i>A</i>	9.84	507	✓	✓
216.35465	19(2, 18) – 18(3, 16) <i>E</i>	6.59	109	✓	✓
216.35995	19(2, 18) – 18(1, 17) <i>A</i>	6.58	109	✓	✓
216.51828	34(9, 26) – 34(8, 27) <i>A</i>	9.51	408	✓	✓
216.54009	34(7, 27) – 34(10, 25) <i>E</i>	9.51	408	B	✓
216.58863	33(9, 25) – 33(8, 26) <i>A</i>	9.04	388	✓	✓
216.61044	33(9, 25) – 33(8, 26) <i>E</i>	9.04	388	✓	✓
216.75896	32(6, 27) – 32(5, 28) <i>E</i>	6.88	338	B	✓
216.80896	32(6, 27) – 32(5, 28) <i>A</i>	6.96	338	B	✓
216.83020	18(2, 16) – 17(2, 15) <i>E</i>	46.14	106	✓	✓
216.83885	18(2, 16) – 17(2, 15) <i>A</i>	46.07	106	✓	✓

Table A.2—Continued

Rest Frequency	Transition	$S_{ij}\mu^2$	$E_u$	Detection	
				hot core-SW	compact ridge
(GHz)		(Debye <sup>2</sup> )	(K)		
216.96479	20(1, 20) – 19(1, 19) <i>E</i>	52.71	112	B	B
216.96590	20(1, 20) – 19(1, 19) <i>A</i>	52.82	111	B	B
216.96625	20(0, 20) – 19(0, 19) <i>E</i>	52.81	112	B	B
216.96742	20(0, 20) – 19(0, 19) <i>A</i>	52.83	111	B	B
217.00429	30(4, 26) – 30(4, 27) <i>E</i>	2.62	291	✓	✓
217.07727	30(4, 26) – 30(4, 27) <i>A</i>	2.63	291	✓	✓
217.14275	35(9, 27) – 35(8, 28) <i>A</i>	9.70	429	✓	✓
217.16536	35(9, 27) – 35(8, 28) <i>E</i>	9.70	429	B	✓
217.21584	32(9, 24) – 32(8, 25) <i>A</i>	8.67	368	✓	✓
217.23592	32(9, 24) – 32(8, 25) <i>E</i>	8.67	368	B	✓
217.26668	30(4, 26) – 30(3, 27) <i>A</i>	5.56	291	✓	✓
217.33797	37(10, 27) – 37(9, 28) <i>E</i>	10.41	485	✓	✓
217.51710	8(5, 4) – 8(3, 5) <i>A</i>	0.02	38	B	✓
217.79416	32(6, 27) – 32(4, 28) <i>A</i>	2.98	338	✓	✓
218.05680	19(6, 14) – 19(4, 15) <i>E</i>	0.41	137	✓	✓
218.06057	19(6, 14) – 19(4, 15) <i>A</i>	0.41	137	✓	✓
218.25959	31(9, 23) – 31(8, 24) <i>A</i>	8.31	349	✓	✓
218.28084	17(1, 16) – 16(1, 15) <i>E</i>	43.54	100	✓	✓
218.29789	17(3, 14) – 16(3, 13) <i>A</i>	43.60	100	✓	✓
218.58532	36(9, 28) – 36(8, 29) <i>A</i>	10.14	451	B	✓
218.59334	27(7, 21) – 27(5, 22) <i>A</i>	1.23	258	B	✓
218.60704	36(9, 28) – 36(8, 29) <i>E</i>	9.99	451	✓	✓
219.08994	34(7, 28) – 34(5, 29) <i>E</i>	3.09	388	B	✓
219.10866	34(7, 28) – 34(5, 29) <i>A</i>	3.10	388	B	✓
219.26318	36(6, 30) – 36(6, 31) <i>A</i>	3.43	429	B	✓
219.41727	30(5, 26) – 30(4, 27) <i>E</i>	5.49	292	✓	✓
219.48370	30(5, 26) – 30(4, 27) <i>A</i>	5.55	292	✓	✓
219.57904	28(9, 19) – 28(8, 20) <i>A</i>	7.29	295	✓	✓
219.59210	28(9, 19) – 28(6, 22) <i>E</i>	7.26	295	✓	✓



Table A.2—Continued

Rest Frequency	Transition	$S_{ij}\mu^2$	$E_u$	Detection	
				hot core-SW	compact ridge
(GHz)		(Debye <sup>2</sup> )	(K)		
219.60016	30(9, 22) – 30(8, 23) <i>E</i>	7.94	330	✓	✓
219.60736	30(5, 26) – 30(3, 27) <i>E</i>	2.61	292	B	✓
219.67311	30(5, 26) – 30(3, 27) <i>A</i>	2.62	292	B	✓
220.16689	17(4, 13) – 16(4, 12) <i>E</i>	42.92	103	✓	✓
220.19029	17(4, 13) – 16(4, 12) <i>A</i>	42.93	103	✓	✓
220.43282	33(5, 28) – 33(5, 29) <i>A</i>	3.06	357	B	✓
220.78615	28(3, 25) – 28(3, 26) <i>E</i>	2.13	248	✓	✓
220.81185	18(3, 16) – 17(2, 15) <i>E</i>	4.43	106	✓	✓
220.81519	18(3, 16) – 17(2, 15) <i>A</i>	4.48	106	✓	✓
220.81955	24(2, 23) – 24(1, 24) <i>A</i>	1.37	169	B	✓
220.86870	28(3, 25) – 28(3, 26) <i>A</i>	2.13	248	✓	✓
220.88894	18(17, 2) – 17(17, 1) <i>A</i>	5.17	293	B	✓
220.90106	18(17, 1) – 17(17, 0) <i>E</i>	5.17	293	✓	✓
220.91035	18(17, 2) – 17(17, 1) <i>E</i>	5.20	293	✓	✓
220.92617	18(16, 2) – 17(16, 1) <i>A</i>	10.05	271	✓	✓
220.93518	18(16, 2) – 17(16, 1) <i>E</i>	10.05	271	✓	✓
220.96661	37(9, 29) – 37(8, 30) <i>E</i>	10.24	473	B	✓
220.97798	18(15, 3) – 17(15, 2) <i>A</i>	14.69	250	✓	✓
220.99833	18(15, 4) – 17(15, 3) <i>E</i>	14.69	250	✓	✓
221.02507	36(6, 30) – 36(5, 31) <i>A</i>	8.45	429	✓	✓
221.04999	18(14, 4) – 17(14, 3) <i>E</i>	18.98	231	✓	✓
221.06693	18(14, 5) – 17(14, 4) <i>E</i>	18.98	231	✓	✓
221.07598	29(9, 21) – 29(8, 22) <i>A</i>	7.66	312	✓	✓
221.08618	29(9, 21) – 29(8, 22) <i>E</i>	7.57	312	✓	✓
221.13972	18(13, 5) – 17(13, 4) <i>E</i>	22.97	213	B	B
221.14113	18(13, 5) – 17(13, 4) <i>A</i>	22.98	213	B	B
221.15854	18(13, 6) – 17(13, 5) <i>E</i>	22.98	213	✓	✓
221.26068	18(12, 6) – 17(12, 5) <i>E</i>	26.59	196	✓	✓
221.26560	18(12, 7) – 17(12, 6) <i>A</i>	26.59	196	✓	✓

Table A.2—Continued

Rest Frequency	Transition	$S_{ij}\mu^2$	$E_u$	Detection	
				hot core-SW	compact ridge
(GHz)		(Debye <sup>2</sup> )	(K)		
221.26569	18(12, 6) – 17(12, 5) <i>A</i>	26.68	196	✓	✓
221.28090	18(12, 7) – 17(12, 6) <i>E</i>	26.59	196	✓	✓
221.29389	28(4, 25) – 28(3, 26) <i>E</i>	4.12	248	✓	✓
221.32184	28(4, 25) – 28(2, 26) <i>E</i>	2.12	248	✓	✓
221.37482	28(4, 25) – 28(3, 26) <i>A</i>	4.11	248	✓	✓
221.42457	18(11, 7) – 17(11, 6) <i>E</i>	29.99	181	B	✓
221.43302	18(11, 7) – 17(11, 6) <i>A</i>	30.08	181	✓	✓
221.44563	18(11, 8) – 17(11, 7) <i>E</i>	29.99	181	✓	✓
221.64934	18(10, 8) – 17(10, 7) <i>E</i>	33.09	167	✓	✓
221.66048	18(4, 15) – 17(4, 14) <i>E</i>	45.31	112	✓	✓
221.67075	18(10, 9) – 17(10, 8) <i>E</i>	33.09	167	✓	✓
221.67467	18(4, 15) – 17(4, 14) <i>A</i>	45.32	112	✓	✓
221.71716	10(4, 6) – 9(3, 7) <i>A</i>	1.68	43	✓	✓
221.74611	26(5, 22) – 26(2, 24) <i>E</i>	2.77	207	✓	✓
221.74862	26(5, 22) – 26(3, 24) <i>E</i>	1.53	207	✓	✓
221.76298	26(2, 24) – 26(1, 25) <i>A</i>	2.75	207	✓	✓
221.84111	26(3, 24) – 26(2, 25) <i>A</i>	2.75	207	✓	✓
221.84391	26(3, 24) – 26(1, 25) <i>A</i>	1.53	207	✓	✓
221.96442	18(9, 9) – 17(9, 8) <i>E</i>	35.98	155	B	B
221.97932	18(9, 10) – 17(9, 9) <i>A</i>	35.90	155	✓	✓
221.98570	18(9, 10) – 17(9, 9) <i>E</i>	35.89	155	✓	✓
222.00501	11(5, 6) – 11(3, 9) <i>E</i>	0.05	56	B	✓
222.28943	37(9, 29) – 36(10, 26) <i>E</i>	1.97	473	B	✓
222.35551	27(9, 18) – 27(8, 19) <i>A</i>	6.92	278	✓	✓
222.36695	27(9, 18) – 27(8, 19) <i>E</i>	6.69	278	✓	✓
222.42140	18(8, 10) – 17(8, 9) <i>E</i>	38.41	144	✓	✓
222.43825	18(8, 11) – 17(8, 10) <i>A</i>	38.41	144	B	B
222.44036	18(8, 10) – 17(8, 9) <i>A</i>	38.41	144	B	B
222.44206	18(8, 11) – 17(8, 10) <i>E</i>	38.41	144	B	B

Table A.2—Continued

Rest Frequency	Transition	$S_{ij}\mu^2$	$E_u$	Detection	
				hot core-SW	compact ridge
(GHz)		(Debye <sup>2</sup> )	(K)		
222.61360	8(5, 4) – 7(4, 4) <i>E</i>	2.10	38	✓	✓
222.63075	28(9, 20) – 28(8, 21) <i>A</i>	7.28	295	✓	✓
222.63508	28(9, 20) – 28(8, 20) <i>E</i>	7.25	295	✓	✓
222.64933	8(5, 4) – 7(4, 3) <i>A</i>	2.12	38	✓	✓
222.65732	8(5, 3) – 7(4, 3) <i>E</i>	2.10	38	✓	✓
222.70916	8(5, 3) – 7(4, 4) <i>A</i>	2.12	38	✓	✓
222.86138	18(7, 12) – 17(7, 10) <i>E</i>	0.31	134	✓	B
223.03786	19(4, 16) – 18(3, 15) <i>E</i>	4.94	117	✓	✓
223.05172	19(2, 17) – 18(3, 16) <i>A</i>	4.95	117	✓	✓
223.11923	18(7, 12) – 17(7, 11) <i>A</i>	40.62	134	✓	✓
223.12509	18(7, 11) – 17(7, 10) <i>E</i>	40.39	134	✓	✓
223.13501	18(7, 12) – 17(7, 11) <i>E</i>	40.32	134	✓	✓
223.16274	18(7, 11) – 17(7, 10) <i>A</i>	40.70	134	✓	✓
223.34801	18(6, 13) – 17(6, 11) <i>E</i>	0.35	125	B	✓
223.39866	18(7, 11) – 17(7, 11) <i>E</i>	0.30	134	B	✓
223.46534	11(4, 8) – 10(3, 7) <i>E</i>	1.76	50	✓	✓
223.50046	11(4, 8) – 10(3, 7) <i>A</i>	1.77	50	✓	✓
223.53851	43(8, 35) – 43(7, 36) <i>E</i>	11.36	618	B	✓
223.59223	43(8, 35) – 43(7, 36) <i>A</i>	11.36	618	✓	✓
223.62449	37(8, 30) – 37(7, 31) <i>E</i>	9.54	463	B	✓
223.63491	37(8, 30) – 37(7, 31) <i>A</i>	9.54	463	✓	✓
223.64534	12(5, 7) – 12(3, 10) <i>A</i>	0.10	63	B	✓
223.82145	35(11, 25) – 35(2, 33) <i>E</i>	8.37	409	✓	✓
223.85393	35(7, 29) – 35(6, 30) <i>A</i>	8.36	409	✓	B
224.02187	18(6, 13) – 17(6, 12) <i>E</i>	42.26	125	B	B
224.02410	18(6, 13) – 17(6, 12) <i>A</i>	42.62	125	B	B
224.16796	27(9, 19) – 27(8, 20) <i>E</i>	6.68	278	✓	✓
224.17335	27(9, 19) – 27(8, 20) <i>A</i>	6.91	278	B	✓
224.29599	38(9, 30) – 38(8, 31) <i>A</i>	10.64	496	B	✓

Table A.2—Continued

Rest Frequency	Transition	$S_{ij}\mu^2$	$E_u$	Detection	
				hot core-SW	compact ridge
(GHz)		(Debye <sup>2</sup> )	(K)		
224.31315	18(5, 14) – 17(5, 13) <i>E</i>	44.18	118	✓	✓
224.32831	18(5, 14) – 17(5, 13) <i>A</i>	44.18	118	✓	✓
224.48622	26(9, 18) – 26(8, 18) <i>E</i>	0.89	262	B	✓
224.58221	18(6, 12) – 17(6, 11) <i>E</i>	42.19	125	✓	✓
224.60001	26(9, 17) – 26(8, 18) <i>A</i>	6.54	262	B	✓
224.60934	18(6, 12) – 17(6, 11) <i>A</i>	42.53	125	✓	✓
224.61879	26(9, 17) – 26(8, 18) <i>E</i>	5.65	262	✓	✓
224.96406	36(10, 26) – 36(9, 27) <i>A</i>	10.09	463	✓	✓
225.02937	36(10, 26) – 36(9, 27) <i>E</i>	9.92	463	✓	✓
225.12058	27(6, 21) – 26(7, 20) <i>A</i>	1.78	252	B	✓
225.25615	18(6, 12) – 17(6, 12) <i>E</i>	0.35	125	B	✓
225.60877	19(3, 16) – 18(3, 15) <i>E</i>	48.63	117	✓	✓
225.61867	19(3, 17) – 18(3, 16) <i>A</i>	48.63	117	✓	✓
225.85536	6(6, 1) – 5(5, 1) <i>E</i>	2.53	36	✓	✓
225.90065	6(6, 0) – 5(5, 0) <i>E</i>	2.53	36	B	✓
225.92860	6(6, 1) – 5(5, 0) <i>A</i>	2.53	36	✓	✓
225.92861	6(6, 0) – 5(5, 1) <i>A</i>	2.53	36	✓	✓
225.99938	30(9, 21) – 29(8, 21) <i>E</i>	1.83	312	✓	✓
226.08117	30(7, 23) – 29(8, 22) <i>A</i>	1.78	312	B	✓
226.33511	25(9, 17) – 25(8, 17) <i>E</i>	1.54	246	B	✓
226.46764	25(9, 16) – 25(8, 17) <i>E</i>	4.62	246	✓	✓
226.53018	33(2, 31) – 33(3, 30) <i>E</i>	6.96	358	✓	✓
226.56142	35(7, 29) – 35(5, 30) <i>A</i>	3.23	409	B	✓
226.57502	33(8, 25) – 32(9, 24) <i>E</i>	1.87	379	B	✓
226.58135	33(6, 28) – 33(5, 29) <i>A</i>	6.96	358	B	✓
226.62935	20(1, 19) – 19(2, 18) <i>E</i>	6.98	120	✓	✓
226.63521	20(1, 19) – 19(2, 18) <i>A</i>	7.06	120	✓	✓
226.71306	20(2, 19) – 19(2, 18) <i>E</i>	52.04	120	✓	✓
226.71869	20(2, 19) – 19(2, 18) <i>A</i>	52.05	120	✓	✓

Table A.2—Continued

Rest Frequency	Transition	$S_{ij}\mu^2$	$E_u$	Detection	
				hot core-SW	compact ridge
(GHz)		(Debye <sup>2</sup> )	(K)		
226.77313	20(1, 19) – 19(1, 18) <i>E</i>	52.04	120	✓	✓
226.77871	20(1, 19) – 19(1, 18) <i>A</i>	51.94	120	✓	✓
226.85682	20(2, 18) – 19(3, 17) <i>E</i>	7.06	120	✓	✓
226.86218	20(2, 19) – 19(1, 18) <i>A</i>	7.06	120	✓	✓
226.97409	25(9, 17) – 25(8, 18) <i>E</i>	4.62	246	✓	✓
227.01949	19(4, 16) – 18(4, 15) <i>E</i>	48.68	117	✓	✓
227.02807	19(2, 17) – 18(2, 16) <i>A</i>	48.69	117	✓	✓
227.10666	25(9, 16) – 25(8, 18) <i>E</i>	1.54	246	B	✓
227.15250	33(6, 28) – 33(4, 29) <i>E</i>	3.04	358	✓	✓
227.20175	33(6, 28) – 33(4, 29) <i>A</i>	3.05	358	✓	✓
227.56094	21(1, 21) – 20(1, 20) <i>E</i>	55.48	122	B	B
227.56199	21(1, 21) – 20(1, 20) <i>A</i>	55.49	122	B	B
227.56274	21(0, 21) – 20(0, 20) <i>A</i>	55.37	122	B	B
227.67322	26(7, 20) – 26(5, 21) <i>A</i>	0.97	242	B	✓
227.71420	26(7, 20) – 26(5, 21) <i>E</i>	0.97	242	B	✓
227.87135	31(4, 27) – 31(4, 28) <i>E</i>	2.66	309	✓	✓
227.94332	31(4, 27) – 31(4, 28) <i>A</i>	2.66	309	B	✓
227.95445	24(9, 15) – 24(8, 16) <i>A</i>	5.77	231	B	✓
227.98625	31(4, 27) – 31(3, 28) <i>E</i>	5.49	309	B	✓
227.99455	24(9, 15) – 24(8, 16) <i>E</i>	4.34	231	✓	B
228.05789	31(4, 27) – 31(3, 28) <i>A</i>	5.49	309	B	✓
228.16491	18(6, 13) – 18(4, 14) <i>A</i>	0.31	125	B	✓
228.20584	24(9, 16) – 24(8, 17) <i>E</i>	4.38	231	✓	✓
228.27042	24(9, 16) – 24(8, 17) <i>A</i>	5.82	231	✓	✓
228.35844	24(9, 15) – 24(8, 17) <i>E</i>	1.43	231	✓	✓
228.49487	14(4, 10) – 14(1, 13) <i>E</i>	0.12	73	B	✓
228.59002	14(4, 10) – 14(1, 13) <i>A</i>	0.12	73	✓	✓
228.62888	18(5, 13) – 17(5, 12) <i>E</i>	44.24	119	✓	✓
228.65140	18(5, 13) – 17(5, 12) <i>A</i>	44.25	119	✓	✓

Table A.2—Continued

Rest Frequency	Transition	$S_{ij}\mu^2$	$E_u$	Detection	
				hot core-SW	compact ridge
(GHz)		(Debye <sup>2</sup> )	(K)		
228.66505	39(9, 31) – 39(8, 32) <i>A</i>	10.83	520	B	✓
228.67921	39(9, 31) – 39(8, 32) <i>E</i>	10.64	520	✓	✓
228.71258	36(9, 27) – 35(10, 26) <i>E</i>	1.99	452	✓	✓
229.08216	23(9, 15) – 23(8, 15) <i>E</i>	0.76	217	B	✓
229.22423	23(9, 14) – 23(8, 15) <i>A</i>	5.43	217	✓	✓
229.25931	23(9, 14) – 23(8, 15) <i>E</i>	4.67	217	B	✓
229.32015	23(9, 15) – 23(8, 16) <i>E</i>	4.67	217	✓	✓
229.38892	23(9, 15) – 23(8, 16) <i>A</i>	5.42	217	✓	✓
229.40502	18(3, 15) – 17(3, 14) <i>E</i>	46.12	111	✓	✓
229.42034	18(3, 15) – 17(3, 14) <i>A</i>	46.12	111	✓	✓
229.47410	20(1, 19) – 19(4, 15) <i>E</i>	3.49	134	✓	✓
229.49206	31(5, 27) – 31(4, 28) <i>A</i>	5.49	309	B	✓
229.49722	23(9, 14) – 23(8, 16) <i>E</i>	0.76	217	B	✓
229.50463	20(3, 17) – 19(4, 16) <i>A</i>	3.49	134	✓	✓
229.59502	19(3, 17) – 18(2, 16) <i>A</i>	4.97	117	✓	✓
229.60676	31(5, 27) – 31(3, 28) <i>A</i>	2.67	310	B	✓
230.11030	22(9, 14) – 22(8, 14) <i>E</i>	0.21	203	B	✓
230.12282	35(8, 28) – 35(6, 29) <i>A</i>	2.57	419	✓	✓
230.16097	35(8, 28) – 35(6, 29) <i>E</i>	2.55	419	B	✓
230.29395	22(9, 13) – 22(8, 14) <i>A</i>	5.08	203	B	✓
230.31231	22(9, 13) – 22(8, 14) <i>E</i>	4.87	203	✓	✓
230.31580	22(9, 14) – 22(8, 15) <i>E</i>	4.87	203	B	✓
230.37659	22(9, 14) – 22(8, 15) <i>A</i>	5.08	203	✓	✓
230.43575	25(1, 24) – 25(0, 25) <i>E</i>	1.38	182	✓	✓
230.44077	25(2, 24) – 25(1, 25) <i>E</i>	1.38	182	✓	✓
230.92011	29(3, 26) – 29(3, 27) <i>E</i>	2.15	264	✓	✓
230.93636	29(3, 26) – 29(2, 27) <i>E</i>	4.12	264	B	✓
231.00438	29(3, 26) – 29(3, 27) <i>A</i>	2.16	264	✓	✓
231.01900	12(4, 9) – 11(3, 8) <i>E</i>	1.80	57	✓	✓

Table A.2—Continued

Rest Frequency	Transition	$S_{ij}\mu^2$	$E_u$	Detection	
				hot core-SW	compact ridge
(GHz)		(Debye <sup>2</sup> )	(K)		
231.04600	12(4, 9) – 11(3, 8) <i>A</i>	1.81	57	B	✓
231.18769	21(9, 13) – 21(8, 14) <i>E</i>	4.71	190	✓	✓
231.19926	21(9, 12) – 21(8, 13) <i>A</i>	4.78	190	✓	✓
231.23920	21(9, 13) – 21(8, 14) <i>A</i>	4.75	190	✓	✓
231.33127	29(4, 26) – 29(2, 27) <i>A</i>	2.15	264	B	✓
231.40224	40(7, 33) – 40(6, 34) <i>E</i>	9.76	532	✓	✓
231.41445	35(10, 25) – 35(9, 26) <i>A</i>	9.48	441	✓	✓
231.42446	38(8, 31) – 38(7, 32) <i>E</i>	9.60	485	✓	✓
231.43718	38(8, 31) – 38(7, 32) <i>A</i>	9.75	485	✓	B
231.46966	35(10, 25) – 35(9, 26) <i>E</i>	9.47	441	✓	B
231.51343	27(2, 25) – 27(1, 26) <i>E</i>	2.75	222	B	✓
231.61200	27(2, 25) – 27(1, 26) <i>A</i>	2.75	222	✓	✓
231.65806	27(3, 25) – 27(2, 26) <i>A</i>	2.75	222	✓	✓
231.93866	20(9, 12) – 20(8, 13) <i>E</i>	4.41	178	✓	✓
231.95522	20(9, 11) – 20(8, 12) <i>E</i>	4.41	178	✓	✓
231.96702	20(9, 11) – 20(8, 12) <i>A</i>	4.41	178	B	✓
232.30577	34(8, 27) – 34(6, 28) <i>A</i>	2.22	398	✓	✓
232.35615	34(8, 27) – 34(6, 28) <i>E</i>	2.22	398	✓	✓
232.37214	34(9, 26) – 34(3, 31) <i>E</i>	3.12	377	B	✓
232.43549	34(5, 29) – 34(5, 30) <i>A</i>	3.12	378	✓	✓
232.57943	19(9, 11) – 19(8, 12) <i>E</i>	4.08	166	✓	✓
232.59727	19(9, 10) – 19(8, 11) <i>E</i>	4.07	166	B	✓
232.61714	19(9, 10) – 19(8, 11) <i>A</i>	4.10	166	✓	✓
232.62520	19(9, 11) – 19(8, 12) <i>A</i>	4.10	166	✓	✓
232.76069	34(9, 26) – 34(4, 30) <i>E</i>	6.98	377	✓	✓
232.82276	34(5, 29) – 34(4, 30) <i>A</i>	6.88	377	B	✓
233.03244	22(0, 22) – 21(5, 17) <i>E</i>	2.53	165	✓	✓
233.08217	22(4, 18) – 21(5, 17) <i>A</i>	2.53	165	B	✓
233.12216	18(9, 10) – 18(8, 11) <i>E</i>	3.74	155	B	✓

Table A.2—Continued

Rest Frequency	Transition	$S_{ij}\mu^2$	$E_u$	Detection	
				hot core-SW	compact ridge
(GHz)		(Debye <sup>2</sup> )	(K)		
233.14065	18(9, 9) – 18(8, 10) <i>E</i>	3.76	155	✓	✓
233.16610	18(9, 9) – 18(8, 10) <i>A</i>	3.76	155	✓	✓
233.16945	18(9, 10) – 18(8, 11) <i>A</i>	3.77	155	✓	✓
233.18150	37(6, 31) – 37(6, 32) <i>A</i>	3.50	452	✓	✓
233.20020	19(17, 2) – 18(17, 1) <i>A</i>	10.12	304	B	✓
233.21277	19(4, 16) – 18(4, 15) <i>E</i>	48.03	123	✓	✓
233.22221	19(17, 3) – 18(17, 2) <i>E</i>	10.12	304	✓	✓
233.22675	19(4, 16) – 18(4, 15) <i>A</i>	47.96	123	✓	✓
233.24679	19(16, 3) – 18(16, 2) <i>A</i>	14.76	282	✓	✓
233.25601	19(16, 3) – 18(16, 2) <i>E</i>	14.76	282	✓	✓
233.26859	19(16, 4) – 18(16, 3) <i>E</i>	14.76	282	✓	✓
233.31012	19(15, 4) – 18(15, 3) <i>A</i>	19.11	261	✓	✓
233.31578	19(15, 4) – 18(15, 3) <i>E</i>	19.11	261	✓	✓
233.33121	19(15, 5) – 18(15, 4) <i>E</i>	19.11	261	✓	✓
233.39466	19(14, 5) – 18(14, 4) <i>A</i>	23.18	242	B	B
233.39668	19(14, 5) – 18(14, 4) <i>E</i>	23.18	242	B	B
233.41443	19(14, 6) – 18(14, 5) <i>E</i>	23.18	242	✓	✓
233.50498	19(13, 6) – 18(13, 5) <i>E</i>	26.87	224	B	B
233.50660	19(13, 7) – 18(13, 6) <i>A</i>	26.87	224	B	B
233.52463	19(13, 7) – 18(13, 6) <i>E</i>	26.96	224	✓	✓
233.57852	17(9, 9) – 17(8, 10) <i>E</i>	3.41	144	✓	✓
233.64988	19(12, 7) – 18(12, 6) <i>E</i>	30.47	208	✓	✓
233.65527	19(12, 8) – 18(12, 7) <i>A</i>	30.37	208	✓	✓
233.67098	19(12, 8) – 18(12, 7) <i>E</i>	30.46	208	✓	✓
233.75392	18(2, 16) – 17(2, 15) <i>E</i>	45.69	114	✓	✓
233.77752	18(4, 14) – 17(4, 13) <i>A</i>	45.76	114	✓	✓
233.84523	19(11, 8) – 18(11, 7) <i>E</i>	33.69	192	✓	✓
233.85423	19(11, 9) – 18(11, 8) <i>A</i>	33.59	192	✓	✓
233.86711	19(11, 9) – 18(11, 8) <i>E</i>	33.59	192	✓	✓



Table A.2—Continued

Rest Frequency	Transition	$S_{ij}\mu^2$	$E_u$	Detection	
				hot core-SW	compact ridge
(GHz)		(Debye <sup>2</sup> )	(K)		
233.92728	42(11, 31) – 42(10, 32) <i>A</i>	11.96	618	B	✓
233.95901	16(9, 8) – 16(8, 9) <i>E</i>	3.07	134	✓	✓
233.97864	16(9, 7) – 16(8, 8) <i>E</i>	3.09	134	✓	✓
234.02371	42(11, 31) – 42(10, 32) <i>E</i>	11.96	618	✓	✓
234.04769	40(9, 32) – 40(8, 33) <i>A</i>	10.78	543	B	✓
234.05863	40(9, 32) – 40(8, 33) <i>E</i>	10.78	544	✓	✓
234.11233	19(10, 9) – 18(10, 8) <i>E</i>	36.62	179	✓	✓
234.12486	19(10, 10) – 18(10, 9) <i>A</i>	36.52	179	✓	✓
234.13460	19(10, 10) – 18(10, 9) <i>E</i>	36.62	179	✓	✓
234.25981	37(6, 31) – 37(5, 32) <i>E</i>	8.30	451	✓	✓
234.27312	15(9, 7) – 15(8, 8) <i>E</i>	2.73	125	✓	✓
234.29326	15(9, 6) – 15(8, 7) <i>E</i>	2.74	125	✓	✓
234.31623	37(6, 31) – 37(5, 32) <i>A</i>	8.29	451	B	✓
234.32876	15(9, 6) – 15(8, 7) <i>A</i>	2.74	125	✓	✓
234.47929	9(5, 5) – 8(4, 4) <i>E</i>	0.20	43	✓	✓
234.48639	19(9, 10) – 18(9, 9) <i>E</i>	39.28	166	✓	✓
234.50223	19(9, 11) – 18(9, 10) <i>A</i>	39.19	166	✓	✓
234.50864	19(9, 11) – 18(9, 10) <i>E</i>	39.18	166	✓	✓
234.52939	14(9, 6) – 14(8, 7) <i>E</i>	2.39	116	✓	✓
234.55012	14(9, 5) – 14(8, 6) <i>E</i>	2.38	116	B	✓
234.58806	14(9, 5) – 14(8, 6) <i>A</i>	2.40	116	✓	✓
234.72653	20(2, 18) – 19(3, 17) <i>E</i>	5.39	128	✓	✓
234.73565	13(9, 5) – 13(8, 6) <i>E</i>	2.03	107	B	B
234.73749	9(5, 5) – 8(4, 4) <i>A</i>	2.16	43	B	B
234.73903	20(2, 18) – 19(3, 17) <i>A</i>	5.45	128	B	B
234.75688	13(9, 4) – 13(8, 5) <i>E</i>	2.03	107	B	✓
234.78336	9(5, 4) – 8(4, 4) <i>E</i>	1.95	43	✓	✓
234.79710	13(9, 4) – 13(8, 5) <i>A</i>	2.04	107	✓	✓
234.89899	12(9, 4) – 12(8, 5) <i>E</i>	1.67	100	✓	✓

Table A.2—Continued

Rest Frequency	Transition	$S_{ij}\mu^2$	$E_u$	Detection	
				hot core-SW	compact ridge
(GHz)		(Debye <sup>2</sup> )	(K)		
234.91680	9(5, 4) – 8(4, 5) <i>A</i>	2.15	43	✓	✓
234.92057	12(9, 3) – 12(8, 4) <i>E</i>	1.68	100	✓	✓
234.94342	36(7, 30) – 36(5, 31) <i>A</i>	3.35	430	✓	✓
234.96309	12(9, 3) – 12(8, 4) <i>A</i>	1.67	100	✓	✓
235.02583	11(9, 3) – 11(8, 4) <i>E</i>	1.29	93	✓	✓
235.02994	19(8, 11) – 18(8, 10) <i>E</i>	41.56	155	✓	✓
235.04648	19(8, 12) – 18(8, 11) <i>A</i>	41.57	155	✓	✓
235.05138	19(8, 12) – 18(8, 11) <i>E</i>	41.65	155	✓	✓
235.09216	11(9, 2) – 11(8, 3) <i>A</i>	1.30	93	✓	✓
235.12201	10(9, 2) – 10(8, 3) <i>E</i>	0.89	86	✓	✓
235.14449	10(9, 1) – 10(8, 2) <i>E</i>	0.89	86	B	✓
235.19049	10(9, 1) – 10(8, 2) <i>A</i>	0.90	86	✓	✓
235.19274	9(9, 1) – 9(8, 2) <i>E</i>	0.47	80	✓	✓
235.26327	9(9, 1) – 9(8, 2) <i>A</i>	0.47	80	✓	✓
235.31520	11(3, 8) – 10(2, 9) <i>E</i>	0.68	46	✓	✓
235.37523	11(3, 8) – 10(2, 9) <i>A</i>	0.68	46	B	✓
235.60227	19(7, 13) – 18(7, 11) <i>E</i>	1.11	145	B	✓
235.84454	19(7, 13) – 18(7, 12) <i>A</i>	43.75	145	✓	✓
235.86597	19(7, 13) – 18(7, 12) <i>E</i>	42.63	145	✓	✓
235.88711	19(7, 12) – 18(7, 11) <i>E</i>	42.63	145	✓	✓
235.93235	19(7, 12) – 18(7, 11) <i>A</i>	43.66	145	✓	✓
236.15070	19(7, 12) – 18(7, 12) <i>E</i>	1.12	145	✓	✓
236.36553	20(3, 18) – 19(3, 17) <i>A</i>	51.27	128	✓	✓
236.44334	15(5, 10) – 15(3, 13) <i>E</i>	0.16	88	B	✓
236.49247	34(6, 29) – 34(5, 30) <i>E</i>	6.87	378	✓	✓
236.58655	6(4, 2) – 5(2, 3) <i>A</i>	0.02	23	B	✓
236.74370	19(5, 15) – 18(5, 14) <i>E</i>	47.01	130	✓	✓
236.74879	34(10, 24) – 34(9, 25) <i>E</i>	9.04	420	B	✓
236.75969	19(5, 15) – 18(5, 14) <i>A</i>	47.02	130	✓	✓

Table A.2—Continued

Rest Frequency	Transition	$S_{ij}\mu^2$	$E_u$	Detection	
				hot core-SW	compact ridge
(GHz)		(Debye <sup>2</sup> )	(K)		
236.80059	19(6, 14) – 18(6, 13) <i>E</i>	45.46	137	✓	✓
236.81031	19(6, 14) – 18(6, 13) <i>A</i>	45.56	137	✓	✓
236.88101	34(6, 29) – 34(4, 30) <i>E</i>	3.10	378	B	✓
237.23860	33(8, 26) – 33(6, 27) <i>A</i>	1.87	377	✓	✓
237.26120	21(1, 20) – 20(2, 19) <i>E</i>	7.44	132	✓	✓
237.26679	21(1, 20) – 20(2, 19) <i>A</i>	7.52	132	✓	✓
237.29747	20(4, 17) – 19(4, 16) <i>E</i>	51.30	128	✓	✓
237.30597	20(2, 18) – 19(2, 17) <i>A</i>	51.40	128	✓	✓
237.30954	21(2, 20) – 20(2, 19) <i>E</i>	54.70	132	✓	✓
237.31508	21(2, 20) – 20(2, 19) <i>A</i>	54.71	132	✓	✓
237.34487	21(1, 20) – 20(1, 19) <i>E</i>	54.71	132	✓	✓
237.35039	21(1, 20) – 20(1, 19) <i>A</i>	54.71	132	✓	✓
237.36505	8(3, 6) – 7(1, 7) <i>E</i>	0.04	27	B	✓
237.39319	21(2, 19) – 20(3, 18) <i>E</i>	7.53	132	✓	✓
237.39858	21(2, 20) – 20(1, 19) <i>A</i>	7.44	132	B	✓
237.80763	19(6, 13) – 18(6, 12) <i>E</i>	45.46	137	✓	✓
237.82983	19(6, 13) – 18(6, 12) <i>A</i>	45.56	137	✓	✓
237.87993	17(6, 12) – 17(4, 13) <i>E</i>	0.23	115	✓	✓
237.91834	17(6, 12) – 17(4, 13) <i>A</i>	0.24	115	B	✓
238.11798	7(6, 2) – 6(5, 2) <i>E</i>	2.53	40	✓	✓
238.15588	22(1, 22) – 21(1, 21) <i>E</i>	58.16	134	B	B
238.15631	22(0, 22) – 21(0, 21) <i>E</i>	58.16	134	B	B
238.15730	22(0, 22) – 21(0, 21) <i>A</i>	58.17	134	B	B
238.19009	7(6, 2) – 6(5, 1) <i>A</i>	2.53	40	✓	✓
238.35264	25(7, 19) – 25(5, 20) <i>A</i>	0.76	226	B	✓
238.39195	25(7, 19) – 25(5, 20) <i>E</i>	0.76	226	✓	✓
238.48438	32(4, 28) – 32(4, 29) <i>E</i>	2.69	328	✓	✓
238.53427	39(10, 30) – 39(9, 31) <i>A</i>	11.05	531	B	✓
238.55621	32(4, 28) – 32(4, 29) <i>A</i>	2.70	328	B	✓

Table A.2—Continued

Rest Frequency	Transition	$S_{ij}\mu^2$	$E_u$	Detection	
				hot core-SW	compact ridge
(GHz)		(Debye <sup>2</sup> )	(K)		
238.57345	39(10, 30) – 39(9, 31) <i>E</i>	10.85	531	✓	✓
238.57772	38(10, 29) – 38(9, 30) <i>A</i>	10.51	508	✓	✓
238.62473	32(4, 28) – 32(3, 29) <i>A</i>	5.49	328	✓	✓
238.92680	20(3, 17) – 19(4, 16) <i>E</i>	5.47	128	✓	✓
238.93248	20(3, 18) – 19(2, 17) <i>A</i>	5.47	128	✓	✓
239.04127	48(12, 36) – 48(11, 37) <i>A</i>	14.53	797	B	✓
239.15577	48(12, 36) – 48(11, 37) <i>E</i>	14.15	797	✓	✓
239.24086	37(10, 28) – 37(9, 29) <i>A</i>	10.32	485	B	✓
239.24469	40(10, 31) – 40(9, 32) <i>A</i>	11.38	555	B	✓
239.27843	37(10, 28) – 37(9, 29) <i>E</i>	10.15	485	✓	✓
239.28305	40(10, 31) – 40(9, 32) <i>E</i>	11.17	555	B	✓
239.41674	10(2, 8) – 9(1, 9) <i>E</i>	0.15	36	✓	✓
239.47271	32(5, 28) – 32(4, 29) <i>E</i>	5.49	328	B	✓
239.49359	10(2, 8) – 9(1, 9) <i>A</i>	0.15	36	B	✓
239.54125	32(5, 28) – 32(4, 29) <i>A</i>	5.48	328	✓	✓
239.89169	8(3, 6) – 7(0, 7) <i>A</i>	0.05	27	B	✓
239.92044	39(8, 32) – 39(7, 33) <i>E</i>	9.62	509	✓	B
239.92752	44(8, 36) – 44(7, 37) <i>E</i>	11.23	645	B	✓
239.93517	39(8, 32) – 39(7, 33) <i>A</i>	9.79	509	✓	✓
240.02108	19(1, 18) – 18(1, 17) <i>E</i>	48.55	122	✓	✓
240.03461	19(3, 16) – 18(3, 15) <i>A</i>	48.55	122	✓	✓
240.16280	26(1, 25) – 26(1, 26) <i>E</i>	0.82	196	✓	✓
240.16561	26(2, 25) – 26(1, 26) <i>E</i>	1.38	196	✓	✓
240.28104	26(1, 25) – 26(1, 26) <i>A</i>	0.82	196	B	✓
240.28383	26(2, 25) – 26(1, 26) <i>A</i>	1.38	196	B	✓
240.36208	10(2, 8) – 9(0, 9) <i>E</i>	0.09	36	B	✓
240.40880	41(9, 33) – 41(8, 34) <i>E</i>	10.88	569	✓	✓
240.43837	10(2, 8) – 9(0, 9) <i>A</i>	0.09	36	B	✓
241.06847	30(3, 27) – 30(2, 28) <i>A</i>	4.16	281	✓	B

Table A.2—Continued

Rest Frequency	Transition	$S_{ij}\mu^2$	$E_u$	Detection	
				hot core-SW	compact ridge
(GHz)		(Debye <sup>2</sup> )	(K)		
241.25789	30(4, 27) – 30(2, 28) <i>A</i>	2.17	281	✓	B
241.33567	28(2, 26) – 28(1, 27) <i>E</i>	2.75	237	✓	B
241.43753	28(2, 26) – 28(1, 27) <i>A</i>	2.77	237	✓	B
242.43959	14(4, 11) – 13(3, 10) <i>E</i>	1.96	73	✓	✓
242.45343	14(4, 11) – 13(3, 10) <i>A</i>	1.94	73	B	✓
242.83539	37(7, 31) – 37(6, 32) <i>E</i>	8.26	452	B	✓
242.87157	19(5, 14) – 18(5, 13) <i>E</i>	47.14	130	✓	✓
242.89602	19(5, 14) – 18(5, 13) <i>A</i>	47.15	130	✓	✓
243.56460	34(10, 25) – 34(9, 26) <i>A</i>	9.03	420	✓	✓
243.59166	34(8, 27) – 34(7, 27) <i>E</i>	9.14	420	B	✓
243.86206	35(5, 30) – 35(5, 31) <i>E</i>	3.16	398	✓	✓
243.97365	37(7, 31) – 37(5, 32) <i>E</i>	3.45	452	B	✓
244.00438	37(7, 31) – 37(5, 32) <i>A</i>	3.46	452	B	✓
244.10297	35(5, 30) – 35(4, 31) <i>E</i>	6.97	398	✓	✓
244.16231	35(5, 30) – 35(4, 31) <i>A</i>	6.97	398	✓	✓
244.48967	32(10, 22) – 32(9, 23) <i>A</i>	8.40	380	B	✓
244.51900	32(10, 22) – 32(9, 23) <i>E</i>	8.23	380	B	✓
244.58030	20(4, 16) – 19(4, 15) <i>E</i>	50.64	135	✓	✓
244.59401	20(4, 17) – 19(4, 16) <i>A</i>	50.64	135	✓	✓
244.65312	16(5, 11) – 16(3, 14) <i>A</i>	0.16	98	B	✓
244.84960	32(8, 25) – 32(6, 26) <i>A</i>	1.54	357	B	✓
244.87111	11(3, 8) – 10(1, 9) <i>E</i>	0.30	46	✓	✓
245.13823	21(1, 20) – 20(4, 16) <i>E</i>	4.05	147	✓	✓
245.16576	21(3, 18) – 20(4, 17) <i>A</i>	4.05	147	✓	✓
245.31530	15(4, 11) – 15(2, 14) <i>E</i>	0.07	83	B	✓
245.37027	33(10, 24) – 33(9, 25) <i>A</i>	8.77	399	✓	✓
245.39342	33(8, 26) – 33(7, 27) <i>E</i>	8.74	399	B	✓
245.42720	15(4, 11) – 15(2, 14) <i>A</i>	0.07	83	✓	✓
245.44689	20(19, 2) – 19(19, 1) <i>A</i>	5.18	363	✓	✓

Table A.2—Continued

Rest Frequency	Transition	$S_{ij}\mu^2$	$E_u$	Detection	
				hot core-SW	compact ridge
(GHz)		(Debye <sup>2</sup> )	(K)		
245.46557	20(19, 1) – 19(19, 0) <i>E</i>	5.18	363	B	✓
245.46846	20(19, 2) – 19(19, 1) <i>E</i>	5.21	363	B	✓
245.47575	20(18, 2) – 19(18, 1) <i>A</i>	10.11	339	✓	✓
245.49181	20(18, 2) – 19(18, 1) <i>E</i>	10.16	339	✓	✓
245.50908	25(5, 20) – 24(6, 19) <i>E</i>	2.18	214	✓	✓
245.51755	20(17, 3) – 19(17, 2) <i>A</i>	14.83	316	✓	✓
245.53030	20(17, 3) – 19(17, 2) <i>E</i>	14.83	315	✓	✓
245.58397	20(16, 4) – 19(16, 3) <i>E</i>	19.23	294	✓	✓
245.59730	20(16, 5) – 19(16, 4) <i>E</i>	19.23	294	B	✓
245.65108	20(15, 6) – 19(15, 5) <i>A</i>	23.27	273	✓	✓
245.65678	20(15, 5) – 19(15, 4) <i>E</i>	23.36	273	✓	✓
245.67298	20(15, 6) – 19(15, 5) <i>E</i>	23.37	273	✓	✓
245.75215	20(14, 7) – 19(14, 6) <i>A</i>	27.13	254	B	B
245.75227	20(14, 6) – 19(14, 5) <i>A</i>	27.23	254	B	B
245.77264	20(14, 7) – 19(14, 6) <i>E</i>	27.12	254	✓	✓
245.81939	41(7, 34) – 41(6, 35) <i>E</i>	9.71	556	B	✓
245.88310	20(13, 7) – 19(13, 6) <i>E</i>	30.71	236	B	B
245.88524	20(13, 7) – 19(13, 6) <i>A</i>	30.83	236	B	B
245.90368	20(13, 8) – 19(13, 7) <i>E</i>	30.82	236	✓	✓
246.02750	21(4, 18) – 20(3, 17) <i>E</i>	5.95	140	✓	✓
246.03889	21(2, 19) – 20(3, 18) <i>A</i>	5.87	140	✓	✓
246.05482	20(12, 8) – 19(12, 7) <i>E</i>	34.15	219	✓	✓
246.06074	20(12, 9) – 19(12, 8) <i>A</i>	34.03	219	B	B
246.06083	20(12, 8) – 19(12, 7) <i>A</i>	34.15	219	B	B
246.12596	7(4, 3) – 6(2, 4) <i>A</i>	0.04	27	ND	✓
246.19601	38(6, 32) – 38(6, 33) <i>A</i>	3.57	474	B	✓
246.28534	20(11, 9) – 19(11, 8) <i>E</i>	37.09	204	✓	✓
246.29507	20(11, 10) – 19(11, 9) <i>A</i>	37.09	204	✓	✓
246.30823	20(11, 10) – 19(11, 9) <i>E</i>	37.09	204	✓	✓

Table A.2—Continued

Rest Frequency	Transition	$S_{ij}\mu^2$	$E_u$	Detection	
				hot core-SW	compact ridge
(GHz)		(Debye <sup>2</sup> )	(K)		
246.44490	15(4, 11) – 15(3, 13) <i>E</i>	0.10	83	B	✓
246.45615	10(5, 6) – 9(4, 5) <i>E</i>	0.67	49	B	✓
246.57737	35(6, 30) – 35(5, 31) <i>E</i>	6.87	398	✓	✓
246.60000	20(10, 10) – 19(10, 9) <i>E</i>	39.88	190	✓	✓
246.61336	20(10, 11) – 19(10, 10) <i>A</i>	39.89	190	✓	✓
246.62319	20(10, 11) – 19(10, 10) <i>E</i>	39.99	190	✓	✓

Table A.3. Transitions of the *Trans* and *Gauche* conformers of ET observed with the ALMA.

Rest Frequency (GHz)	Transition	$S_{ij}\mu^2$ (Debye <sup>2</sup> )	$E_u$ (K)	Detection	
				hot core-SW	compact ridge
<i>Trans</i> conformer					
213.85626	13(0, 13) – 12(1, 12)	12.83	74	✓	✓
214.18012	22(5, 17) – 22(4, 18)	23.10	245	✓	✓
214.26774	9(2, 8) – 8(1, 7)	6.53	43	✓	✓
214.95629	18(11, 7) – 19(10, 10)	2.02	295	✓	ND
215.37564	21(2, 20) – 21(1, 21)	22.88	196	✓	✓
215.45224	26(4, 23) – 25(5, 20)	9.50	316	✓	✓
215.61072	20(3, 17) – 19(4, 16)	7.27	191	B	✓
216.62542	9(8, 1) – 10(7, 4)	0.32	118	✓	ND
217.80369	5(3, 3) – 4(2, 2)	5.99	24	✓	✓
218.46123	5(3, 2) – 4(2, 3)	5.98	24	B	✓
218.55450	21(5, 16) – 21(4, 17)	21.98	226	✓	✓
218.65408	7(2, 5) – 6(1, 6)	5.50	29	✓	✓
218.94327	35(4, 31) – 35(3, 32)	37.58	560	✓	B
219.17369	30(3, 27) – 30(2, 28)	32.39	410	B	✓
220.15478	24(3, 22) – 24(2, 23)	25.92	263	✓	✓
221.61296	34(6, 28) – 34(5, 29)	35.94	548	✓	✓
222.21729	20(5, 15) – 20(4, 16)	20.86	208	✓	✓
222.51950	26(4, 23) – 26(3, 24)	27.84	316	✓	✓
224.11927	24(4, 20) – 23(5, 19)	8.46	275	B	✓
225.21036	19(5, 14) – 19(4, 15)	19.74	191	✓	✓
226.39549	22(2, 21) – 22(1, 22)	23.95	214	✓	✓
226.58134	26(2, 24) – 26(1, 25)	28.24	305	✓	B
226.66170	10(2, 9) – 9(1, 8)	7.05	51	✓	✓
227.60608	18(5, 13) – 18(4, 14)	18.62	175	B	✓
229.37325	33(6, 27) – 33(5, 28)	34.84	519	✓	✓
229.49113	17(5, 12) – 17(4, 13)	17.48	160	✓	✓
229.77930	27(4, 24) – 27(3, 25)	28.92	339	✓	✓
230.14482	25(3, 23) – 25(2, 24)	27.00	284	B	B



Table A.3—Continued

Rest Frequency	Transition	$S_{ij}\mu^2$	$E_u$	Detection	
				hot core-SW	compact ridge
(GHz)		(Debye <sup>2</sup> )	(K)		
230.95378	16(5, 11) – 16(4, 12)	16.34	146	✓	B
230.98460	29(5, 25) – 28(6, 22)	10.17	399	✓	ND
230.99137	14(0, 14) – 13(1, 13)	13.89	86	✓	✓
231.56090	20(5, 16) – 20(4, 17)	20.87	208	✓	✓
231.73761	19(5, 15) – 19(4, 16)	19.74	191	✓	B
232.03463	18(5, 14) – 18(4, 15)	18.62	175	✓	✓
232.31850	23(5, 19) – 23(4, 20)	24.21	264	✓	✓
232.40481	17(5, 13) – 17(4, 14)	17.48	160	✓	✓
232.54796	17(11, 7) – 18(10, 8)	1.66	280	✓	✓
232.80883	16(5, 12) – 16(4, 13)	16.34	146	✓	✓
232.85088	28(5, 23) – 27(6, 22)	9.66	375	✓	ND
232.92850	14(5, 9) – 14(4, 10)	14.02	120	✓	✓
233.57102	13(5, 8) – 13(4, 9)	12.84	108	✓	✓
233.95112	13(5, 9) – 13(4, 10)	12.84	108	✓	✓
234.05112	12(5, 7) – 12(4, 8)	11.65	97	✓	✓
234.25516	12(5, 8) – 12(4, 9)	11.65	97	✓	✓
234.40645	11(5, 6) – 11(4, 7)	10.43	87	✓	✓
234.48134	31(3, 28) – 31(2, 29)	33.46	436	✓	✓
234.66627	10(5, 5) – 10(4, 6)	9.18	78	✓	✓
234.71457	10(5, 6) – 10(4, 7)	9.18	78	✓	✓
234.72560	23(1, 22) – 23(0, 23)	50.23	233	B	B
234.75882	6(3, 4) – 5(2, 3)	6.41	29	✓	✓
234.85303	9(5, 4) – 9(4, 5)	7.90	69	✓	B
234.87361	9(5, 5) – 9(4, 6)	7.90	69	✓	✓
234.98424	8(5, 3) – 8(4, 4)	6.56	62	✓	✓
234.99191	8(5, 4) – 8(4, 5)	6.56	62	✓	B
235.07349	7(5, 2) – 7(4, 3)	5.15	55	✓	✓
235.13151	6(5, 1) – 6(4, 2)	3.64	49	✓	✓
235.98333	14(1, 14) – 13(0, 13)	16.03	86	✓	✓

Table A.3—Continued

Rest Frequency	Transition	$S_{ij}\mu^2$	$E_u$	Detection	
				hot core-SW	compact ridge
(GHz)		(Debye <sup>2</sup> )	(K)		
236.29907	6(3, 3) – 5(2, 4)	6.41	29	✓	✓
236.32517	26(5, 22) – 26(4, 23)	27.52	327	✓	✓
237.52412	23(2, 22) – 23(1, 23)	25.02	233	✓	✓
237.63879	28(4, 25) – 28(3, 26)	30.01	362	✓	✓
238.70176	11(2, 10) – 10(1, 9)	7.58	60	✓	✓
240.11024	27(2, 25) – 27(1, 26)	29.31	327	✓	✓
240.45095	26(3, 24) – 26(2, 25)	28.08	305	✓	B
243.55694	8(2, 6) – 7(1, 7)	6.01	36	✓	✓
244.90813	32(6, 26) – 31(7, 25)	10.85	491	✓	ND
245.15728	29(5, 25) – 29(4, 26)	30.80	399	✓	✓
<i>Gauche conformer</i>					
213.76008	13(1, 13) – 12(1, 12), $v_t=1-1$	20.65	135	✓	✓
213.87270	32(7, 26) – 32(6, 26), $v_t=0-1$	18.92	556	✓	ND
214.05616	21(10, 11) – 22(9, 13), $v_t=1-0$	2.15	376	✓	ND
214.43462	17(3, 15) – 16(4, 13), $v_t=1-0$	3.24	200	✓	ND
215.36727	13(1, 13) – 12(1, 12), $v_t=0-0$	20.65	131	✓	✓
215.93156	11(0, 11) – 10(1, 9), $v_t=1-0$	6.06	115	✓	✓
216.02627	10(3, 8) – 10(2, 8), $v_t=1-0$	6.02	118	✓	✓
216.41562	13(0, 13) – 12(0, 12), $v_t=0-0$	20.77	131	✓	✓
216.52169	8(4, 4) – 7(3, 4), $v_t=0-1$	5.00	106	✓	✓
216.65968	8(4, 5) – 7(3, 5), $v_t=0-1$	5.00	106	✓	✓
217.54815	5(1, 4) – 4(0, 4), $v_t=1-0$	3.64	76	✓	✓
217.84716	30(7, 24) – 30(6, 24), $v_t=0-1$	17.65	504	✓	ND
218.79621	35(7, 28) – 35(6, 30), $v_t=0-1$	20.80	642	✓	ND
218.94832	36(7, 29) – 36(6, 31), $v_t=0-1$	21.43	672	✓	ND
219.06702	22(4, 19) – 22(3, 19), $v_t=1-0$	13.31	292	✓	B
219.27029	9(3, 7) – 9(2, 7), $v_t=1-0$	5.37	110	✓	✓
219.39206	14(2, 12) – 13(1, 12), $v_t=0-1$	5.19	151	B	✓
220.12701	10(2, 8) – 10(1, 10), $v_t=1-0$	6.25	113	✓	ND

Table A.3—Continued

Rest Frequency	Transition	$S_{ij}\mu^2$	$E_u$	Detection	
				hot core-SW	compact ridge
(GHz)		(Debye <sup>2</sup> )	(K)		
220.44347	30(7, 23) – 30(6, 25), $v_t=0-1$	17.65	504	✓	✓
221.81168	8(3, 6) – 8(2, 6), $v_t=1-0$	4.72	103	✓	✓
222.14170	26(7, 20) – 26(6, 20), $v_t=0-1$	15.10	409	✓	✓
222.16062	27(7, 20) – 27(6, 22), $v_t=0-1$	15.74	431	✓	✓
222.62600	26(2, 24) – 25(3, 22), $v_t=0-1$	6.43	358	✓	ND
222.64283	26(7, 19) – 26(6, 21), $v_t=0-1$	15.10	409	✓	✓
222.67711	13(2, 12) – 12(2, 11), $v_t=0-0$	20.28	137	✓	✓
222.74214	13(2, 12) – 12(2, 11), $v_t=1-1$	20.28	142	✓	B
222.75240	25(7, 19) – 25(6, 19), $v_t=0-1$	14.46	387	✓	B
223.23324	12(2, 11) – 11(1, 11), $v_t=0-1$	4.60	126	B	✓
223.24146	24(7, 18) – 24(6, 18), $v_t=0-1$	13.81	366	✓	✓
223.62958	23(7, 17) – 23(6, 17), $v_t=0-1$	13.16	346	✓	✓
223.69502	7(3, 5) – 7(2, 5), $v_t=1-0$	4.06	96	✓	✓
223.74813	23(7, 16) – 23(6, 18), $v_t=0-1$	13.16	346	✓	B
224.07085	7(7, 1) – 7(6, 1), $v_t=0-1$	1.14	140	B	✓
224.14513	8(7, 2) – 8(6, 2), $v_t=0-1$	2.15	147	B	✓
224.16627	21(7, 15) – 21(6, 15), $v_t=0-1$	11.85	309	✓	B
224.22200	9(7, 3) – 9(6, 3), $v_t=0-1$	3.07	154	✓	✓
224.29910	10(7, 4) – 10(6, 4), $v_t=0-1$	3.93	162	✓	✓
224.30383	17(1, 17) – 16(2, 15), $v_t=1-0$	4.28	185	✓	B
224.33928	20(7, 14) – 20(6, 14), $v_t=0-1$	11.18	291	✓	✓
224.36174	20(7, 13) – 20(6, 15), $v_t=0-1$	11.18	291	✓	B
224.37376	11(7, 5) – 11(6, 5), $v_t=0-1$	4.75	171	✓	✓
224.44306	12(7, 6) – 12(6, 6), $v_t=0-1$	5.54	181	✓	✓
224.47371	19(7, 12) – 19(6, 14), $v_t=0-1$	10.51	275	✓	B
224.50376	13(7, 7) – 13(6, 7), $v_t=0-1$	6.29	192	✓	✓
224.54091	18(7, 12) – 18(6, 12), $v_t=0-1$	9.84	259	✓	✓
224.54724	18(7, 11) – 18(6, 13), $v_t=0-1$	9.84	259	✓	✓
224.55244	14(7, 8) – 14(6, 8), $v_t=0-1$	7.03	204	✓	✓

Table A.3—Continued

Rest Frequency	Transition	$S_{ij}\mu^2$	$E_u$	Detection	
				hot core-SW	compact ridge
(GHz)		(Debye <sup>2</sup> )	(K)		
224.59698	16(7, 10) – 16(6, 10), $v_t=0-1$	8.46	230	✓	B
224.66995	3(2, 1) – 2(1, 1), $v_t=1-0$	2.02	71	✓	✓
224.73929	11(3, 9) – 10(2, 9), $v_t=0-1$	5.01	123	✓	✓
224.82313	13(1, 12) – 12(1, 11), $v_t=0-0$	20.65	135	✓	✓
224.87264	13(11, 2) – 12(11, 1), $v_t=1-1$	5.90	286	✓	✓
224.88357	13(10, 3) – 12(10, 2), $v_t=1-1$	8.48	260	✓	✓
224.90658	13(9, 5) – 12(9, 4), $v_t=1-1$	10.81	237	✓	✓
224.92383	16(2, 15) – 15(3, 13), $v_t=1-0$	3.45	179	✓	✓
224.94604	13(8, 6) – 12(8, 5), $v_t=1-1$	12.90	216	✓	✓
225.00120	6(3, 4) – 6(2, 4), $v_t=1-0$	3.38	90	✓	✓
225.00899	13(7, 6) – 12(7, 5), $v_t=1-1$	14.75	197	✓	✓
225.10519	13(10, 3) – 12(10, 2), $v_t=0-0$	8.48	255	✓	✓
225.10988	13(6, 7) – 12(6, 6), $v_t=1-1$	16.35	181	✓	✓
225.13050	13(8, 6) – 12(8, 5), $v_t=0-0$	12.90	211	✓	✓
225.17061	13(7, 6) – 12(7, 5), $v_t=0-0$	14.75	192	✓	✓
225.24881	13(6, 7) – 12(6, 6), $v_t=0-0$	16.35	176	✓	✓
225.27885	13(5, 9) – 12(5, 8), $v_t=1-1$	17.70	168	✓	✓
225.28285	13(5, 8) – 12(5, 7), $v_t=1-1$	17.70	168	✓	✓
225.39973	13(5, 9) – 12(5, 8), $v_t=0-0$	17.70	163	✓	✓
225.45691	13(3, 11) – 12(3, 10), $v_t=1-1$	19.66	148	✓	✓
225.54569	13(4, 10) – 12(4, 9), $v_t=1-1$	18.81	157	✓	✓
225.56011	13(3, 11) – 12(3, 10), $v_t=0-0$	19.67	144	✓	B
225.66028	13(4, 10) – 12(4, 9), $v_t=0-0$	18.80	152	✓	B
225.67110	13(4, 9) – 12(4, 8), $v_t=1-1$	18.80	157	✓	✓
225.79689	13(4, 9) – 12(4, 8), $v_t=0-0$	18.80	152	✓	✓
225.83609	5(3, 3) – 5(2, 3), $v_t=1-0$	2.67	85	✓	✓
226.05693	14(0, 14) – 13(0, 13), $v_t=1-1$	22.37	146	✓	✓
226.73025	3(3, 0) – 3(2, 2), $v_t=1-0$	1.06	78	B	✓
227.10890	5(3, 2) – 5(2, 4), $v_t=1-0$	2.67	85	✓	B

Table A.3—Continued

Rest Frequency	Transition	$S_{ij}\mu^2$	$E_u$	Detection	
				hot core-SW	compact ridge
(GHz)		(Debye <sup>2</sup> )	(K)		
227.29475	13(3, 10) – 12(3, 9), $v_t=1-1$	19.67	149	✓	✓
227.58083	12(3, 9) – 11(2, 9), $v_t=0-1$	5.30	133	✓	✓
227.59077	6(3, 3) – 6(2, 5), $v_t=1-0$	3.38	90	✓	✓
227.76082	3(2, 2) – 2(1, 2), $v_t=1-0$	2.02	71	B	✓
227.89191	13(1, 12) – 12(1, 11), $v_t=1-1$	20.65	140	✓	✓
228.02905	13(3, 10) – 12(3, 9), $v_t=0-0$	19.67	144	✓	✓
228.28855	11(1, 10) – 10(2, 8), $v_t=1-0$	2.48	119	✓	✓
228.52283	7(3, 4) – 7(2, 6), $v_t=1-0$	4.06	96	✓	✓
228.88665	9(3, 6) – 9(2, 8), $v_t=1-0$	5.37	110	✓	✓
229.24255	20(4, 16) – 19(5, 14), $v_t=1-0$	3.64	257	✓	✓
229.24944	25(3, 22) – 25(2, 24), $v_t=0-1$	15.31	343	✓	ND
230.23074	13(2, 11) – 12(2, 10), $v_t=1-1$	20.28	143	✓	B
230.67255	13(2, 11) – 12(2, 10), $v_t=0-0$	20.28	139	✓	✓
230.69655	8(3, 5) – 8(2, 7), $v_t=1-0$	4.72	103	✓	✓
230.79376	6(5, 1) – 5(4, 1), $v_t=0-1$	5.56	105	✓	✓
230.90000	23(11, 12) – 24(10, 14), $v_t=1-0$	2.30	439	B	✓
231.56869	18(1, 18) – 17(2, 16), $v_t=1-0$	4.58	199	✓	B
231.66873	14(1, 14) – 13(1, 13), $v_t=0-0$	22.26	142	✓	✓
231.78985	31(5, 27) – 31(4, 27), $v_t=1-0$	18.71	506	✓	✓
232.00849	11(2, 9) – 11(1, 11), $v_t=1-0$	6.86	122	✓	ND
232.49137	14(0, 14) – 13(0, 13), $v_t=0-0$	22.37	142	✓	✓
232.59655	14(1, 14) – 13(1, 13), $v_t=1-1$	22.26	147	B	B
233.71428	9(4, 5) – 8(3, 5), $v_t=0-1$	5.25	114	✓	✓
233.92471	13(0, 13) – 12(1, 11), $v_t=1-0$	7.27	136	✓	✓
234.36056	15(0, 15) – 14(1, 13), $v_t=1-0$	8.49	158	B	✓
235.75642	35(5, 30) – 35(4, 32), $v_t=0-1$	21.18	616	✓	ND
237.59811	12(3, 9) – 12(2, 11), $v_t=1-0$	7.29	138	✓	✓
238.49875	19(1, 19) – 18(2, 17), $v_t=1-0$	4.88	214	✓	ND
238.56819	6(1, 5) – 5(0, 5), $v_t=1-0$	4.24	81	✓	✓

Table A.3—Continued

Rest Frequency	Transition	$S_{ij}\mu^2$	$E_u$	Detection	
				hot core-SW	compact ridge
(GHz)		(Debye <sup>2</sup> )	(K)		
239.18595	16(0, 16) – 15(1, 14), $v_t=1-0$	9.09	171	✓	✓
239.47808	14(2, 13) – 13(2, 12), $v_t=0-0$	21.91	148	✓	✓
239.55137	14(2, 13) – 13(2, 12), $v_t=1-1$	21.91	153	✓	✓
239.91214	21(4, 18) – 20(5, 16), $v_t=1-0$	3.93	274	✓	ND
240.50454	33(2, 31) – 32(3, 29), $v_t=0-1$	8.54	531	✓	ND
240.65398	4(2, 2) – 3(1, 2), $v_t=1-0$	2.27	75	✓	✓
240.78219	15(2, 13) – 14(1, 13), $v_t=0-1$	5.50	163	✓	✓
242.17545	14(11, 4) – 13(11, 3), $v_t=1-1$	8.56	297	✓	✓
242.19130	14(10, 4) – 13(10, 3), $v_t=1-1$	10.96	272	✓	✓
242.22128	14(9, 6) – 13(9, 5), $v_t=1-1$	13.12	248	✓	✓
242.27115	14(8, 6) – 13(8, 5), $v_t=1-1$	15.06	228	✓	✓
242.34984	14(7, 7) – 13(7, 6), $v_t=1-1$	16.78	209	✓	✓
242.42989	14(10, 4) – 13(10, 3), $v_t=0-0$	10.96	266	✓	✓
242.47558	14(6, 8) – 13(6, 7), $v_t=1-1$	18.26	193	✓	✓
242.52421	14(7, 8) – 13(7, 7), $v_t=0-0$	16.78	204	✓	✓
242.62569	14(6, 8) – 13(6, 7), $v_t=0-0$	18.26	188	✓	✓
242.68501	14(5, 10) – 13(5, 9), $v_t=1-1$	19.52	180	✓	✓
242.69303	14(5, 9) – 13(5, 8), $v_t=1-1$	19.52	180	✓	✓
242.77010	14(3, 12) – 13(3, 11), $v_t=1-1$	21.34	160	✓	✓
242.81645	14(5, 10) – 13(5, 9), $v_t=0-0$	19.51	175	✓	✓
242.82510	14(5, 9) – 13(5, 8), $v_t=0-0$	19.51	175	✓	✓
242.99596	14(4, 11) – 13(4, 10), $v_t=1-1$	20.54	169	✓	✓
243.12032	14(4, 11) – 13(4, 10), $v_t=0-0$	20.54	164	✓	✓
243.13859	13(3, 10) – 12(2, 10), $v_t=0-1$	5.59	144	B	✓
243.20652	14(4, 10) – 13(4, 9), $v_t=1-1$	20.54	169	B	✓
243.30550	17(0, 17) – 16(1, 15), $v_t=1-0$	9.70	185	✓	✓
243.34972	14(4, 10) – 13(4, 9), $v_t=0-0$	20.54	164	✓	✓
243.48628	35(2, 33) – 34(3, 31), $v_t=0-1$	9.14	587	✓	ND
244.00985	12(3, 10) – 11(2, 10), $v_t=0-1$	5.30	133	✓	✓

Table A.3—Continued

Rest Frequency	Transition	$S_{ij}\mu^2$	$E_u$	Detection	
				hot core-SW	compact ridge
(GHz)		(Debye <sup>2</sup> )	(K)		
244.63395	14(1, 13) – 13(1, 12), $v_t=1-1$	22.25	152	✓	✓
245.32714	14(3, 11) – 13(3, 10), $v_t=1-1$	21.34	160	✓	✓
245.44511	12(2, 10) – 12(1, 12), $v_t=1-0$	7.48	132	B	B
246.41476	14(3, 11) – 13(3, 10), $v_t=0-0$	21.34	156	✓	✓

Table A.4. Unblended lines of the formic acid (t-HCOOH) toward the hot core-SW and hot core-north.

Rest Frequency	Transition	$S_{ij}\mu^2$	$E_u$	Detection	
				hot core-SW	hot core-north
(GHz)		(Debye <sup>2</sup> )	(K)		
220.03797	10(0, 10) – 9(0, 9)	20.14	59	✓	✓
223.91557	10(2, 9) – 9(2, 8)	19.39	72	✓	✓
224.91183	10(7, 3) – 9(7, 2)	10.30	215	✓	✓
224.92908	10(6, 5) – 9(6, 4)	12.93	174	B	✓
224.97676	10(5, 6) – 9(5, 5)	15.15	139	✓	✓
225.08544	10(4, 7) – 9(4, 6)	16.97	110	✓	✓
225.09121	10(4, 6) – 9(4, 5)	16.97	110	✓	✓
225.51255	10(3, 7) – 9(3, 6)	18.38	88	B	✓
228.54408	10(2, 8) – 9(2, 7)	19.40	73	✓	B
231.50561	10(1, 9) – 9(1, 8)	19.99	64	✓	B
236.71720	11(1, 11) – 10(1, 10)	22.03	72	✓	✓
241.14625	11(0, 11) – 10(0, 10)	22.15	70	✓	✓

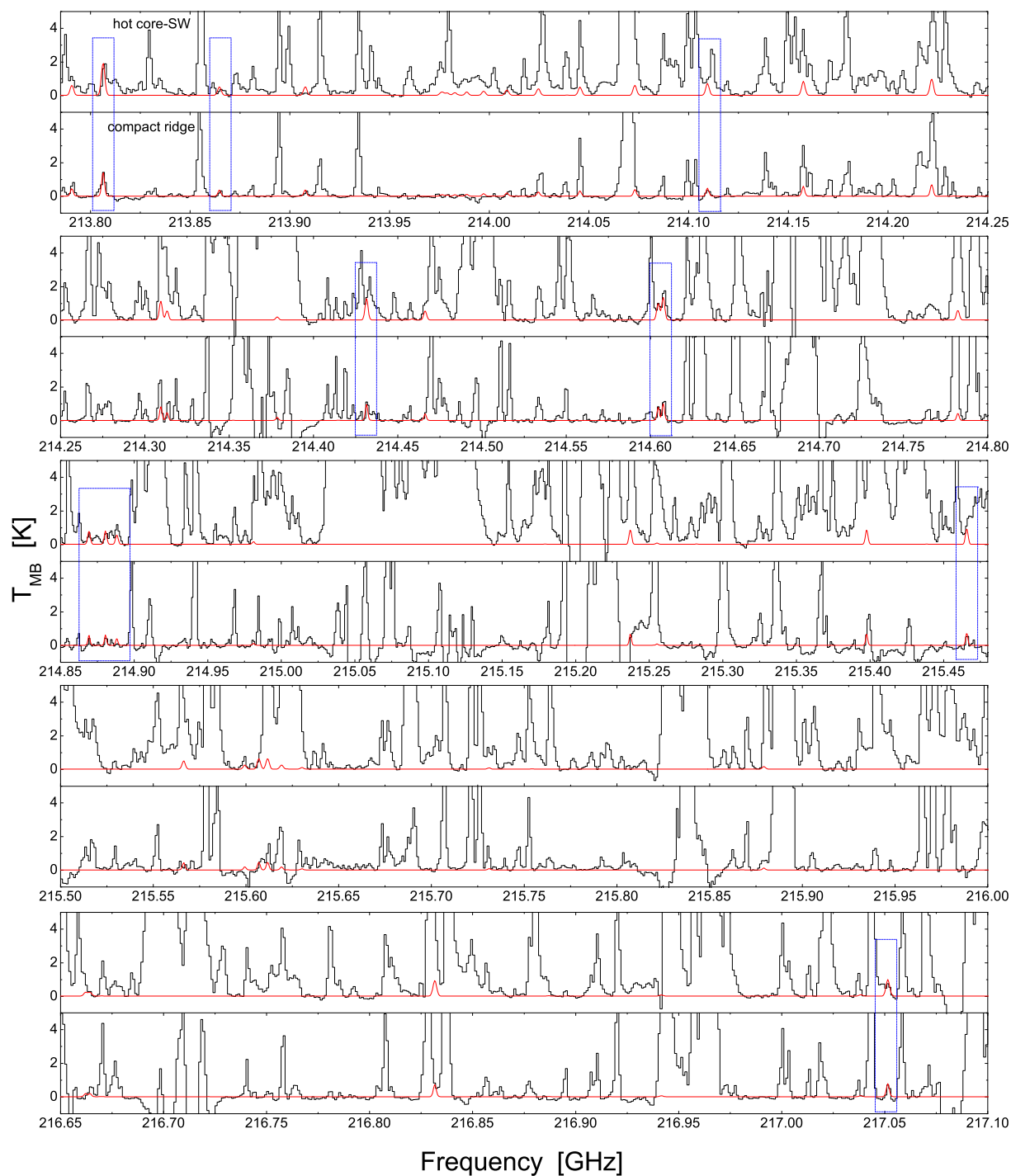


Fig. A.1.— Transitions of the *trans* and *gauche* conformers of EF ( $C_2H_5OCHO$ ) from transitions 213.785 GHz to 217.100 GHz toward the hot core and compact ridge. The black curve is the observed spectra, and the red line indicates the simulated LTE spectra. Transitions with an blue box around it are listed in Table A.1.



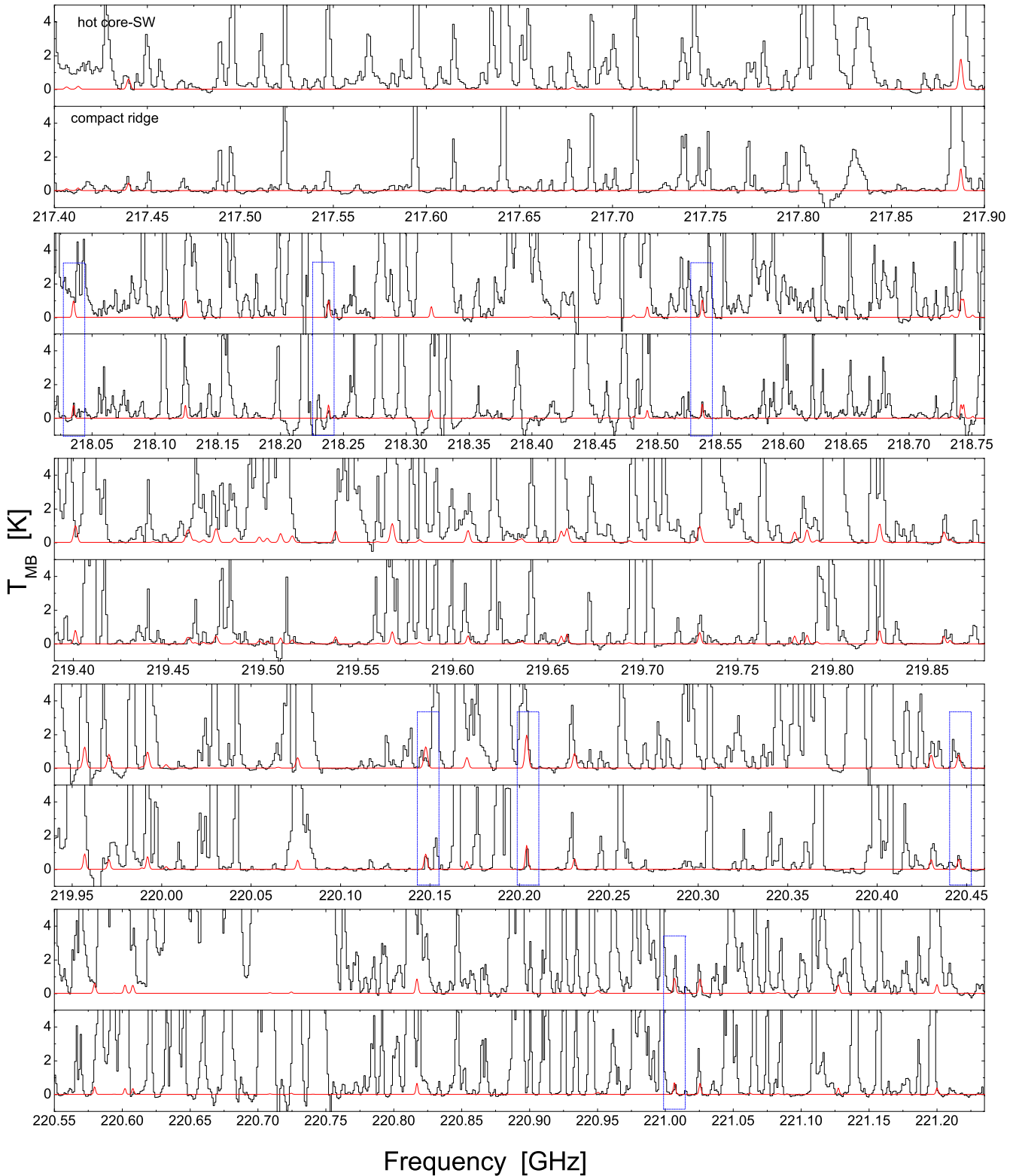


Fig. A.1.— Continued, from transitions 217.400 to 221.235 GHz. The spectral range of 218.76 to 219.39 GHz is not showed in figure, because there is no EF detectable lines in this range.

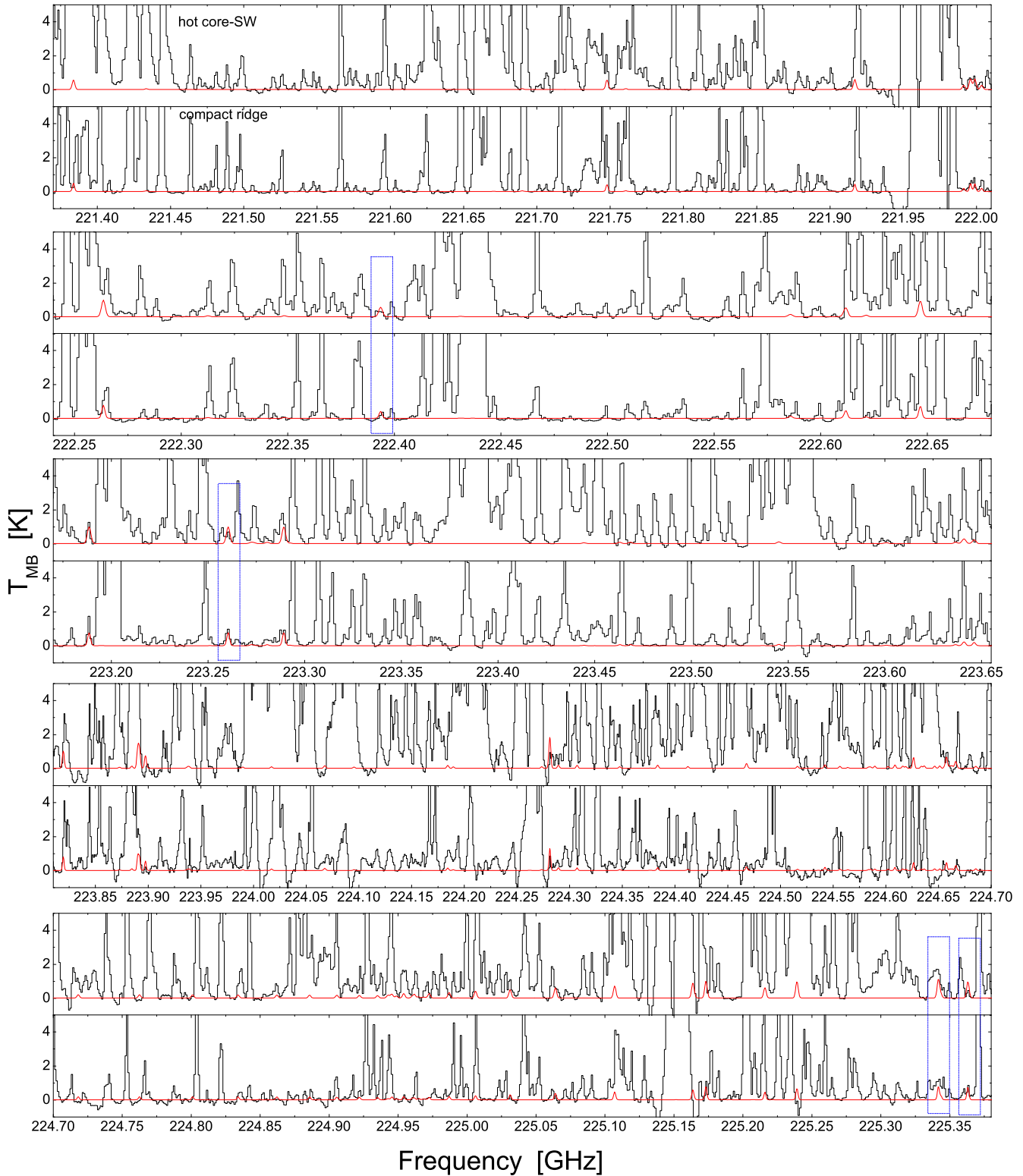


Fig. A.1.— Continued, from transitions 221.370 to 225.380 GHz. The range of 222.68-223.17 GHz without detectable lines is not showed.

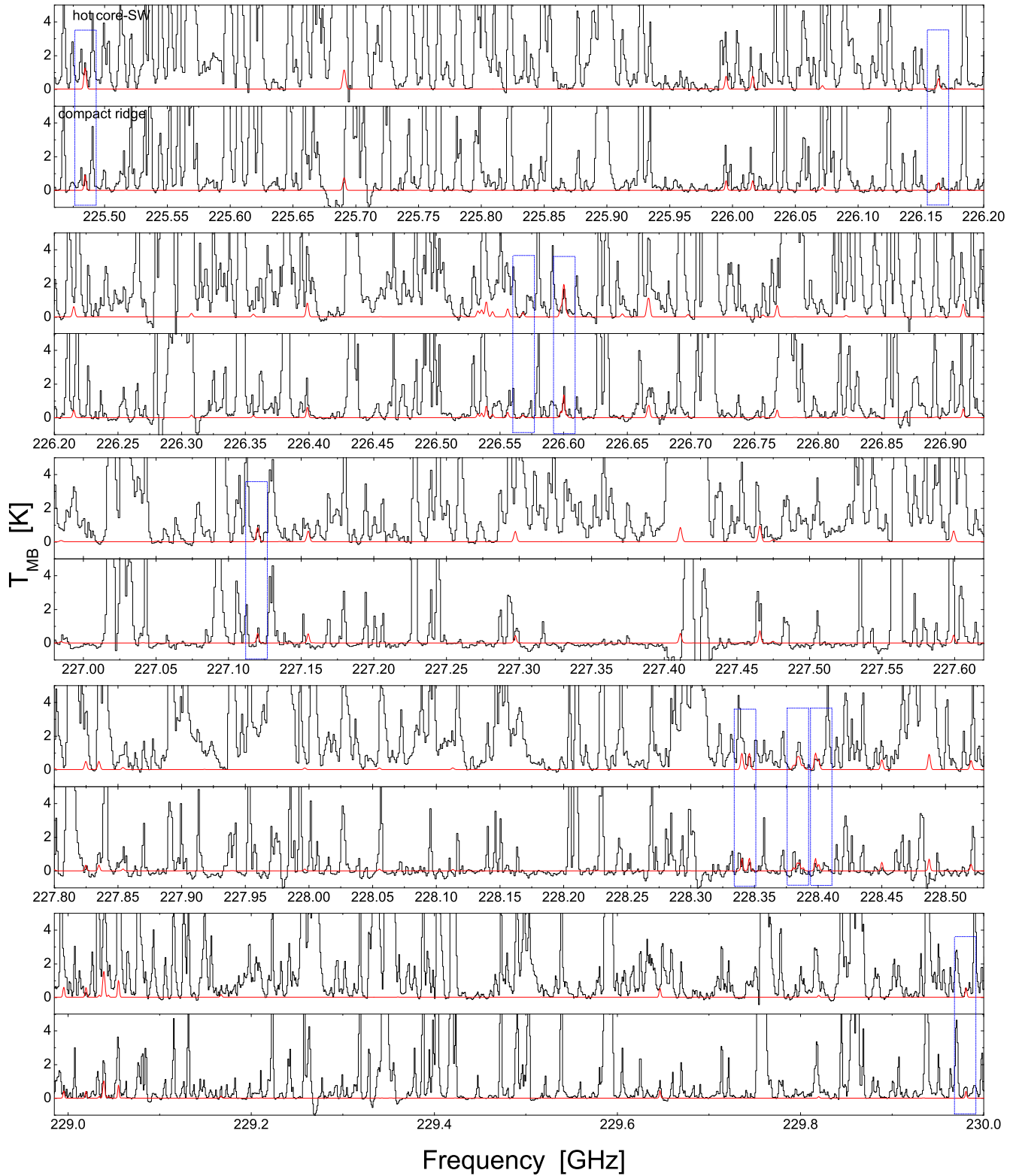


Fig. A.1.— Continued, from transitions 225.46 to 230.00 GHz.

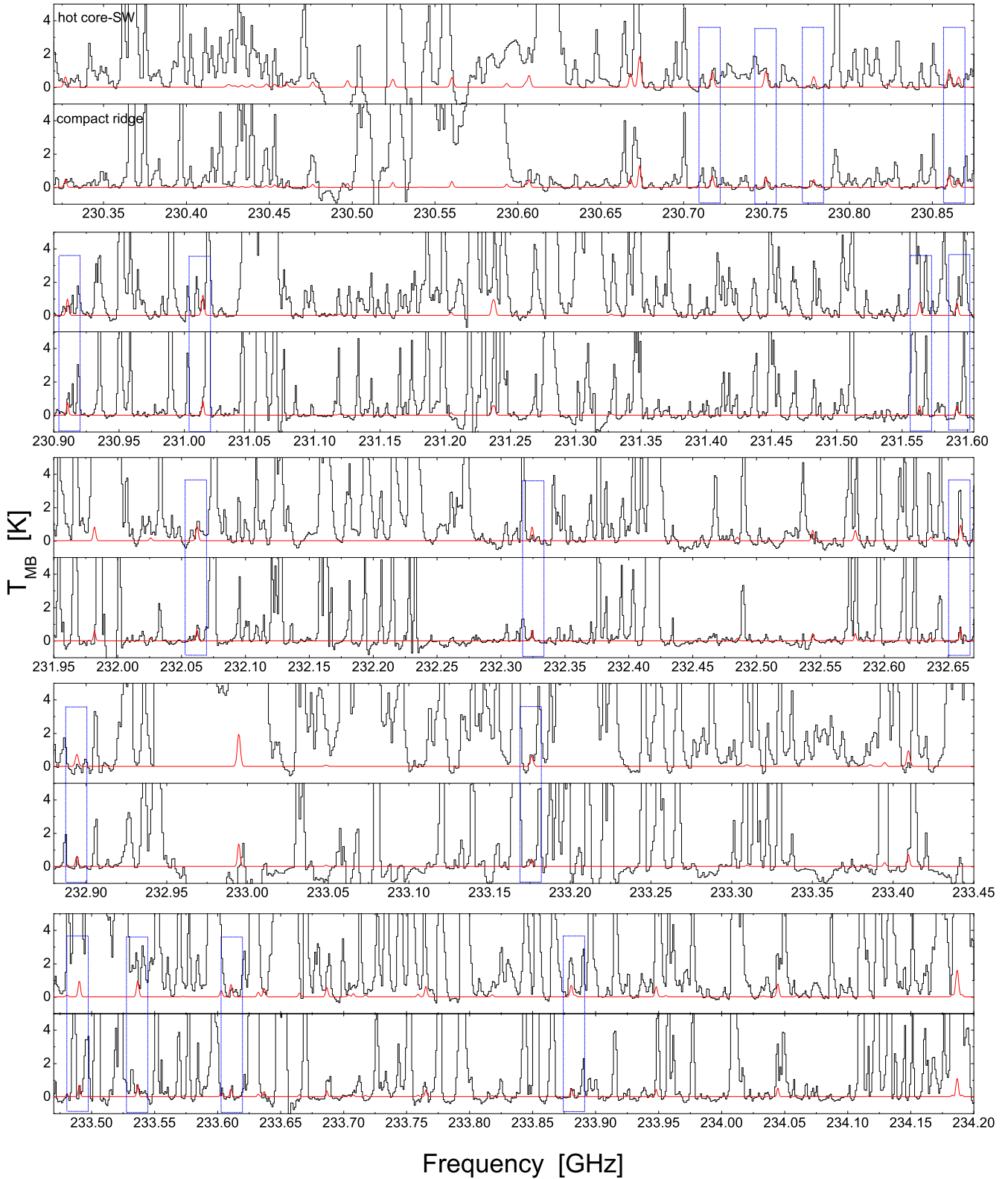


Fig. A.1.— Continued, from transitions 230.320 to 234.200 GHz.

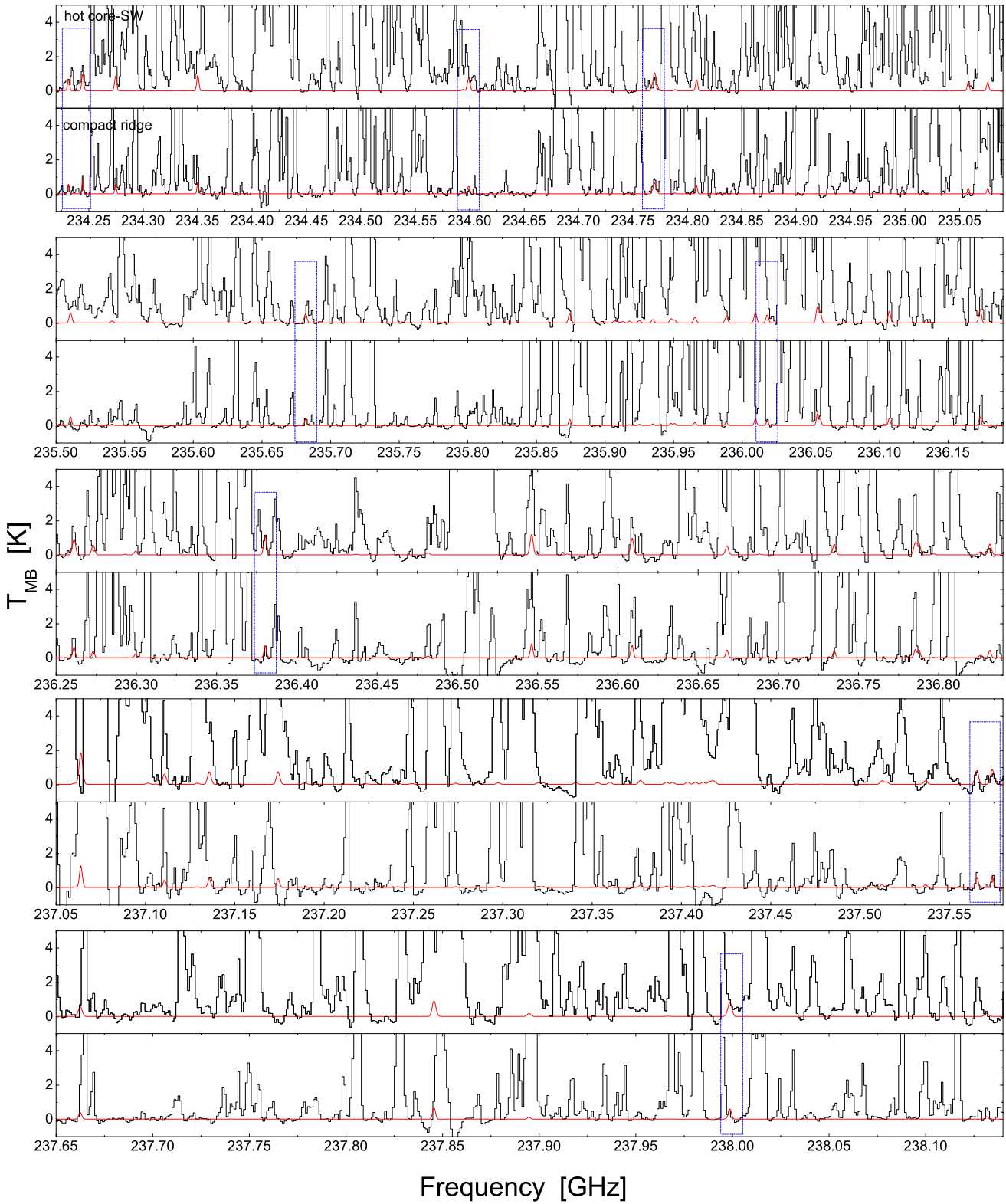


Fig. A.1.— Continued, from transitions 234.220 to 238.140 GHz.

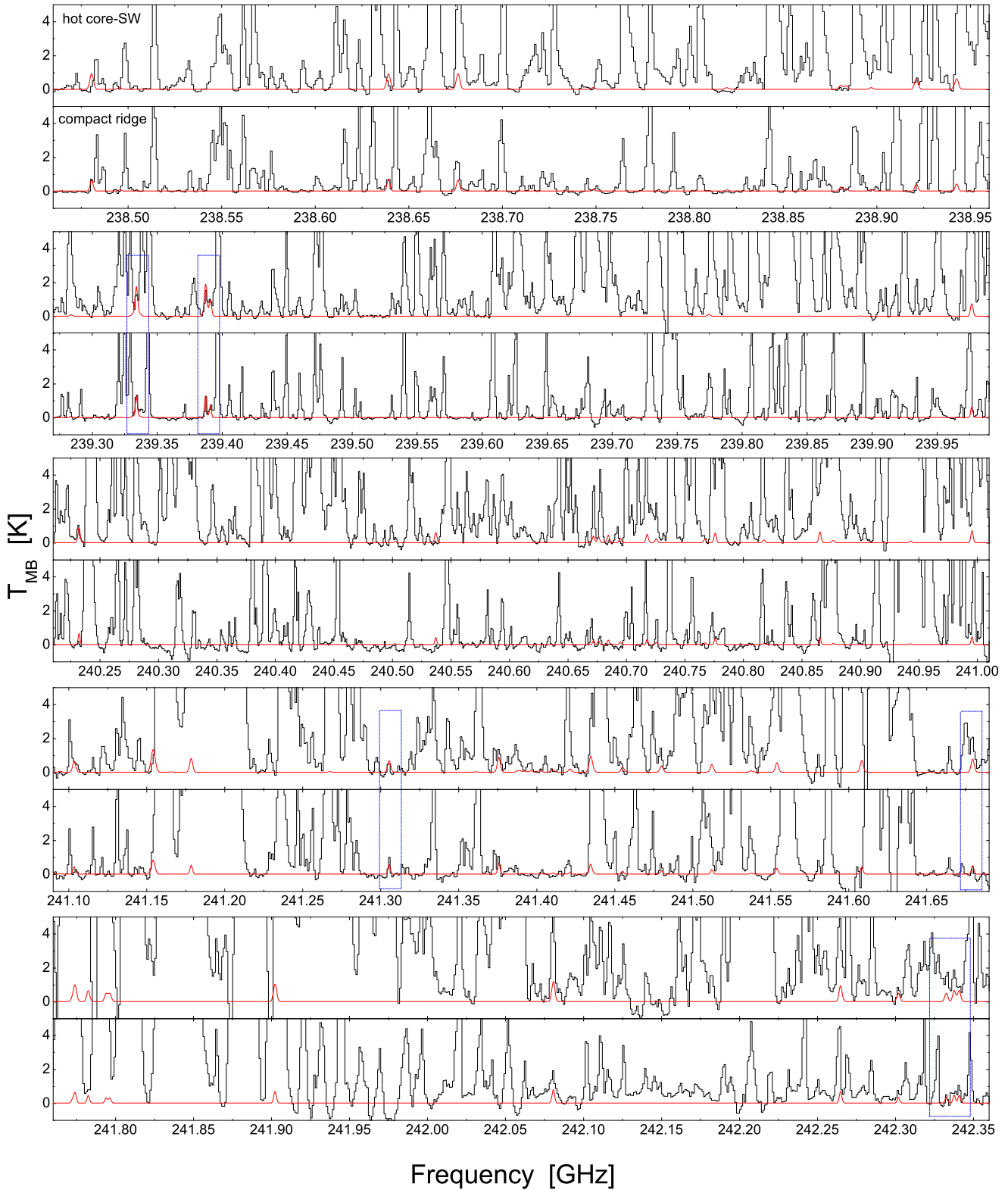


Fig. A.1.— Continued, from transitions 238.460 to 242.360 GHz.

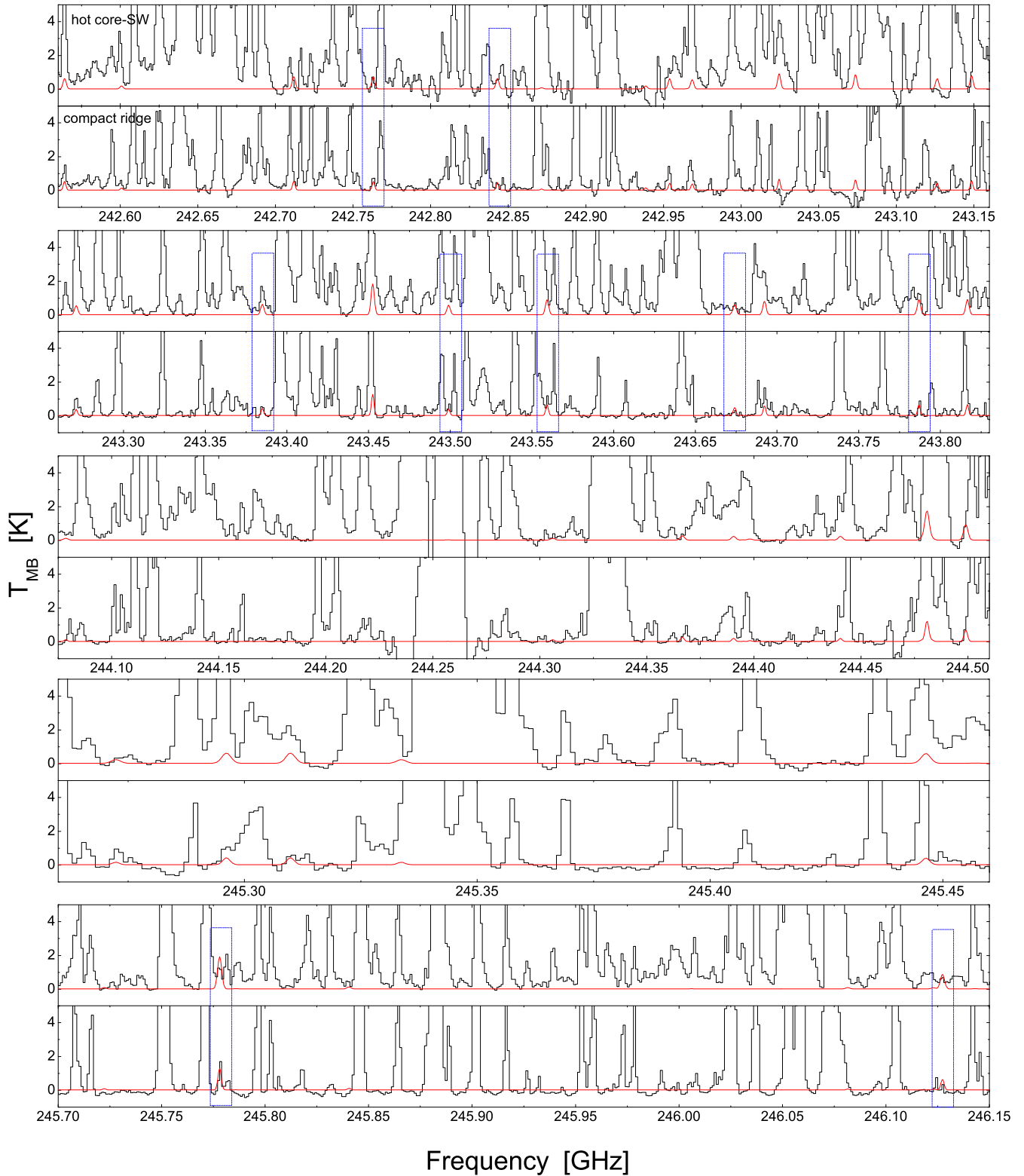


Fig. A.1.— Continued, from transitions 242.560 to 246.150 GHz.